THE PREDICTION OF AMORPHOUS SOLID DISPERSION PERFORMANCE IN VIVO FROM IN VITRO EXPERIMENTS

by

Venecia Rochelle Wilson

A Dissertation

Submitted to the Faculty of Purdue University

In Partial Fulfillment of the Requirements for the degree of

Doctor of Philosophy

Department of Industrial & Physical Pharmacy

West Lafayette, Indiana

December 2018

THE PURDUE UNIVERSITY GRADUATE SCHOOL
STATEMENT OF COMMITTEE APPROVAL

Dr. Lynne S. Taylor, Chair

    Department of Industrial & Physical Pharmacy

Dr. Stephen Beaudoin

    Davidson School of Chemical Engineering

Dr. Dor Ben-Amotz

    Department of Chemistry

Dr. Stephen R. Byrn

    Department of Industrial & Physical Pharmacy

Dr. Kevin J. Edgar

    Virginia Polytechnic Institute and State University

Approved by:

    Dr. Rodolfo Pinal

        Head of the Graduate Program

To everyone who motivated me to something greater than myself. I pray the best of your today is the worst of your tomorrow.

ACKNOWLEDGMENTS

To those that I didn't mention by name, I want to thank you for time, encouragement, criticism, love, and conversations. We did it!

TABLE OF CONTENTS

LIST OF TABLES

LIST OF FIGURES

ABSTRACT

Author: Wilson, Venecia,R. PhD
Institution: Purdue University
Degree Received: December 2018
Title: The Prediction of Amorphous Solid Dispersion Performance in vivo from in vitro Experiments
Committee Chair: Lynne S. Taylor

Enabling formulations are growing in popularity due to the large number of drugs within the pharmaceutical development pipeline that possess poor water solubility. These sophisticated formulation techniques can increase the solubility of the drug in aqueous media and/or aid in their dissolution. Amorphous solid dispersions (ASDs) are of particular interest due to their ability to generate highly supersaturated solutions upon dissolution. Typically, an ASD consists of amorphous drug homogenously blended with an amphiphilic polymer. The polymer has several roles including to facilitate drug release, as well as to inhibit crystallization of the drug from the solid matrix and from the supersaturated solution generated following dissolution. A phenomenon termed liquid-liquid phase separation (LLPS) or glass-liquid phase separation (GLPS) can occur during ASD dissolution when the amorphous solubility is exceeded. Here the drug attains its maximum thermodynamic activity in solution with the excess drug forming a second phase consisting of colloidal amorphous aggregates. It has been hypothesized that the presence of the colloidal amorphous aggregates could be advantageous *in vivo* since they can act as a drug reservoir and subsequently maintain the drug at its maximum thermodynamic activity in the gastro-intestinal fluid following solution depletion arising from permeation across the gastrointestinal membrane. However, there are few *in vivo* studies which test this hypothesis. If colloids form, the polymer must also inhibit crystallization from the drug-rich phase. Hence, the polymer has many roles during ASD dissolution making rational polymer selection for ASD formulation a complex process. While many studies, both past and present, probe drug release during dissolution, a limited number of studies address a mechanistic understanding of the polymer role during dissolution. The purpose of this study was to 1) investigate the interplay of the polymer's ability to inhibit crystallization (thought to be primarily through hydrophobic interactions) and to facilitate drug release (via hydrophilic interaction with the aqueous media) on ASD performance and 2) determine the *in vivo* relevance of colloidal amorphous aggregates. Herein, a preliminary

correlation was established between *in vitro* diffusion cell experiments and the amount of drug absorbed in rats. Further, it was found that rapid drug release through use of a relatively hydrophilic polymer is essential, and that the best crystallization inhibitors may be too hydrophobic to achieve adequate release. Therefore, a polymer needs to be an adequate crystallization inhibitor, but be able to release the drug upon oral administration. The implications from this study provides the necessary foundation for assessing ASD phase behavior and performance *in vitro* in order to make improved *in vivo* predictions. Ultimately, this research is expected to improve the speed of life-saving drugs progressing through the development pipeline and reduce drug development costs by reducing the need for animal testing.

CHAPTER 1.   INTRODUCTION

1.1   Research Significance

The likelihood of a drug progressing to the market is predicated on its safety and efficacy. Approximately 65% of commercially available medications are dosed orally[1], which is in part due to the ease of manufacturability and patient preference. The efficacy of an orally delivered compound is dependent upon its solubility and permeability; the drug must solubilize in the body's aqueous environment and be absorbed in the digestive tract by crossing tissue membrane, then reach its site of action and trigger a desired therapeutic effect. Unfortunately, it has been reported that approximately 90% of new molecular entities (NME) in development have poor aqueous solubility[2]; resulting in decreased absorption and reduced efficacy of potentially life-saving compounds. Consequently, several enabling formulation techniques have been developed which can improve drug aqueous solubility by modifying the physical and/or chemical state of the drug (Figure 1-1).

Of particular interest in the context of this research, are amorphous solid dispersions (ASD) and self-emulsifying drug delivery systems (SEDDS). In both formulations, the active pharmaceutical ingredient (API) remains chemically unchanged and excipients are formulated with the drug to aid in its solubilization and dissolution in solution. In SEDDS, the drug is pre-dissolved in a mixture of surfactant and triglycerides; *in vivo* the mixture forms an emulsion due to agitation caused by gastro-intestinal motility. The SEDDS must undergo digestion for drug to be released from the oily droplets[3]. The major advantage of SEDDS is that the API is pre-dissolved consequently, dissolution limited absorption is avoided. Whereas with an ASD, the drug is homogenously mixed with polymer. Polymer aides in the release of the drug, therefore, dissolution limited absorption could still occur if: the drug-polymer interaction is stronger than polymer-water interaction, drug rich domains form at the ASD-water interface and retards dissolution, or crystallization occurs within the ASD or in solution; all of which would be a result of the dissolution of the ASD being slower than the absorption of the drug. Traditionally, ASDs are formulated with polymers that have been repurposed for ASD[4–7]. The lack of chemically diverse polymers limits the number drugs that can be formulated as an ASD since the drug-polymer interaction will impact drug release

and extent of supersaturation during ASD dissolution. Both types of enabling formulations will be investigated their ability to enhance the absorption of a fast crystallizing poorly water-soluble compound. The purpose of this dissertation is to investigate the interplay of phase transitions that occur during ASD dissolution and its impact on *in vivo* performance. The introduction is subsequently organized to first provide fundamental understanding of thermodynamics of supersaturation, followed by ASD preparation and its dissolution outcomes, and lastly a description of drug permeation and absorption both *in vitro* and *in vivo*.

1.2 Thermodynamic Activity of Drug in Enabling Formulations

The simplest way of screening the effectiveness of the enabling formulations at increasing the solubility of compounds in dissolution media is to measure their effective concentration in solution. The thermodynamic activity i.e. the effective concentration, is given by the following equation[8]

$$a = \gamma c_i \qquad (1\text{-}1)$$

where a is the activity, γ is the activity coefficient, c_i is the concentration of species i, and $c*$ is the standard state concentration of species i. The thermodynamic activity coefficient will be at unity if both of the following criteria are true: 1) dilute aqueous solution of the species under investigation 2) an absence of specific interactions between the species of interest and other species in solution[8].

$$a = c_i \qquad (1\text{-}2)$$

The concentration of drug in solution can also be related to the chemical potential[9]:

$$\frac{\mu - \mu*}{RT} = S - 1 = \frac{c_i}{c*} - 1 \qquad (1\text{-}3)$$

μ is the chemical potential of the drug in solution, $\mu*$ is the standard state chemical potential of the drug in solution, R is the universal gas constant, T is the temperature, and S is the supersaturation level of the drug. The supersaturation is thus a measure of the excess chemical potential of solute relative to its standard state. For systems where the activity coefficient is unity, supersaturation can be estimated from the ratio of the solute concentration to the solute concentration at saturation. For amorphous solid dispersions formulated with polymers which do not change the standard state chemical potential of the drug, supersaturation can be directly calculated from effective concentration. Conversely, lipid based formulations such as SEDDS which contain solubilizing

excipients will increase the equilibrium solubility of the drug which will result in the thermodynamic activity coefficient unequal to 1.

1.3 Thermodynamic Properties of Supersaturated Solutions

A supersaturated solution is obtained when the chemical potential of the drug in solution is greater than the chemical potential of the drug in its solid state[10].When this is the case, the solution is no longer in thermodynamic equilibrium and a driving force for crystallization will now exist; with the driving force being proportional to the difference between the chemical potential in solution and solid. If the crystallization kinetics is not instantaneous, highly supersaturated solutions can be created in which the chemical potential will reach a maximum, termed the amorphous solubility[11–14].

1.3.1 Amorphous Solubility

Amorphous material lacks long-range order which gives it a solubility advantage over the crystalline form. The amorphous solubility can be calculated using Hoffman[15] and Murdande[16] equations respectively:

$$\Delta G_{c \to a} = \frac{\Delta H_f (T_m - T) T}{T_m^2} \qquad (1\text{-}4)$$

$$C_a = C_{eq} e^{[\Delta G_{c \to a} - I(a_2)]/RT} \qquad (1\text{-}5)$$

where $\Delta G_{c \to a}$ is the chemical potential of transitioning from a crystalline solid to amorphous material, ΔH_f is the enthalpy of formation, T_m is the melting temperature, T is the experimental temperature, C_{eq} is the equilibrium solubility, $-I(a_2)$ is the moisture sorption factor, and R is the universal gas constant.

Any addition of drug to the solution once the amorphous solubility has been reached will result in the formation of an amorphous precipitate, which will be a glass or supercooled liquid depending on the glass transition temperature of the water-saturated amorphous system. If the experimental temperature is below the glass transition temperature, the amorphous material will precipitate as a glass, and if it is above, as a supercooled liquid[12,17]. Glass-liquid phase separation (GLPS)/ liquid-liquid phase separation (LLPS) is a metastable state in respect to the crystalline form[18,19] (Figure

1-2.). Figure 1-3 depicts the chemical potential of the drug and the phase changes that can occur in a highly supersaturated solution:

1) $\mu^{solution} < \mu^{solid}$: Initially the compound will readily dissolve since the system is undersaturated.

2) $\mu^{solution} > \mu^{solid}$: The concentration of compound in solution will increase above the equilibrium solubility i.e. crystalline solubility.

3) $\mu^{solution}$ at a maximum: Once a certain concentration is exceeded, amorphous precipitate (supercooled liquid or glass) can form in solution. Further addition of the compound to solution would result in more amorphous precipitate.

4) $\mu^{solution}$ is decreasing: Crystallization occurs resulting in a decrease in concentration and chemical potential.

5) $\mu^{solution} = \mu^{solid}$: The system has reached equilibrium.

The precipitation of amorphous drug is not unique to amorphous based formulations, it was shown that amorphous precipitate formed during digestion of cinnarizine self micro-emulsifying drug delivery system[20].

1.3.2 Crystallization Theory

1.3.2.1 Nucleation

Crystallization is a two-step process: nucleation followed by crystal growth. Nucleation can be described as primary homogeneous or heterogeneous or secondary (Figure 1-4). Primary nucleation is nucleation in the absence of seed crystals and secondary occurs in the presence of seed crystals[10]. There are two popular models to describe nucleation: classical nucleation theory (CNT) and two step nucleation with the former being widely accepted as the simplified depiction of crystallization[21], Figure 1-5. CNT postulates that in a supersaturated solution, solute molecules associate with one another to form nuclei; at sizes below a critical size, termed the critical radius, the nuclei will have a tendency to re-dissolve whereas at sizes above the nuclei is stable and will have a tendency to grow. The critical radius is determined by the free energy required to create a new surface (ΔG_s) and free energy released from condensing the solute from solution (ΔG_v). The formation of a new surface requires energy while the condensation of the solute from solution expels energy. The total free energy of the nuclei could be described as:

$$\Delta G = \Delta G_s + \Delta G_v \quad \text{(1-6)}$$

Whereby the total free energy of the system can also be described by the radius, r, of the nuclei formed in solution and its interfacial tension, γ:

$$\Delta G = \frac{4}{3}\pi r^3 \Delta G_v + 4\pi r^2 \gamma \quad \text{(1-7)}$$

At the maximum total free energy of the system, the solute will have a thermodynamic driving force to crystallize hence in equation 1-8 the radius at the maximum total free energy can be found by taking the derivative of G and equating it to zero, this is described as the critical radius (equation 1-9).

$$\frac{d(\Delta G)}{dr} = 0 \quad \text{(1-8)}$$

$$r_c = \frac{2\gamma}{\Delta G_v} \quad \text{(1-9)}$$

There are several assumptions that are made[21]:

1) Clusters are spherical
2) Nucleation is a steady-state process
3) Nuclei are in the same ordered arrangement as the crystal
4) Nuclei are stationary
5) Nuclei grow by monomer addition
6) Curvature of the clusters are independent of surface tension

In the case of homogeneous nucleation, the nucleation rate, J, can be described by the Arrehenius equation:

$$J = Ae^{-\left(\frac{\Delta G_{crit}}{kT}\right)} \quad \text{(1-10)}$$

$$\Delta G_{crit} = \frac{4\pi r_c^2}{3} \quad \text{(1-11)}$$

$$J = Ae^{\left[-16\pi\gamma^3 v^2 \big/ 3k^3 T^3 (lnS)^2\right]} \quad \text{(1-12)}$$

Where A is a constant, Υ is the interfacial tension between the cluster and liquid, v is the molecular volume, k is the Boltzmann constant, T is the experimental temperature, and S is the supersaturation[10].

The major difference between CNT, described above, and two-step nucleation theory is the assumption that nuclei spatial arrangement is constant over time i.e. the orientation of the nuclei

is the same as that of the crystal[21]. Two-step nucleation theory states the initial orientation of the molecule cluster is independent of the crystal structure arrangement[21]. This theory has been widely accepted as a more probable accurate depiction of crystallization in comparison to CNT.

1.3.2.2 Crystal Growth

Once the nucleus is stable in solution, it will grow into a crystal. Crystal growth occurs by molecules diffusing from the bulk media to the stable nuclei or crystal and then subsequent attachment of the molecule to the surface in the crystal arrangement[10,22]. The type of crystal growth, diffusion limited or integration limited, will depend on the physiochemical properties of the drug and the experimental conditions[22]. Diffusion limited growth can be described mathematically (equation 1-13) where m is mass, t is time, R_G is crystal growth, k_d is the diffusion growth rate, c is concentration of drug in bulk media, and c_i is the concentration of at the crystal interface[10].

$$\text{Diffusion limited: } \frac{dm}{dt} = R_G = k_d(c - c_i) \qquad (1\text{-}13)$$

Integration limited growth is described by:

$$\text{Integration limited: } \frac{dm}{dt} = R_G = k_I(c_i - c^*)^r \qquad (1\text{-}14)$$

where k_r: integration growth rate, c^*: equilibrium concentration, and r: integration order[10]. Solution additives such as polymers have been shown to retard crystal growth. In diffusion limited crystal growth, the polymer will need to slow and/or halt the diffusion of molecules to the crystal surface by increasing solution viscosity. In the case of integration limited growth, the polymer will need block integration sites on the crystal surface, which would be facilitated by strong interactions between the drug and polymer; while in diffusion limited the growth, the polymer-solute interaction is of less importance.

1.4   Amorphous Solid Dispersion

The role of the polymer in ASDs is to prevent crystallization in the solid-state, facilitate the release of drug into solution during ASD dissolution, and inhibit crystallization of drug in solution. The ability of the polymer to delay crystallization in solution is dependent upon its physiochemical properties: molecular weight[23], rigidity[24], degree of substitution of key functional groups[25], hydrophobicity and bulkiness of substituents[26], and amphilicity[27] . In addition, drug crystallization

will be driven by the physiochemical properties of the drug, pKa of media, and the favorable interactions that exist between the polymer and the drug.

During storage, conditions such as relative humidity and temperature are important factors to consider for solid-state crystallization inhibition. It has been proposed and confirmed that glass transition temperature, T_g, is an indirect measure of molecular mobility of the ASD[28,29]. If the T_g of ASD is greater that the T_g of the amorphous drug, the kinetic barrier of crystallization is higher for the ASD than the amorphous drug alone. The miscibility of the drug within the polymer and the overall thermodynamics of mixing will impact the glass transition temperature of the amorphous solid dispersion[30].

1.4.1 Drug-Polymer Miscibility

In miscible drug-polymer systems, the drug is homogeneously mixed with the polymer to kinetically stabilize the amorphous drug. The entropy and enthalpy of mixing affects the miscibility of the drug-polymer system which can be estimated from the volume fraction of each component[31,32]:

$$\frac{\Delta G}{RT} = \frac{\Phi_{drug}}{m_{drug}} ln\Phi_{drug} + \frac{\Phi_{polymer}}{m_{polymer}} ln\Phi_{polymer} + \chi\Phi_{drug}\Phi_{polymer} \qquad (1\text{-}15)$$

Φ_{drug} :volume fraction of drug m_{drug} mole fraction of drug, $\Phi_{polymer}$:volume fraction of polymer, $m_{polymer}$:mole fraction of polymer, χ :Flory-Huggins interaction parameter. When the Flory-Huggins interaction parameters is a sufficiently large positive value, the cohesive forces of each individual component are stronger than the adhesion force and the mixture is unfavorable which is classified as endothermic mixing[33]. Conversely, if it is a small positive or negative value, adhesion forces promote mixing which is called exothermic mixing[33]. It was proposed by Hansen[34] the Flory-Huggins interaction parameter could be estimated by the cohesion energy density via the solubility parameter:

$$\chi = V \frac{(\delta_{drug} - \delta_{polymer})^2}{RT} \qquad (1\text{-}16)$$

where V is the molar volume, δ_{drug} is the drug solubility parameter, and $\delta_{polymer}$ is the polymer solubility parameter[33]. However, this approach can only yield zero or positive values of the interaction parameter.

There are several different proposed ways to calculate solubility parameter[34–37] to predict the miscibility of drug and polymers; the difference amongst the different parameters are the interpretation of the temperature and volume relationship. Hansen and Hoy solubility parameters are unique in that the solubility parameter can be calculated based upon the molecule's expected intramolecular interactions: dispersive, hydrogen bonding, and polar[34,35,38]. The individual interaction solubility parameters are calculated independently using Hansen's method[34], whereas, with Hoy the dispersive interaction value is dependent upon the polar and hydrogen bonding interaction values[35].

$$\text{Dispersive Hansen Solubility Parameter}^{34}: \delta_d = \sqrt{\frac{E_D}{V}} \qquad (1\text{-}17)$$

$$\text{Dispersive Hoy Solubility Parameter}^{35}: \delta_d = \sqrt{\delta_t^2 - \delta_p^2 - \delta_h^2} \qquad (1\text{-}18)$$

Where δ_d is dispersive portion of the solubility parameter, E_D is dispersive potential energy, δ_t is total solubility parameter, δ_p is polar solubility parameter, and δ_h is the hydrogen bonding solubility parameter. The miscibility of a system using solubility parameters can be estimated by the solubility parameter distance. The greater the solubility parameter distance (Ra), the less probable that the two components will be miscible[34]:

$$(Ra)^2 = 4(\delta_{d_{drug}} - \delta_{d_{polymer}})^2 + (\delta_{p_{drug}} - \delta_{P_{polymer}})^2 + (\delta_{h_{drug}} - \delta_{h_{polymer}})^2 \qquad (1\text{-}19)$$

It is assumed that species are uncharged in solubility parameter calculations, thus they can only qualitatively provide an estimate of drug and polymer miscibility in their respective unionized state. A more thorough approach such as molecular dynamic simulations can be used to better predict drug-polymer interactions[39].

Immiscibility of the polymer and amorphous drug could lead to crystallization due to the polymer no longer being in the vicinity of the drug to inhibit solid-state crystallization. In a phenomena described as amorphous-amorphous phase separation (AAPS), drug rich domains form in the homogenous ASD[40–42]. Moisture induced, the most reported cause of AAPS, occurs when the ASD absorbs water during storage or once introduced to aqueous media during dissolution; in those systems, the polymer-water interaction is stronger than the drug-polymer interaction. Hence, the miscibility of the drug and polymer can change in the presence of moisture, so while the solubility parameter and Flory-Huggins interaction parameter can be used to predict drug-polymer

miscibility, they do not address miscibility in aqueous solution. AAPS, which is undesired, can be experimentally determined through fluorescence spectroscopy and atomic force microscopy[42,43].

1.4.2 ASD Dissolution

If the polymer is water soluble and is able to stabilize the drug in solution, then the ASD can be described as dissolving via a spring-parachute mechanism. Within the spring-parachute mechanism, the drug is able to remain in a supersaturated state for an extended period of time in comparison to the dissolution of the pure amorphous form of the drug[44] (Figure 1-6). The dissolution rate and supersaturation achieved in solution will depend on the drug loading i.e. for very different dissolution profiles could be observed for the same drug and polymer combination with varying drug loadings[45–48]. It is often assumed that a lower drug loading ASD formulated with a hydrophilic polymer will generate higher supersaturation upon dissolution than a higher drug loading ASD with the same drug and polymer[45,49]. Corrigan proposed in 1985 that this phenomena is due to the hydrophobic drug retarding the release of hydrophilic polymer at high drug loadings[49]. Ideally during ASD dissolution, congruent release of the drug and polymer i.e. polymer controlled dissolution[49] would generate a highly supersaturated solution that undergoes LLPS/GLPS. Previous studies showed that the amorphous aggregates generated during LLPS dissolved more rapidly than externally generated amorphous drug introduced to supersaturated solution of drug ergo colloidal amorphous aggregat3es dissolve at the same speed or faster than undissolved ASD[20,50]. It has been reported for many amorphous solid dispersion systems that colloidal amorphous aggregates form during dissolution[51–54].

There are two ways that the ASD can undergo LLPS/GLPS: 1) the ASD dissolves creating a supersaturated solution in which the amorphous solubility is exceeded thus resulting in any additional drug added to solution forming amorphous aggregates[55] or 2) AAPS occurs in ASD and the polymer dissolves leaving the amorphous aggregates[56]. The polymer's role in facilitating LLPS/GLPS is very different in the two proposed mechanisms, however the author assumes that the more probable situation is the former due to previous studies showing AAPS as a precursor to crystallization[42]. Regardless of the mechanism of formation, once amorphous aggregates are generated, they can rapidly dissolve and maintain the effective concentration of drug in solution[57].

The duration of supersaturation will depend on the drug crystallization kinetics as described in Section 1.3.2.

1.5 Drug Permeation Through Membranes

1.5.1 In vitro Drug Permeation Studies

Orally dosed drugs must permeate through intestinal membrane to reach its site of action except in the case where the intestine is the site of action. Only uncharged unbound drug can passively diffuse across lipophilic membranes such as the small intestine[58]. The rate of passive absorption is directly proportional to the uncharged free drug concentration with the mass flux plateauing at the amorphous solubility; therefore, solubility or dissolution enhancing formulations have the propensity maximize oral bioavailability of BCS Class II compounds that are extensively absorbed passively. A positive correlation between the percent of drug released during ASD dissolution and mean plasma concentration in dogs for ritonavir, sufficiently oral bioavailable compound[59], was observed by Law *et al*[60]. For slow crystallizers such as ritonavir[25], passive absorption is a function of the amount of drug released; however, for drugs that crystallize over biologically relevant timeframes absorption would be dependent on the amount of drug released, in addition to, the crystallization kinetics of the compound. This is due to absorption being a dynamic process that is dependent upon the difference of the chemical potential of the drug in the apical and basal side of a membrane, as well as, permeation rate of the drug[61]. In traditional ASD dissolution, only the chemical potential of the drug in the apical side of the membrane is considered.

Side-by-side diffusion cell experiments are used to temporally model the chemical potential difference across the apical and basal side of membranes by measure drug flux across a membrane of choice [19,57,62]. The device contains a bi-compartmental system that is separated by a membrane; the formulation is placed in the donor compartment and the concentration of drug in the receiver compartment is used to calculate the mass flux, J[63].

$$J = \frac{Da}{h\gamma_m} \qquad (1\text{-}20)$$

D is the solute diffusivity, a is the activity of drug in the donor compartment (calculated by equation 1-1), h is the thickness of the membrane, γ_m is the activity coefficient of the drug in the membrane.

It has been observed by the Taylor lab that the mass flux of drug linearly increases with initial drug concentration in the donor compartment up to the amorphous solubility[17,19,57,62,64]. At concentrations above the amorphous solubility, the mass flux will plateau due to the maximum free drug concentration being achieved and maintained in donor compartment by the re-dissolution of amorphous aggregates. Raina *et al*, that the amorphous aggregates act as a depot replenishing drug that has diffused to the receiver compartment[19] (Figure 1-7); more amorphous aggregates could correlate to longer duration of supersaturation at the amorphous solubility and consequently, more drug absorbed.

1.5.2   In vivo Drug Absorption

Animal studies are conducted during preclinical drug development to assess a drug's toxicology and pharmacology. Due to costs and ethical considerations, drug development scientists are seeking to correlate *in vitro* studies with *in vivo* animal studies to minimize the amount of animals used in preclinical studies. Food and Drug Administration (FDA) describe in vitro-in vivo correlation (IVIVC) as the "relationship between an *in vitro* attribute of a dosage form and a relevant *in vivo* response"[65]. In the late 1980s , the United States Pharmacopeia (USP) published four correlation levels of IVIVC for oral dosage forms; the highest level A is achieved when a model is established that correlates in vitro dissolution with in vivo dissolution and level D, the lowest, when only a qualitative correlation is established[65]. Complex dissolution apparatuses that can mimic gastro-intestinal conditions such as pH shift, fluid dynamics, temperature, intestinal fluid contents are commercially available. However, the FDA has reported that the majority of dissolution tests are performed in Apparatus I and II in non-biorelevant conditions[1] which indicates the need for simplistic cost effective bio-relevant dissolution apparatuses which results can be correlated with *in vivo* animal study outcomes. To the author's knowledge, no IVIVC has been reported for a drug formulated as an ASD in which the experimental design employed concurrently investigates drug release and absorption.

1.6   Hypotheses

The goal of the proposed study is to model the *in vivo* absorption of poorly water-soluble drug molecules through understanding the thermodynamic and kinetic properties of its enabling formulation *in vitro*. This study will be carried out by testing the following hypotheses:

- *The maximum free drug concentration that can be achieved is the amorphous solubility limit. To reach this limit for a fast crystallizing compound formulated as an amorphous solid dispersion, the polymer must stabilize the amorphous drug in solid-state and amorphous precipitate in solution. In solution, such polymers must be water soluble and possess sufficient hydrophobic substituents which can interact with the drug thereby inhibiting crystallization.*

- *The mass flux of a drug across a membrane is an indicator of the thermodynamic activity of the drug in solution and can be used to predict the qualitative in vivo absorption of various formulations of a model compound which is absorbed predominantly via passive transport.*

1.7   Research Overview

This dissertation is organized as such:

1) Chapter 1 provides fundamental understanding of phase transitions that occur in supersaturated solutions, the utility of amorphous solids in formulation development, and the dynamic process of drug absorption *in vitro* and *in vivo*.

2) Chapter 2 studies demonstrate the importance of drug phase behavior during ASD dissolution and its implication on *in vivo* performance in rats.

3) In Chapter 3, novel cellulose derivatives with varying effectiveness of inhibiting crystallization of drug were prepared as ASDs. Their performance was compared to the model compound commercial formulation in rats.

4) Chapter 4 investigates the drug-polymer interactions and the polymer's ability to inhibit crystallization in systems that have undergone GLPS.
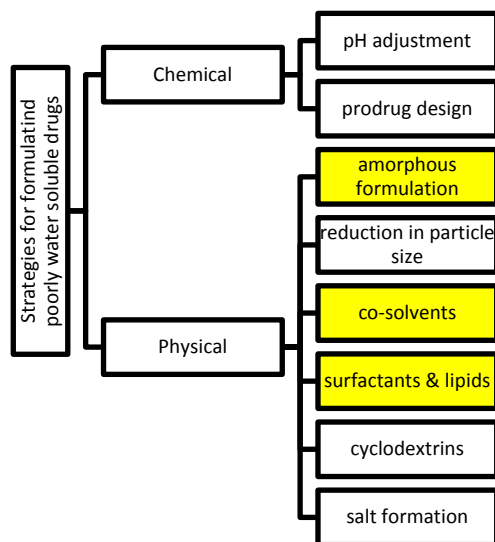
Figure 1-1. Adapted from Rodriguez-Aller *et al*[2]. The types of enabling formulations, formulations which increase the solubility of poorly aqueous soluble compounds. The boxes highlighted in yellow are formulation techniques investigated in this study.
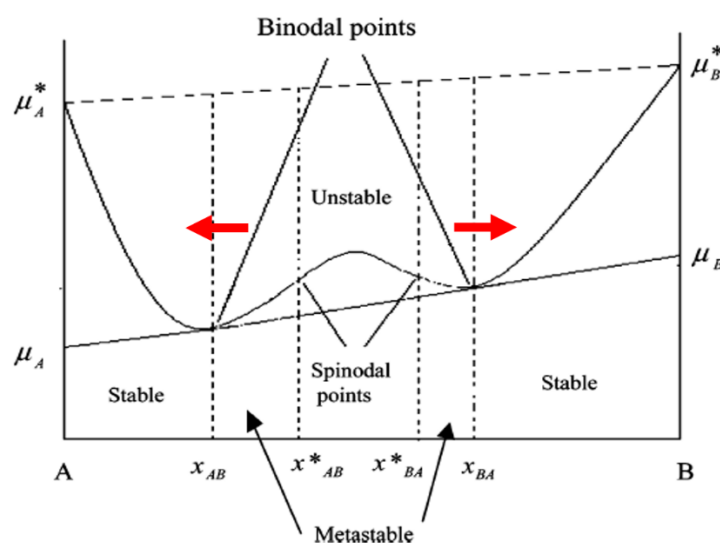
Figure 1-2. Addition of drug at a concentration much beyond the amorphous solubility results in a highly unstable system. To compensate for the instability, LLPS or GLPS occurs to shift the system from unstable to a stable region (with respect to LLPS), indicated by the red arrows. It should be noted that the system is still metastable with respect to the crystalline phase. Figure adapted from Deneau and Steele[18].
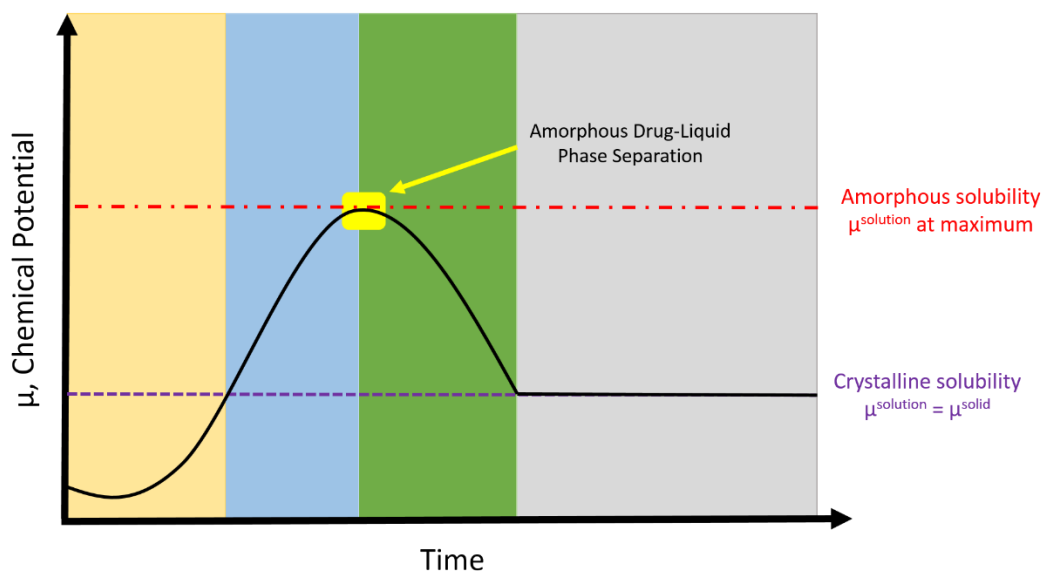
Figure 1-3. Chemical potential versus time plot depicts the various phase changes that occur in under and supersaturated solutions. 1) Orange: undersaturated solution, 2) Blue: supersaturated solution, 3) Yellow box: amorphous precipitate forms in solution, 4) Green: crystallization, 5) Gray: solution in equilibrium
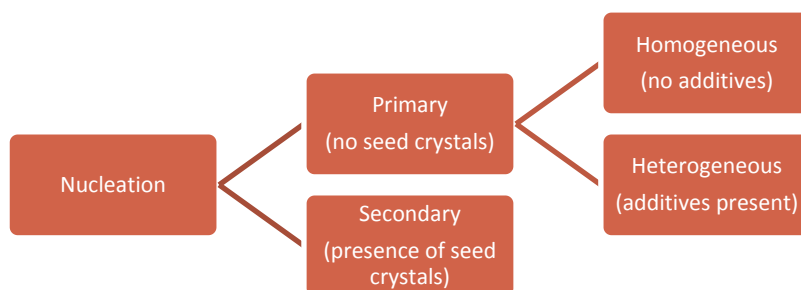
Figure 1-4. Based upon the crystallization environment, there are different nucleation processes that can occur. Figure adapted from Mullin[11].
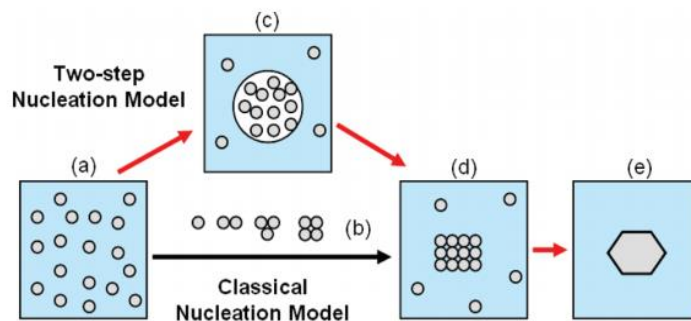
Figure 1-5. Figure taken from Erdemir *et al*[26]. Pathway for classical nucleation theory: a) supersaturated solution, b) ordered clusters of the drug molecule, d) stable nuclei formed, and e) crystal formation. Pathway for two step nucleation: a) supersaturated solution, c) liquid-like cluster, d) stable nuclei formed, and e) crystal formation.
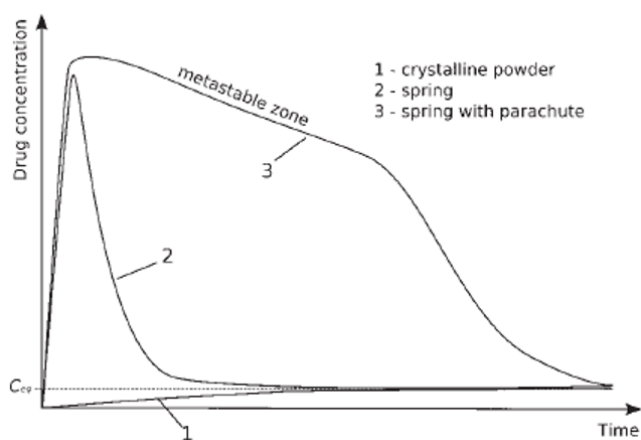
Figure 1-6. Taken from Brouwers *et al*[39]. The solubility advantage of an amorphous solid dispersion versus amorphous drug versus crystalline drug.
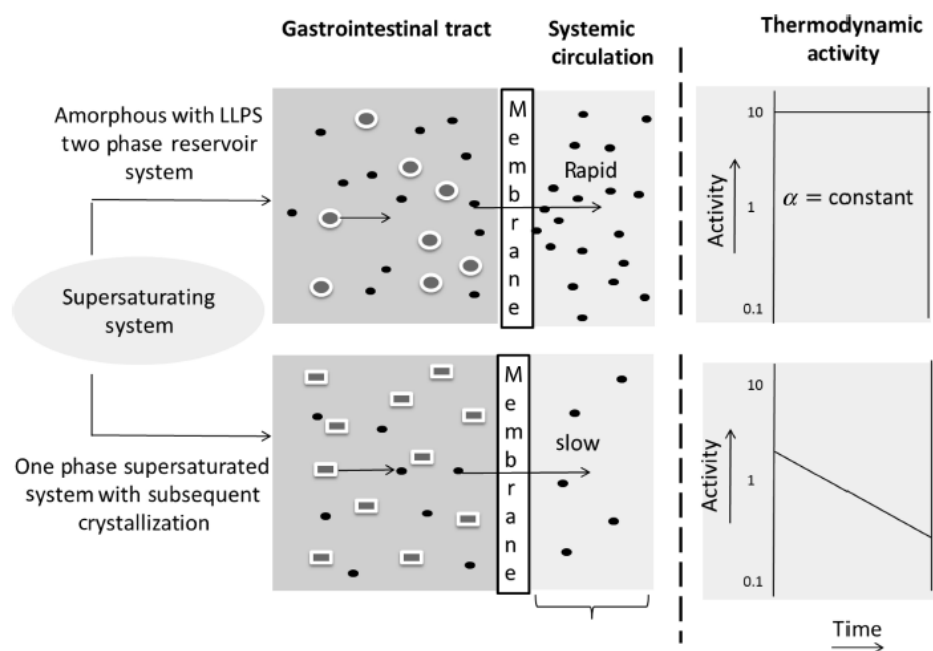
Figure 1-7. Figure taken from Raina et al[19]. The top figure depicts the mass flowrate and activity of a system in which LLPS has occurred; the bottom figure depicts the mass flowrate and activity of a supersaturated solution in which LLPS hasn't occurred and when crystallization occurs.

1.8 References

[1] I. E. Shohin, D. Y. Grebenkin, E. A. Malashenko, Y. M. Stanishevskii, and G. V. Ramenskaya, "A brief review of the FDA dissolution methods database," *Dissolution Technologies*. 2016.

[2] M. Rodriguez-Aller, D. Guillarme, J. L. Veuthey, and R. Gurny, "Strategies for formulating and delivering poorly water-soluble drugs," *J. Drug Deliv. Sci. Technol.*, vol. 30, pp. 342–351, 2015.

[3] S. A. Charman, W. N. Charman, M. C. Rogge, T. D. Wilson, F. J. Dutko, and C. W. Pouton, "Self-Emulsifying Drug Delivery Systems: Formulation and Biopharmaceutic Evaluation of an Investigational Lipophilic Compound," *Pharm. Res. An Off. J. Am. Assoc. Pharm. Sci.*, 1992.

[4] Y.-Y. Tseng and S.-J. Liu, "Nanofibers used for the delivery of analgesics," *http://dx.doi.org/10.2217/nnm.15.23*, 2015.

[5] C. Ding, M. Zhang, and G. Li, "Rheological properties of collagen/hydroxypropyl methylcellulose (COL/HPMC) blended solutions," *J. Appl. Polym. Sci.*, vol. 131, no. 7, p. n/a-n/a, Apr. 2014.

[6] F. Tajarobi, A. Larsson, H. Matic, and S. Abrahmsén-Alami, "The influence of crystallization inhibition of HPMC and HPMCAS on model substance dissolution and release in swellable matrix tablets," *Eur. J. Pharm. Biopharm.*, vol. 78, no. 1, pp. 125–133, 2011.

[7] B. Volker, *Polyvinylpyrrolidone Excipients for Pharmaceuticals*. Berlin/Heidelberg: Springer-Verlag, 2005.

[8] D. Ben-Amotz, *Understanding Physical Chemistry*. Chennai: John Wiley & Sons, 2014.

[9] A. S. Myerson, *Handbook of Industrial Crystallization*, 2nd ed. Woburn: Butterworth-Heinemann, 2002.

[10] J. W. Mullin, *Crystallization*. Oxford: Butterworth-Heinemann, 2001.

[11] L. Almeida e Sousa, S. M. Reutzel-Edens, G. A. Stephenson, L. S. Taylor, L. Almeida e. Sousa, S. M. Reutzel-Edens, G. A. Stephenson, and L. S. Taylor, "Assessment of the Amorphous 'Solubility' of a Group of Diverse Drugs Using New Experimental and Theoretical Approaches," *Mol Pharm*, vol. 12, no. 2, pp. 484–495, 2014.

[12] G. A. Ilevbare and L. S. Taylor, "Liquid–Liquid Phase Separation in Highly Supersaturated Aqueous Solutions of Poorly Water-Soluble Drugs: Implications for Solubility Enhancing Formulations," *Cryst. Growth Des.*, vol. 13, no. 4, pp. 1497–1509, Apr. 2013.

[13] B. C. Hancock and M. Parks, "What is the true solubility advantage for amorphous pharmaceuticals?," *Pharm. Res.*, vol. 17, no. 4, pp. 397–404, 2000.

[14] P. E. Bonnett, K. J. Carpenter, S. Dawson, and R. J. Davey, "Solution crystallisation via a submerged liquid–liquid phase boundary: oiling out," *Chem. Commun.*, no. 6, pp. 698–699, 2003.

[15] J. D. Hoffman, "Thermodynamic driving force in nucleation and growth processes," *J. Chem. Physics1*, vol. 29, no. 5, pp. 1192–1193, 1958.

[16] R. H. Bogner, S. B. Murdande, M. J. Pikal, and R. M. Shanker, "Solubility advantage of amorphous pharmaceuticals: II. application of quantitative thermodynamic relationships for prediction of solubility enhancement in structurally diverse insoluble pharmaceuticals," *Pharm. Res.*, vol. 27, no. 12, pp. 2704–2714, 2010.

[17] L. I. Mosquera-Giraldo and L. S. Taylor, "Glass−Liquid Phase Separation in Highly Supersaturated Aqueous Solutions of Telaprevir," *Mol. Pharm.*, vol. 12, no. 2, pp. 496–503, 2015.

[18] E. Deneau and G. Steele, "An in-line study of oiling out and crystallization," *Org. Process Res. Dev.*, vol. 9, no. 6, pp. 943–950, 2005.

[19] S. A. Raina, G. G. Z. Zhang, D. E. Alonzo, J. Wu, D. Zhu, N. D. Catron, Y. Gao, and L. S. Taylor, "Enhancements and limits in drug membrane transport using supersaturated solutions of poorly water soluble drugs," *J. Pharm. Sci.*, vol. 103, no. 9, pp. 2736–2748, 2014.

[20] P. J. Sassene, M. M. Knopp, J. Z. Hesselkilde, V. Koradia, A. Larsen, T. Rades, and A. MüLlertz, "Precipitation of a poorly soluble model drug during in vitro lipolysis: Characterization and dissolution of the precipitate," *J. Pharm. Sci.*, 2010.

[21] D. Erdemir, A. Y. Lee, and A. S. Myerson, "Nucleation of crystals from solution: Classical and two-step models," *Acc. Chem. Res.*, vol. 42, no. 5, pp. 621–629, 2009.

[22] R. W. Balluffi, S. M. Allen, and W. C. Carter, *Kinetics of Materials*. 2005.

[23] S. Xie, S. K. Poornachary, P. S. Chow, and R. B. H. Tan, "Direct precipitation of micron-size salbutamol sulfate: New insights into the action of surfactants and polymeric additives," *Cryst. Growth Des.*, vol. 10, no. 8, pp. 3363–3371, 2010.

[24] E. Y. Kramarenko, R. G. Khokhlov, P. G. Winkler, A. R. Reineker, and P. Khalatur, "Molecular dynamics simulation study of adsorption of polymer chains with variable degree," *J. Chem. Phys.*, pp. 4806–4813, 1996.

[25] G. A. Ilevbare, H. Liu, J. Pereira, K. J. Edgar, and L. S. Taylor, "Influence of Additives on the Properties of Nanodroplets Formed in Highly Supersaturated Aqueous Solutions of Ritonavir," 2013.

[26] Y. Yani, P. S. Chow, and R. B. H. Tan, "Molecular simulation study of the effect of various additives on salbutamol sulfate crystal habit," *Mol. Pharm.*, vol. 8, no. 5, pp. 1910–1918, 2011.

[27] G. A. Ilevbare, H. Liu, K. J. Edgar, and L. S. Taylor, "Impact of polymers on crystal growth rate of structurally diverse compounds from aqueous solution," *Mol. Pharm.*, vol. 10, no. 6, pp. 2381–2393, 2013.

[28] M. Yoshioka, B. C. Hancock, and G. Zografi, "Crystallization of indomethacin from the amorphous state below and above its glass transition temperature," *J. Pharm. Sci.*, 1994.

[29] B. C. Hancock, S. L. Shamblin, and G. Zografi, "Molecular Mobility of Amorphous Pharmaceutical Solids Below Their Glass Transition Temperatures," *Pharm. Res. An Off. J. Am. Assoc. Pharm. Sci.*, 1995.

[30] W. Tu, Y. Wang, X. Li, P. Zhang, Y. Tian, S. Jin, and L. M. Wang, "Unveiling the dependence of glass transitions on mixing thermodynamics in miscible systems," *Sci. Rep.*, 2015.

[31] P. J. Marsac, T. Li, and L. S. Taylor, "Estimation of drug-polymer miscibility and solubility in amorphous solid dispersions using experimentally determined interaction parameters," *Pharm. Res.*, vol. 26, no. 1, pp. 139–151, 2009.

[32] P. J. Flory, *Principles of Polymer Chemistry*. Ithaca: Cornell University Press, 1953.

[33] S. Thakral and N. K. Thakral, "Prediction of drug-polymer miscibility through the use of solubility parameter based flory-huggins interaction parameter and the experimental validation: PEG as model polymer," *J. Pharm. Sci.*, vol. 102, no. 7, pp. 2254–2263, 2013.

[34] C. M. Hansen, *Hansen Solubility Parameters*. Boca Raton: Taylor & Francis Group, 2007.

[35] K. L. Hoy, "New values of the solubility parameters from vapor pressure data," *J. Paint Technol.*, vol. 42, no. 541, pp. 76–118, 1970.

[36] R. F. Fedors, "A method for estimating both the solubility parameters and molar volumes of liquids," *Polym. Eng. Sci.*, 1974.

[37] R. H. Müller, G. E. Hildebrand, R. Nitzsche, and B.-R. Paulke, "Zetapotential und Partikelladung in der Laborpraxis," *Paperb. APV*, vol. 37, 1996.

[38] C. K. Y. Yiu, N. M. King, D. H. Pashley, B. I. Suh, R. M. Carvalho, M. R. O. Carrilho, and F. R. Tay, "Effect of resin hydrophilicity and water storage on resin strength," *Biomaterials*, vol. 25, no. 26, pp. 5789–5796, 2004.

[39] L. I. Mosquera-Giraldo, C. H. Borca, X. Meng, K. J. Edgar, L. V. Slipchenko, and L. S. Taylor, "Mechanistic Design of Chemically Diverse Polymers with Applications in Oral Drug Delivery," *Biomacromolecules*, vol. 17, no. 11, pp. 3659–3671, 2016.

[40] H. Konno, T. Handa, D. E. Alonzo, and L. S. Taylor, "Effect of polymer type on the dissolution profile of amorphous solid dispersions containing felodipine," *Eur. J. Pharm. Biopharm.*, vol. 70, no. 2, pp. 493–499, 2008.

[41] A. C. Rumondor and L. S. Taylor, "Effect of polymer hygroscopicity on the phase behavior of amorphous solid dispersions in the presence of moisture," *Mol. Pharm.*, vol. 7, no. 2, pp. 477–490, 2010.

[42] H. S. Purohit and L. S. Taylor, "Phase separation kinetics in amorphous solid dispersions upon exposure to water," *Mol. Pharm.*, vol. 12, no. 5, pp. 1623–1635, 2015.

[43] N. Li, J. D. Ormes, and L. S. Taylor, "Leaching of Lopinavir Amorphous Solid Dispersions in Acidic Media," *Pharm. Res.*, vol. 33, no. 7, pp. 1723–1735, 2016.

[44] J. Brouwers, M. E. Brewster, and P. Augustijns, "Supersaturating drug delivery systems: The answer to solubility-limited oral bioavailability?," *Journal of Pharmaceutical Sciences*, vol. 98, no. 8. pp. 2549–2572, 2009.

[45] D. E. Alonzo, Y. Gao, D. Zhou, H. Mo, G. G. Z. Z. Zhang, and L. S. Taylor, "Dissolution and precipitation behavior of amorphous solid dispersions," *J. Pharm. Sci.*, vol. 100, no. 8, pp. 3316–3331, 2011.

[46] M. J. Jackson, U. S. Kestur, M. A. Hussain, and L. S. Taylor, "Dissolution of Danazol Amorphous Solid Dispersions: Supersaturation and Phase Behavior as a Function of Drug Loading and Polymer Type," *Mol. Pharm.*, 2016.

[47] N. S. Trasi and L. S. Taylor, "Dissolution performance of binary amorphous drug combinations - Impact of a second drug on the maximum achievable supersaturation," *Int. J. Pharm.*, 2015.

[48] T. Xie and L. S. Taylor, "Dissolution Performance of High Drug Loading Celecoxib Amorphous Solid Dispersions Formulated with Polymer Combinations," *Pharm. Res.*, vol. 33, no. 3, pp. 739–750, 2016.

[49] O. I. Corrigan, "Mechanisms of dissolution of fast release solid dispersions," *Drug Dev. Ind. Pharm.*, 1985.

[50] M. E. Matteucci, B. K. Brettmann, T. L. Rogers, E. J. Elder, R. O. Williams, and K. P. Johnston, "Design of potent amorphous drug nanoparticles for rapid generation of highly supersaturated media," *Mol. Pharm.*, 2007.

[51] T. Tachibana and A. Nakamura, "A methode for preparing an aqueous colloidal dispersion of organic materials by using water-soluble polymers: Dispersion ofB-carotene by polyvinylpyrrolidone," *Kolloid-Zeitschrift Zeitschrift für Polym.*, vol. 203, no. 2, pp. 130–133, Jun. 1965.

[52] L. I. Mosquera-Giraldo, N. Li, V. R. Wilson, B. L. B. Nichols, K. J. Edgar, and L. S. Taylor, "Influence of Polymer and Drug Loading on the Release Profile and Membrane Transport of Telaprevir," *Mol. Pharm.*, vol. 15, no. 4, pp. 1700–1713, Apr. 2018.

[53] N. Li and L. S. Taylor, "Tailoring supersaturation from amorphous solid dispersions," *J. Control. Release*, vol. 279, pp. 114–125, 2018.

[54] A. Elkhabaz, S. Sarkar, J. K. Dinh, G. J. Simpson, and L. S. Taylor, "Variation in Supersaturation and Phase Behavior of Ezetimibe Amorphous Solid Dispersions upon Dissolution in Different Biorelevant Media," *Mol. Pharm.*, 2018.

[55] A. S. Indulkar, J. E. Waters, H. Mo, Y. Gao, S. A. Raina, G. G. Z. Zhang, and L. S. Taylor, "Origin of Nanodroplet Formation Upon Dissolution of an Amorphous Solid Dispersion: A Mechanistic Isotope Scrambling Study," *J. Pharm. Sci.*, vol. 106, no. 8, pp. 1998–2008, 2017.

[56] P. Harmon, K. Galipeau, W. Xu, C. Brown, and W. P. Wuelfing, "Mechanism of Dissolution-Induced Nanoparticle Formation from a Copovidone-Based Amorphous Solid Dispersion," *Mol. Pharm.*, 2016.

[57] A. S. Indulkar, Y. Gao, S. A. Raina, G. G. Z. Zhang, and L. S. Taylor, "Exploiting the Phenomenon of Liquid-Liquid Phase Separation for Enhanced and Sustained Membrane Transport of a Poorly Water-Soluble Drug," *Mol. Pharm.*, vol. 13, no. 6, pp. 2059–2069, 2016.

[58] P. A. SHORE, B. B. BRODIE, and C. A. HOGBEN, "The gastric secretion of drugs: a pH partition hypothesis.," *J. Pharmacol. Exp. Ther.*, vol. 119, no. 3, pp. 361–369, 1957.

[59] R. Lledó-García, A. Nácher, L. Prats-García, V. G. Casabó, and M. Merino-Sanjuán, "Bioavailability and pharmacokinetic model for ritonavir in the rat," *J. Pharm. Sci.*, 2007.

[60] D. Law, E. A. Schmitt, K. C. Marsh, E. A. Everitt, W. Wang, J. J. Fort, S. L. Krill, and Y. Qiu, "Ritonavir-PEG 8000 Amorphous Solid Dispersions: In Vitro and in Vivo Evaluations," *J. Pharm. Sci.*, vol. 93, no. 3, pp. 563–570, 2004.

[61] W. L. Hayton, "Rate-limiting barriers to intestinal drug absorption: A review," *J. Pharmacokinet. Biopharm.*, vol. 8, no. 4, pp. 321–334, Aug. 1980.

[62] S. A. Raina, G. G. Z. Zhang, D. E. Alonzo, J. Wu, D. Zhu, N. D. Catron, Y. Gao, and L. S. Taylor, "Impact of Solubilizing Additives on Supersaturation and Membrane Transport of Drugs," *Pharm. Res.*, vol. 32, no. 10, pp. 3350–3364, 2015.

[63] W. I. Higuchi and T. Higuchi, "Theoretical Analysis of Diffusional Movement Through Heterogeneous Barriers**University of Wisconsin, S-hool of Pharmacy, hladison 6," *J. Am. Pharm. Assoc. (Scientific ed.)*, vol. 49, no. 9, pp. 598–606, 1960.

[64] N. S. Trasi and L. S. Taylor, "Thermodynamics of Highly Supersaturated Aqueous Solutions of Poorly Water-Soluble Drugs - Impact of a Second Drug on the Solution Phase Behavior and Implications for Combination Products," *J. Pharm. Sci.*, vol. 104, no. 8, pp. 2583–2593, 2015.

[65] FDA, "Guidance for Industry Extended Release Oral Dosage Forms: Development, Evaluation, and Application of In Vitro/In Vivo Correlations U.S.," *Evaluation*. 1997.

CHAPTER 2.   RELATIONSHIP BETWEEN AMORPHOUS SOLID DISPERSION IN VIVO ABSORPTION AND IN VITRO DISSOLUTION: PHASE BEHAVIOR DURING DISSOLUTION, SPECIATION, AND MEMBRANE MASS TRANSPORT

2.1   Abstract

Enzalutamide is a fast crystallizing, hydrophobic compound that has solubility limited absorption *in vivo*. Given the low aqueous solubility of this compound, it was of interest to evaluate amorphous formulations *in vitro* and *in vivo*. Amorphous solid dispersions (ASD) of enzalutamide were prepared with the hydrophilic polymers, hydroxypropyl methylcellulose acetate succinate (HPMCAS) and copovidone (PVPVA). A side-by-side diffusion cell was developed as an *in vitro* characterization tool to discriminate enzalutamide ASDs based upon the solute thermodynamic activity achieved during dissolution and its impact on the subsequent membrane transport rates, phase behavior, and drug speciation. The same formulations were then tested *in vivo* in rats using oral dosing of ASD suspensions. Different levels of plasma exposure were observed between the ASDs, which could be correlated to the phase behaviors of the ASDs following dissolution. Unsurprisingly, ASDs that underwent crystallization show lower plasma exposures. However, differences were also observed between ASDs that dissolved to form nanosized amorphous drug aggregates versus those that dissolved to yield only supersaturated solutions, with the former outperforming the latter in terms of the plasma exposure. These observations highlight the importance of thoroughly understanding the phase behavior of an amorphous formulation following dissolution and the need to discriminate between different types of precipitation, specifically crystallization versus glass liquid phase separation to form nanosized amorphous aggregates.

2.2   Introduction

The majority of new molecular entities in the drug development pipeline have poor water solubility[1]. This, in combination with the fact that the majority of patients prefer orally dosed formulations, presents a challenge for formulators[2–4] . There are several different enabling formulation strategies including salt formation, complexation with cyclodextrins, self-emulsifying drug delivery systems, and amorphous solid dispersions, all of which can increase solubility and

subsequently bioavailability[5,6]. Amorphous solid dispersions (ASD) are of particular interest since this formulation approach does not involve chemical changes to the compound, yields a solid formulation, and, for some drugs, the amorphous material can provide a solubility advantage over the crystalline form of several-fold [7–11].

An amorphous solid dispersion is ideally a homogeneous mixture of amorphous drug with a hydrophilic polymer. Because the drug in the dispersion is generally in a higher energy state than its crystalline counterpart (the exception being when the drug is below its solubility limit in the polymer), crystallization can occur in the dispersion upon storage. Crystallization can also take place during dissolution, either in the hydrated matrix or from the supersaturated solution generated by dissolution of the ASD under non-sink conditions. An additional phase separation phenomenon that can occur in aqueous media during ASD dissolution is glass-liquid phase separation (GLPS) or liquid-liquid phase separation (LLPS) [12–15]. This phase transformation occurs when the amorphous solubility (the highest free drug concentration that can be achieved in solution) is exceeded and (if crystallization is avoided) water-saturated colloidal amorphous drug aggregates form in solution[12,15]. The colloidal drug aggregates exist in metastable equilibrium with the supersaturated solution until crystallization occurs. If the hydrated amorphous drug has a glass transition temperature (T_g) that is above the operating temperature, then this process is termed glass-liquid phase separation, while for systems below the T_g, the process is liquid-liquid phase separation. Raina *et al.* proposed that these amorphous aggregates would be advantageous for oral delivery since they could act as a depot and replenish drug that is absorbed *in vivo*[13], thus maintaining the supersaturation at an optimized level. Indulkar *et al* demonstrated the reservoir effect in an *in vitro* membrane transport study[16]. However, there is little *in vivo* data to support this supposition.

The goal of the current study was to extend these previous *in vitro* studies and determine the role of ASD formulation performance in terms of potential for amorphous aggregate formation on *in vivo* absorption. The model drug employed was enzalutamide (Figure 2-1), which is indicated for use in castration resistant prostate cancer[17]. Enzalutamide is a Biopharmaceutics Classification System (BCS) class II compound and exhibits solubility limited absorption. The commercial product is Xtandi®, a lipid based formulation in a soft gel capsule. ASDs of enzalutamide were

formulated with copovidone (PVPVA) and hydroxypropyl methylcellulose acetate succinate (HPMCAS) (Figure 2-1), two of the most common polymers used in commercial ASD formulations[8,11]. A side-by-side diffusion cell was then used to evaluate the mass flow profiles for of various ASDs following dissolution. The tendency of the ASDs to undergo glass-liquid phase separation (GLPS) was also probed. Subsequently, these ASDs were dosed to rats to evaluate the *in vivo* exposure profiles, and correlations were sought between *in vitro* behavior and *in vivo* performance.

2.3   Materials & Methods

2.3.1   Materials

Enzalutamide (Enz) was purchased from ChemShuttle (Hayward, California). Methanol and dichloromethane were obtained from Fisher Scientific (Hampton, New Hampshire). 4-4-diethylaminostryrl-N-methylpyridinium (4-Di-2-Asp) was purchased from Life Technologies (Grand Island, New York) and Nile Red from Sigma Aldrich (St. Louis, Missouri). Kollidon VA64, also called copovidone, (PVPVA) and hydroxypropyl methylcellulose acetate succinate MF grade (HPMCAS-MF) were obtained from BASF (Ludwigshaven,Germany) and Shin-Etsu Co. Ltd (Tokyo, Japan), respectively. The molecular structures of the drug and polymers are shown in Figure 2-1. Spectra/ Por 1 (regenerated cellulose membrane MW cutoff: 6-8 kD) was purchased from Spectrum Laboratories Inc., (Rancho Dominguez, CA). Male Sprague-Dawley rats were obtained from Charles River Laboratories (Wilmington, MA).

2.3.2   Methods

2.3.2.1   Crystalline Solubility Measurements

Triplicate samples containing an excess amount of crystalline enzalutamide in 50 mM phosphate buffer pH 6.5, 37°C were stirred for 48 hours. The undissolved solid was separated from the supernatant by ultracentrifugation at 35,000 rpm for 15 minutes in an Optima L-100 XP Ultracentrifuge (Beckman Coulter, Inc., Brea, California). The enzalutamide concentration in the supernatant was analyzed using an Agilent 1260 Infinity high performance liquid chromatography (HPLC) system (Santa Clara, California). The HPLC method used was 20.0 µL injection volume with an Agilent ZORBAX Eclipse Plus C18 5 µm 4.6 x 150 mm column (Agilent Technologies,

Santa Clara, California). The sample was eluted using a mobile phase composed of 60% methanol and 40% water by volume at a 0.75 mL/min flowrate. An ultraviolet (UV) detector at a wavelength of 237 nm was used. A calibration curve was constructed over the concentration range of 500 ng/mL–20 mg/mL of enzalutamide. A good linear fit weighted with $1/x^2$ was achieved with an R^2 value of 0.9902.

2.3.2.2   Experimental Amorphous Solubility Measurements

The amorphous solubility was determined by two techniques: fluorescence spectroscopy using an environment sensitive probe and ultraviolet (UV) extinction[12,13,18].

2.3.2.2.1   Fluorescence Spectroscopy

A solution of 2 µg/mL 4-Di-2-Asp in 50 mM phosphate buffer pH 6.5 was prepared and equilibrated at 37°C. Enzalutamide stock solution (10 mg/mL in methanol) was added to the buffer with stirring at 300 rpm to generate enzalutamide concentrations ranging from 10-65 µg/mL. Fluorescence emission spectra were acquired 10 seconds after the addition of enzalutamide using a Shimadzo RF-5301 PC Spectrofluorophotometer (Kyoto, Japan). The excitation wavelength was 488 nm, excitation slit width was 20 nm, emission slit width was 3 nm, and a sampling interval of 0.2 nm was used. A notable blue shift in the emission peak spectrum was used to determine the amorphous solubility.

2.3.2.2.2   Ultraviolet Extinction

A 10 mg/mL stock solution of enzlutamide was continuously added to 50 mM pH 6.5 phosphate buffer at a rate of 35 µL/min using a KD Scientific Legato 200 Syringe Pump (Holliston, MA). This experiment was also performed in the presence of 900 µg/mL of polymer pre-dissolved in buffer to determine if the polymer impacted the amorphous solubility. The solution was maintained at 37°C and stirred at 300 rpm. The extinction at 445 nm was monitored using a SI Photonic UV Spectrophotometer (Tucson, Arizona) with a 0.5cm dip probe. Experiments were performed in triplicate.

2.3.2.3   Differential Scanning Calorimetry

Thermal analysis was performed using a TA Instruments DSC Q2000 (New Castle, Delaware) analyzing 4-5 mg of enzalutamide in Tzero aluminum pans with hermetically sealed Tzero

aluminum lids (TA Instruments, New Castle, Delaware). The differential scanning calorimetry (DSC) was calibrated for enthalpy and temperature using indium and tin. The melting point and glass transition temperature were determined by heating the sample at a rate of 10°Cmin^{-1} to approximately 2°C above the melting point, rapidly cooling at a rate of 20°Cmin^{-1} to 0°C followed by re-heating at a rate of 10°Cmin^{-1} to 20°C below the melting point. Samples were analyzed in triplicate.

2.3.2.4 Moisture Sorption of Amorphous Enzalutamide

The moisture sorption isotherm of amorphous enzalutamide was measured using a gravimetric analyzer (SGA-100, VTI Corporation, Hialeah, FL). 4-5 mg of amorphous enzalutamide was exposed to increasing relative humidity (RH) from 5% to 95%. Samples were dried prior to RH exposure. The drying equilibrium criterion was 0.01% w/w change within 5 minutes with a maximum drying time of 3 hours. The maximum equilibration time for each RH step was 3 hours with a similar equilibrium criterion as for drying. Samples were analyzed in triplicate.

2.3.2.5 Theoretical Amorphous Solubility

The theoretical amorphous solubility of enzalutamide was determined by applying the Hoffman equation[19] to estimate the free energy difference between the amorphous and crystalline forms of the drug (ΔG_{a-c}).

$$\Delta G_{a \rightarrow c} = \frac{\Delta H_f (T_m - T)T}{(T_m)^2} \quad (2\text{-}1)$$

Where ΔH_f is the enthalpy of fusion, T_m is the melting temperature, and T is the experimental temperature. The amorphous solubility was then estimated using the approach proposed by Murdande[20]:

$$C_{amorphous} = C_{eq} \times \exp[-I(a_2)] \times \exp\left[\frac{\Delta G_c}{RT}\right] \quad (2\text{-}2)$$

Where ΔGc is the calculated free energy difference, R is the universal gas constant, T is the experimental temperature,, C_{eq} is the equilibrium solubility of the crystal, and, *exp([-I(a₂)])* is a term that describes the activity of the water-saturated amorphous drug, and is estimated from the water sorption profile.

2.3.2.6   Mass of Enzalutamide Aggregates Generated During Glass-Liquid Phase Separation

2.3.2.6.1   Ultracentrifugation

Samples of enzalutamide in pH 6.5 phosphate buffer (12 mL) containing a known concentrations of drug above the amorphous solubility (ranging from 45 µg/mL to 100 µg/mL) were prepared. A concentrated stock solution of 10 mg/mL enzalutamide in methanol was used to prepare the aqueous solutions. The samples were centrifuged as described above. The supernatant was discarded and the amorphous pellet was dried for 2 days at 5 mm Hg in a vacuum oven. The mass of the dried pellet was determined using a Mettler Toledo XS105 DualRange Analytical Balance (Mettler Toledo, Columbus, Ohio). Experiments were performed in triplicate.

2.3.2.6.2   Fluorescence Spectroscopy

12 mL samples of enzalutamide (ranging from 45 µg/mL to 100 µg/mL) in 2 µg/mL Nile Red in phosphate buffer were prepared. The samples were vortexed for 5 seconds prior to taking a measurement. The fluorescence emission spectrum was determined on a Shimadzo RF-5301 PC Spectrofluorophotometer (Kyoto, Japan) at an excitation wavelength of 520 nm with a sampling interval of 0.2nm and excitation slit width of 3 nm and emission slit width of 10 nm. This was performed in triplicate.

2.3.2.7   Amorphous Solid Dispersion Performance

2.3.2.7.1   Formulation Preparation.

Amorphous solid dispersions (ASD) were prepared by rotary evaporation. Two drug loadings were prepared: 10 and 50 wt. % drug using either PVPVA or HPMCAS-MF as the ASD polymer. For PVPVA dispersions the solvent system was 50:50 dichloromethane:methanol (v/v) while for HPMCAS dispersions, a 75:25 dichloromethane:acetone (v/v) mixture was used. The solvent was rapidly removed using rotary evaporation on a Buchi Rotovapor R-215 (New Castle, Delaware) with a water bath temperature of 30ºC until a solid formed in the vial at which point the temperature was increased to 40ºC. Samples were stored for 12 hours under 5 mm Hg vacuum to remove any residual solvent. Upon removal from the vacuum oven, ASDs were ground to fine powder using a mortar and pestle.

2.3.2.7.2   Amorphous Solid Dispersion Dissolution.

ASD dissolution experiments were performed in triplicate. The concentration of enzalutamide was monitored *in situ* using a UV dip probe (pION μDiss, Pion Inc., Billerica, MA). The total concentration of enzalutamide added to solution was 100 μg/mL in 12.5 mL of pH 6.5 phosphate buffer. Samples were stirred at 300 rpm at 37°C.

2.3.2.7.3   Amorphous Solid Dispersion Dissolution in the Presence of an Environment Sensitive Fluorescence Probe

A solution containing 2 μg/mL of Nile Red in pH 6.5 phosphate buffer was prepared by adding a small amount of a concentrated solution of Nile Red in methanol to the buffer. The amount of ASD subsequently added to this solution was such that, if all solids dissolve, the final enzalutamide concentration is 100 μg/mL. After 1 hour of dissolution, 2 mL samples were removed and filtered using a 1.0 μm Tisch Glass Fiber Syringe Filter (North Bend, Ohio) to remove undissolved ASD particles. The filtrate was then excited at 520 nm on Shimadzo RF-5301 PC Spectrofluorophotometer and the emission spectrum was collected with an excitation slit width of 5 nm and emission slit width of 5 nm. Analysis was performed in triplicate.

2.3.2.7.4   Characterization of Enzalutamide Speciation for Amorphous Solid Dispersions to be Dosed as Suspension to Rats.

ASD dissolution was performed for 1 hour in pH 6.5 buffer containing 2 μg/mL Nile Red, stirring at 300 rpm at room temperature (22°C±2°C). 2 mL samples were removed and filtered using a 5.0 μm Whatman PVDF Syringe Filter (Maidstone, United Kingdom) pre-saturated by initially filtering 10 mL of a 40 μg/mL enzalutamide solution containing 5 μg/mL HPMCAS. 10 μL of the ASD filtrate was added to 1.990 mL of 40 μg/mL enzalutamide with 5 μg/mL HPMCAS and 2 μg/mL of Nile Red in pH 6.5 50 mM phosphate buffer. This solution was used to dilute the filtrate since the signal of the undiluted sample was too high for the detector. The diluent solution contained dissolved enazalutamide at approximately the amorphous solubility to prevent dissolution of amorphous aggregates formed during ASD dissolution and contained HPMCAS to prevent rapid crystallization. The quantity of aggregates was estimated from the intensity of Nile Red fluorescence peak, and knowledge of the amount of ASD added to the dissolution medium and the amorphous solubility. The speciation was then estimated in terms of the amount of

molecularly dissolved drug, colloidal species and residual solid enzalutamide (either undissolved ASD, aggregates that have undergone agglomeration or crystallized material larger than 5µm).

2.3.2.8 Mass Flow Rate Measurements

2.3.2.8.1 Supersaturated Enzalutamide Solutions

The mass flow rate was measured using a PermeGear Side-by-Side Diffusion Cell (Hellertown, Pennsylvania) with a regenerated cellulose dialysis membrane (Spectra/ Por 1, Spectrum Laboratories Inc., Rancho Dominguez, California) separating the donor and receiver compartment. The orifice diameter was 30mm. 30 mL buffer containing 5 µg/mL HPMCAS (to prevent crystallization) was added to each compartment. Supersaturated solutions of enzalutamide were generated in the donor compartment by adding aliquots of a concentrated methanol solution of enzalutamide. The total methanol concentration was less than 1% and an equal amount of methanol was added to the receiver compartment. Aliquots of 75 µL were taken every 5 minutes from the receiver compartment and analyzed using the HPLC method described above. The mass flow rate was determined from the slope of a concentration versus time plot. Experiments were performed in triplicate.

2.3.2.8.2 Mass Flow Rate Measurements for Solutions Derived from Amorphous Solid Dispersion Dissolution

ASDs were stirred in approximately 30 mL of pH 6.5 phosphate buffer for 1 hour prior to being placed in the donor compartment. The receiver compartment contained the same volume of pH 6.5 phosphate buffer as the donor compartment. Aliquots (75 µL) were taken every 5 minutes from the receiver compartment and analyzed via HPLC using the method described above.
The mass flow rate (dm/dt) was determined from the slope of a concentration versus time plot. The flux (J) can then be calculated by dividing the mass flow rate by the membrane surface area (A):

$$J = \frac{dm}{dt \times A} \qquad (2\text{-}3)$$

The flux is directly proportional to the thermodynamic activity of the drug in solution:

$$J = \frac{Da}{h\gamma_m} \qquad (2\text{-}4)$$

Where D is the solute diffusivity, a is the activity of the drug in solution, h is the thickness of the membrane , and γ_m is the activity coefficient of the drug in the membrane. All terms, with the

exception of *a*, are assumed to be constants for a given experimental set-up[21,22]. Thus, the mass flowrate can be related to thermodynamic activity of the drug in solution:

$$\frac{dm}{dt \times A} = \frac{Da}{h\gamma_m} \qquad (2\text{-}5)$$

Hence, the enzalutamide thermodynamic activity in the donor compartment of the diffusion cell can be inferred from the measured mass flowrate. Experiments were performed in triplicate.

2.3.2.9   Rat Studies

Male Sprague-Dawley rats were administered ASD suspensions by oral gavage at a dose volume of 10 mL/kg. Animals were allowed free access to food and water prior to and during dosing. Serial blood samples were collected into K_2EDTA anticoagulant for plasma concentration analysis at 0.25, 0.5, 1, 2, 3, 6, 9, 12, 24, 48 and 72 hours after dosing. All plasma was separated by centrifugation at a speed of 3000 g for 10 minutes at~4°C and stored frozen at a temperature below -15°C until analysis.

2.3.2.9.1   Enzalutamide Concentration Determination in Rat Plasma

Plasma samples were assessed for enzalutamide levels by LC-MS/MS. Standards of known concentrations were prepared in plasma and processed with the unknown samples. A 10 µL aliquot of plasma was precipitated with 275 µL of acetonitrile containing internal standard (diclofenac). Samples were vortexed and then centrifuged. A 100 µL volume of supernatant was combined with 200 µL of 0.1% formic acid in water for each sample. Supernatants were analyzed on a Sciex API5500™ mass spectrometer with a Turbo-Ion Spray source using multiple reaction monitoring at m/z 465 > 209 (Framingham, Massachusetts). Separation was performed with 0.1% formic acid in water and 0.1% formic acid in acetonitrile gradient on a Fortis Pace C18 5µm, 30 x 2.1 mm column (Fortis Inc., St. John's, Canada). Peak areas, peak area ratios, and calculated concentrations (determined by comparing peak area ratios of the samples to area ratios of known standards) were determined with Sciex Analyst™ 1.6.2 software. The standard curves met a minimum r-squared value of 0.99 and used the least weighted appropriate regression fit up to $1/x^2$ quadratic.

Peak plasma concentrations (C_{max}) and the time to peak plasma concentration (T_{max}) were determined directly from the plasma concentration data for each animal. Plasma concentration

data were submitted to non-compartmental curve fitting using WinNonlin (Certara, St. Louis, Missouri). The area under the plasma concentration-time curve from 0 to t hours after dosing (AUC_{0-t}, t = time of the last measurable plasma concentration) was calculated using the linear trapezoidal rule. The residual area extrapolated to infinity, determined as the final measured plasma concentration (C_t) divided by the terminal plasma elimination rate constant (β), was added to the AUC_{0-t} to produce the total area under the curve ($AUC_{0-\infty}$).

2.4 Results

2.4.1 Enzalutamide Physiochemical Properties

Various physicochemical characteristics of enzalutamide are listed in Table 2-1. Crystalline enzalutamide has strong intermolecular interactions as evident from the high melting point of 470 K. The glass transition temperature (T_g) is also high, suggesting that at the experimental temperature (37ºC or 310K), amorphous enzalutamide is glassy in nature, even when saturated with water. This was supported by calculation of the T_g using the Fox equation to estimate the impact of water, whereby the water content of amorphous enzalutamide in water was estimated from the moisture sorption profile. The estimated wet T_g value was 79°C or 352K, well above the experimental temperature.

2.4.2 Amorphous and Crystalline Solubility

Crystalline enzalutamide has an aqueous solubility of 2.9 $\pm$ 0.1 µg/mL at 37°C. The presence of a polymer did not appreciably impact the solubility (Table 2-2). Based on the heat of fusion, melting temperature, and moisture sorption, the estimated amorphous solubility is around 39 µg/mL, yielding an expected 13-fold enhancement relative to the crystalline form.

Figure 2 shows the fluorescence and UV extinction data for supersaturated enzalutamide solutions. Based on these data, the experimental amorphous solubility was determined to be approximately 42 µg/mL (Table 2), and is thus in good agreement with the predicted value. As described previously, the amorphous solubility is the highest concentration of free drug that can be achieved in solution[12]. Once the amorphous solubility is exceeded, in the absence of crystallization, any additional drug added to the solution will form amorphous aggregates. In the case of enzalutamide, the amorphous precipitate that formed appears glassy under a cross-polarized microscopy,

consistent with expectations based on the high T_g of the dry amorphous material, the amount of water absorbed by the amorphous material and the estimated wet T_g (Table 2-1).

2.4.3   Non-Sink Amorphous Solid Dispersion Dissolution

From the release data shown in Figure 2-3, the 10:90 Enz:PVPVA ASD had faster release in comparison to the 50:50 Enz:PVPVA ASD. Both systems reached a concentration close to the amorphous solubility, and underwent de-supersaturation shortly after reaching the maximum concentration due to crystallization of the drug. The dissolution profiles of HPMCAS ASDs at the low and high drug loadings were very different. The 10% drug load dispersion reached a maximum concentration of only 10 μg/mL and crystals could be observed in the dissolution medium. In contrast, the 50% drug load ASD reached a concentration corresponding to the amorphous solubility, and showed no de-supersaturation for 7 hours.   The area under the curve (AUC) integrated for different time frames for each ASD is shown in Table 2-3 where it is apparent that the quantitative ranking of AUC for ASDs changed with the integration time frame.

In order to compare the amount of amorphous aggregates that evolve from the various ASDs following dissolution, fluorescence spectroscopy with the environmentally sensitive probe, Nile Red, was employed. Nile Red is poorly fluorescent in water, with the fluorescence intensity increasing dramatically in less polar environments[24–26]. The intensity of Nile Red fluorescence is thus expected to depend on the amount of the drug aggregate phase, since when drug aggregates are present, the probe will preferentially associate with this phase. Figure 4 demonstrates that there is indeed a good correlation between the Nile Red emission intensity and the amount of enzalutamide present as amorphous aggregates. Selected Nile Red emission spectra are shown in Figure 2-5. It is apparent that Nile Red fluorescence is barely detectable in buffer. An increase in intensity accompanied by a blue shift is observed for a 45 μg/mL enzalutamide system; this system has a concentration just above the amorphous solubility, so a small quantity of drug aggregates are expected to be present. A large increase in intensity is seen for the system containing 100 μg/mL of enzalutamide, consistent with a larger extent of drug aggregate formation.   Both of the HPMCAS ASDs yielded a similar Nile Red signal to that observed for water, indicating that neither of those dispersions led to detectable GLPS following dissolution. In the case of the 10:90 Enz:HPMCAS dispersion, this was due to due to rapid crystallization. For the 50:50 Enz:HPMCAS

dispersion, no crystals were observed and hence it is apparent that the dispersion did not dissolve to a concentration higher than the amorphous solubility, explaining the absence of aggregate formation. Dissolution of the 50:50 Enz:PVPVA ASD led to the same Nile Red fluorescence intensity as the system containing 45 μg/mL enzalutamide, indicating a small amount of aggregate formation corresponding to ~3μg/mL of amorphous enzalutamide. In contrast, dissolution of the 10:90 Enz:PVPVA ASD generated a greater extent of amorphous aggregates as evidenced by a more intense Nile Red fluorescence. Using the data shown Figure 2-4, it was estimated that 10:90 Enz:PVPVA dispersion led to approximately 50μg/mL of amorphous enzalutamide aggregates. Thus, the solution composition is expected to be composed of 42 μg/mL of molecularly dissolved enzalutamide, 50 μg/mL of amorphous nanoaggregates and 8 μg/mL of enzalutamide removed by filtration, most likely undissolved ASD or agglomerated nanoparticles, giving a mass balance of a total of 100 μg/mL of enzalutamide in the form of an ASD added to the solution. The size of the amorphous aggregates that formed following dissolution of the PVPVA ASDs was approximately 100 nm in diameter based on DLS measurements. The distribution of various enzalutamide species in the ASD suspensions used to for dosing in *in vivo* experiments was determined using a similar approach as described above, and results are summarized in Table 2-4.

2.4.4   Mass Flow Rate

The measured mass flow rate is dictated by the thermodynamic activity of the drug in solution in the donor compartment as described by equation 2-5. As shown in Figure 2-6, the mass flow rate increases linearly with enzalutamide concentrations up to approximately the amorphous solubility, after which the mass flow remains relatively constant, fluctuating around 0.85μg/min. This phenomenon has been observed previously [13,15,16,22,27] and can be explained by the addition of drug beyond the amorphous solubility resulting in glass liquid phase separation (GLPS)[15]. After GLPS, the concentration of molecularly dissolved drug will remain at the amorphous solubility, while additional drug added to solution will result in the formation of additional amorphous aggregates[15]. At concentrations at and above the GLPS concentration, the thermodynamic activity of the drug in solution is at a maximum[12,28–30] and hence the mass flow rate remains approximately constant. For concentrations below the amorphous solubility, the flux is directly proportional to the solute activity, which scales directly with added drug concentration in this concentration region.

Next, the mass flow rates for solutions generated after dissolution of the ASDs for one hour as well as a crystalline slurry were also measured, with results summarized in Table 2-5. All of the ASDs had higher mass flow in comparison to the crystalline slurry with the 10:90 Enz:PVPVA dispersion having the highest value, while the 50:50 Enz:PVPVA and 50:50 Enz:HPMCAS ASDs showed similar values and the 10:90 Enz:HPMCAS gave the lowest mass flow.

The plasma concentration versus time profiles for the four ASDs following oral dosing, as well as a control formulation consisting of a suspension of crystalline material, are shown in Figure 2-7. It is apparent that the highest concentrations were achieved for the 10:90 Enz:PVPVA dispersion, while the 10:90 Enz:HPMCAS ASD gave the lowest values out of the dispersion samples, with a concentration-time profile similar to that of the crystalline control. It is interesting to note that the 50:50 Enz:HPMCAS ASD had a slower absorption phase as compared to the PVPVA formulations, and the 50:50 Enz:PVPVA was slower than the 10:90 Enz:PVPVA ASD, consistent with the *in vitro* dissolution profiles. From the pharmacokinetic profiles, the maximum systemic concentration (C_{max}) and the area under the curve over the 48 hour experimental timeframe (AUC_{0-48}) were extracted. These were then plotted against the *in vitro* mass flow values obtained from the side-by-side diffusion cell with the data summarized in Figure 8. It is apparent that there is a good correlation between both C_{max} and AUC_{0-48} and the mass flow rates observed for the various dispersions.

2.5   Discussion

With an increase in the number of poorly soluble drugs, it is important to understand how supersaturation, the types of species, and their relative quantities formed upon dissolution from enabling formulations impact oral drug absorption[1]. Enzalutamide was selected as a model compound because it exhibits poor oral absorption due to low aqueous solubility rather than as a result of poor permeability[31]. Because of the low aqueous solubility of the crystalline form, enzalutamide is currently marketed as a lipid formulation. With such an enabling formulation, it is well absorbed in humans with an estimated absorption of around 82% at the current clinical dose.[32,33] In addition, *in vivo* variability is relatively low. It remains unionized across the physiological pH range and is not a substrate for P-glycoprotein[33]. These characteristics make

enzalutamide a relevant model compound for studies that probe the impact of supersaturation and speciation on absorption.

The advantage of a supersaturated solution can be understood by considering the simple equation,

$$J = pc \qquad (2\text{-}6)$$

where J is the flux across a biological membrane, p is permeability and c is the concentration available for permeation. Thus, for a high permeability, low solubility compound, the concentration of drug in solution limits the rate of absorption. For solid oral dosage forms, the concentration-time profile will depend both on the dissolution rate, as well as the maximum achievable concentration, which, for a crystalline drug, is dictated by the equilibrium solubility. Consequently, for dissolution rate limited compounds, one can simply increase the rate of dissolution to achieve sufficient concentration for adequate absorption, for example by increasing particle surface area. However, if the absolute value of c is small, as for many compounds with a low crystalline solubility, then the flux will be limited by the magnitude of this value. Supersaturating dosage forms enable increases in flux to be achieved by yielding concentrations greater than crystal solubility.

Care must be taken in defining both concentration and supersaturation in terms of expected impact on membrane transport. It is widely accepted that only free drug concentration provides the driving force for membrane transport. Likewise, the supersaturation ratio (S), should be defined in terms of the ratio of the solute thermodynamic activity (a) to the activity of the crystalline reference (a^*):

$$S = \frac{a}{a^*} = \frac{\gamma c}{\gamma^* c^*} \qquad (1\text{-}7)$$

The supersaturation ratio can also be written in terms of the concentration (c) and the activity coefficient (γ), with * indicating values at standard state[34]. While widely employed, making the approximation that γ/γ^* is unity and hence $S = c/c^*$ may or may not be a valid assumption, depending on the complexity of the medium and the concentration ranges employed[16].

The upper limit of supersaturation that can be achieved is dictated by the spinodal decomposition point, where (in the absence of crystallization) the amorphous form of the drug spontaneously phase separates from the solution. In practical terms, the binodal point is often referred to as the amorphous solubility. At compositions between the binodal and spinodal points, there is a thermodynamic driving force for phase separation but there could be a time lag for this to occur. Whereas, at supersaturations above the spinodal decomposition point, phase separation would be instantaneous. Hence, the free drug concentration is at a maximum in the presence of an amorphous phase, and addition of further drug leads to the formation of more of the amorphous drug-rich phase. Above the amorphous solubility, the supersaturation ratio therefore remains a constant, and does not increase with an increase in the added concentration of the drug. This is exemplified by Figure 2-6, which demonstrates that above the amorphous solubility, the membrane mass flow rate remains constant; membrane transport rate is directly proportional to the supersaturation ratio.

For the formulations evaluated herein, it can be noted that three of the ASDs achieve the amorphous solubility (Figure 2-3), while one dispersion exhibits inferior dissolution performance. These three amorphous dispersions thus lead to an *S* of approximately 13, calculated from the ratio of the amorphous to crystalline solubility values shown in Table 2-2. This clearly translates to an improved *in vitro* mass flow rate (Table 2-5), as well as more extensive absorption and subsequent plasma exposure *in vivo*, as predicted by consideration of simple relationships between membrane transport and free drug concentration. However, given that all three formulations appear to reach the same maximum free drug concentration based on the *in vitro* dissolution data shown in Figure 2-3, simply considering the extent of supersaturation achieved is clearly not adequate to explain the significantly higher *in vivo* absorption achieved with the 10:90 Enz:PVPVA dispersion relative to the 50% drug loading dispersions.

To explain the *in vivo* observations, we return to a consideration of the mechanisms involved in achieving membrane transport following dosing of an oral solid dosage form. First the drug must dissolve in the gastrointestinal (GI) fluid, then diffuse to the apical side of the membrane, partition into the membrane, diffuse across the membrane, and then partition out of the basolateral membrane to enter the bloodstream. Dissolution, diffusion and permeation are necessary processes

coupled in series. Thus, if the solution is saturated with respect to the solid state form that is dissolving, additional material cannot dissolve until material is removed by permeation across the membrane. The interplay of dissolution, diffusion and permeation is not well predicted from conventional non-sink dissolution experiments lacking an absorption compartment; this is evident from the dissolution data shown in Figure 2-3 and the extracted AUC values presented in Table 2-3, which are not predictive of differences seen in the *in vivo* absorption. Specifically, if the permeation step is rapid, as expected for a BCS class II drug such as enzalutamide, dissolution, even from an amorphous formulation, may be the rate limiting step. This was shown in the *in vitro* study by Indulkar *et al* where macroscopic amorphous particles resulted in a lower overall flux profile relative to nano-dimensioned amorphous drug aggregates which could sustain the flux at a maximum value, dictated by the amorphous solubility, due to their rapid dissolution and replenishment of dissolved drug removed by transport across the membrane[16].

Therefore the drug "speciation" during ASD dissolution is important for drug absorption as outlined in Figure 2-9. During ASD dissolution, drug can exist as some combination of drug in undissolved ASD particles, molecularly dissolved drug, amorphous aggregates, and crystalline particles formed in the matrix or by crystallization from the supersaturated solution. The optimal scenario for a BCS Class II compound would be one in which the ASD dissolution rate is rapid leading to GLPS and the formation of nanosized aggregates. In this scenario, the rate of transfer across the membrane (k_{diff}) is at a maximum because the free drug concentration is maintained at the amorphous solubility due to the reservoir effect of amorphous aggregates which have a fast dissolution rate (k_{diss}^{AA}), rapidly replenishing drug absorbed into the body. The route of amorphous aggregate formation shown in Figure 2-9 has been experimentally verified for nifedipine and a similar pathway is invoked for enzalutamide aggregate-forming ASDs [35]. If drug crystallization occurs, both the molecularly dissolved solution concentration and the mass of aggregates will be reduced, with the exact free drug solution concentration profile depending on the relative magnitude of the rate constants, (k_{diss}^{AA}), the crystallization rate constant, k_c, and k_{diff}. Assuming k_c is rapid, which appears to be the case for one of the enzalutamide ASDs (10:90 Enz:HPMCAS), with the majority of drug crystallizing, then the absorption rate becomes dissolution limited and is dictated by the dissolution rate of the crystalline precipitate (k_{diss}^c).

In reviewing the data shown in Table 4, which provides an overview of the physical state of enzalutamide in PVPVA ASDs immediately prior to dosing, it is apparent, that a fraction of the drug is already dissolved in solution, at the amorphous solubility, leading to rapid initial absorption. However, Table 4 and Schematic 1 highlight that the important differences between the 50% and 10% drug load PVPVA dispersions are not just the initial extent of supersaturation attained, but whether the dispersion dissolves to yield amorphous aggregates or not, as well as the extent of amorphous aggregate formation. Herein, it was clearly demonstrated that the 10:90 Enz:PVPVA dispersion dissolves rapidly (high k_{diss}^{ASD}) to form the maximum free drug concentration (the amorphous solubility) with a high yield of amorphous aggregates (Table 2-4). The 50:50 Enz:PVPVA and 50:50 Enz:HPMCAS ASDs either did not form, or formed negligible amounts of amorphous aggregates (Table 2-4 and Figure 2-5). The formation of these amorphous aggregates appears to be of great importance, influencing the extent of *in vivo* absorption; indeed we see approximately 30% greater absorption for an equivalent dose of a dispersion that forms amorphous aggregates versus the dispersions that simply dissolve to achieve the amorphous solubility. Clearly the ASD that crystallizes leads to a dramatic reduction in absorption, highlighting that the type of precipitate formed is important. Referring again to Figure 2-9, the relative magnitudes of k_{diss}^{AA} and k_{diss}^{c} are expected to be quite disparate due to the higher solubility of the amorphous aggregates, as well as their high surface area due to their small size (~100 nm). This is supported by our *in vivo* data that clearly demonstrate that precipitation to a crystalline form has drastically different consequences for absorption extent relative to phase separation to nanosized amorphous aggregates, although both could be described as precipitation events.

Two explanations have been suggested to explain the beneficial properties of amorphous aggregates on *in vivo* absorption. The first is the small size of the aggregates which leads to a reservoir effect. In other words, equilibration between the solution, which is saturated at the amorphous solubility, and the amorphous aggregates is very fast due to their high surface area and prewetted state. This leads to a high and sustained flux value, as demonstrated previously for *in vitro* studies[16]. The second mechanism which has been proposed is related to the unstirred water layer (UWL), a stagnant layer adjacent to the membrane which acts as a barrier for diffusion. Drifting of the highly concentrated amorphous aggregates into the UWL, would provide an

additional mechanism for transport of drug to the membrane and enhance absorption,[36] although dissolution of the drug is clearly still required for the drug to permeate through the membrane. Regardless of the exact mechanism, there is very little *in vivo* data comparing systems that do and don't form amorphous aggregates in terms of impact on absorption. Herein, we observe an approximately 30% increase in AUC for the ASD that forms amorphous aggregates, relative to ASDs that dissolve to the amorphous solubility without forming aggregates. While it is impossible to know the generality of this observation, recent studies have suggested that formation of itraconazole aggregates may be beneficial to absorption[36].

Somewhat remarkably, and as shown in Figure 8, the *in vivo* data shows good correlation with the *in vitro* mass flow data obtained from the dissolved ASDs using a side-by-side diffusion cell. Thus, the ASD which shows the highest mass flow rate, yields the highest AUC and C_{max} values *in vivo*. Although we do not have a great deal of data points for comparison between the *in vitro* and *in vivo* data, this observation is extremely encouraging, suggesting that *in vitro* tests that combine dissolution with mass transport measurements may be useful to screen formulations and identify systems that will have the best *in vivo* performance. Clearly, simply using the dissolution data presented in Figure 2-3 would not lead to adequate discrimination between three of the ASDs. The 10% drug load dispersion with HPMCAS obviously performs poorly in the dissolution test, and this result is somewhat predictive of *in vivo* performance. It is of interest to consider this system a little more closely at this juncture. Typically, an ASD with a lower drug loading might be expected to have improved performance over the correspondingly higher drug loading dispersion. This has been seen for multiple systems during dissolution testing[37–41] and also during *in vivo* testing[40,42]. The origin of the poor performance of this particular ASD is the rapid matrix crystallization of enzalutamide upon contact with water. This effect is not seen for the higher drug loading dispersion with HPMCAS. While crystallization explains the poor dissolution properties in terms of the extent of supersaturation achieved, and the correspondingly low *in vivo* absorption (based on the magnitude of the AUC), the underlying reason for susceptibility of the particular dispersion to crystallization remains to be elucidated.

2.6   Conclusion

In this study, the interplay between drug thermodynamic activity in solution following ASD dissolution, speciation in terms of the presence and weight fraction of drug-rich amorphous aggregates, as well as drug absorption following oral dosing to rats was evaluated. Promising correlations between *in vitro* mass flow measurements and the rate and extent of drug absorbed were observed. In contrast, non-sink closed compartment dissolution testing of the formulations was not particularly predictive of *in vivo* exposure. The formation of amorphous, drug-rich aggregates from one ASD led to a 30% increase in the AUC following oral dosing relative to an ASD that gave a similar maximum supersaturation but did not form aggregates. This observation strongly supports the critical role of drug-rich aggregates in enhancing the oral absorption of drugs with solubility-limited absorption. During ASD formulation development, it is desirable that the ASD particles dissolve, *in vivo*, to produce the maximum yield of amorphous drug-rich aggregates. In addition, we need to ensure that crystallization is inhibited over absorption-relevant timeframes.

Table 2-1. Physiochemical properties of enzalutamide.

Property	Value
Molecular Weight	464.44 g/mol
cLogP*	2.98
Melting Point	470 K
Glass Transition Temperature	362 K
Wet Glass Transition Temperature Calculated with Fox Equation[23]	352 K
Enthalpy of Fusion	33,820 (380) J/mol
pKa*	None between 3 – 11
Estimated moles of water/mole of ENZ at 100% RH	0.50
$I(a_2)$	0.69

*The calculated logP and pKa values were taken from the enzalutamide EMEA document[17].
Standard deviations for thermal measurements were less than ±1K, n=3.

Table 2-2. Summary of the experimental crystalline and amorphous solubility values of enzalutamide. Values in parentheses are the standard deviations, n=3.

Sample	Solubility (μg/mL)
Crystalline (buffer)	2.9 (0.1)
Crystalline (with 5 μg/mL HPMCAS)	1.7 (0.8)
Amorphous (Fluorescence)	42 (3)
Amorphous (Extinction)	42 (2)
Amorphous (Extinction with 900 μg/mL HPMCAS)	43 (2)
Amorphous (Extinction with 900 μg/mL PVPVA)	42 (0)

Table 2-3. Area under the curve (AUC) values for enzalutamide ASDs determined from the dissolution profiles shown in Figure 2-3.

Formulation	AUC_{0-2hr} (μg*h/mL)	AUC_{0-4hr} (μg*h/mL)	AUC_{0-7hr} (μg*h/mL)
50:50 Enz:HPMCAS	64	147	275
10:90 Enz:HPMCAS	16	24	50
50:50 Enz:PVPVA	69	130	180
10:90 Enz:PVPVA	75	127	198

Table 2-4. The speciation of the ASD suspensions dosed to rats after 1 hour of dissolution.

Speciation	10:90 Enz:PVPVA	50:50 Enz:PVPVA
ENZ as free drug in solution*	0.21 mg	0.21 mg
ENZ as amorphous aggregates	37.65 mg	0 mg
ENZ as undissolved ASD or crystals	12.14 mg	49.79 mg

*based on assuming the system dissolved to amorphous solubility

Table 2-5. Mass flow of crystalline slurry and four enzalutamide ASDs.

Formulation	Mass Flowrate (µg/min)
Crystalline slurry	0.063(0.003)
10:90 Enz:HPMCAS	0.147(0.018)
50:50 Enz:HPMCAS	0.437(0.080)
50:50 Enz:PVPVA	0.456(0.021)
10:90 Enz:PVPVA	0.632(0.023)
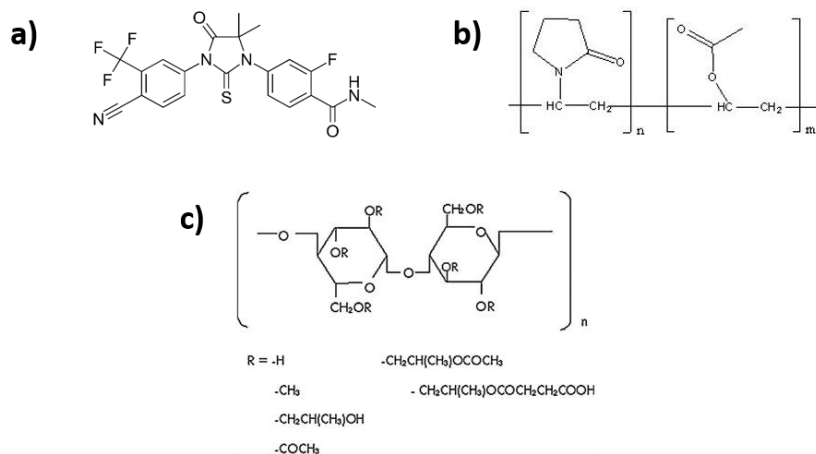
Figure 2-1. Chemical structure of a) enzalutamide, b) PVPVA, and c) HPMCAS.
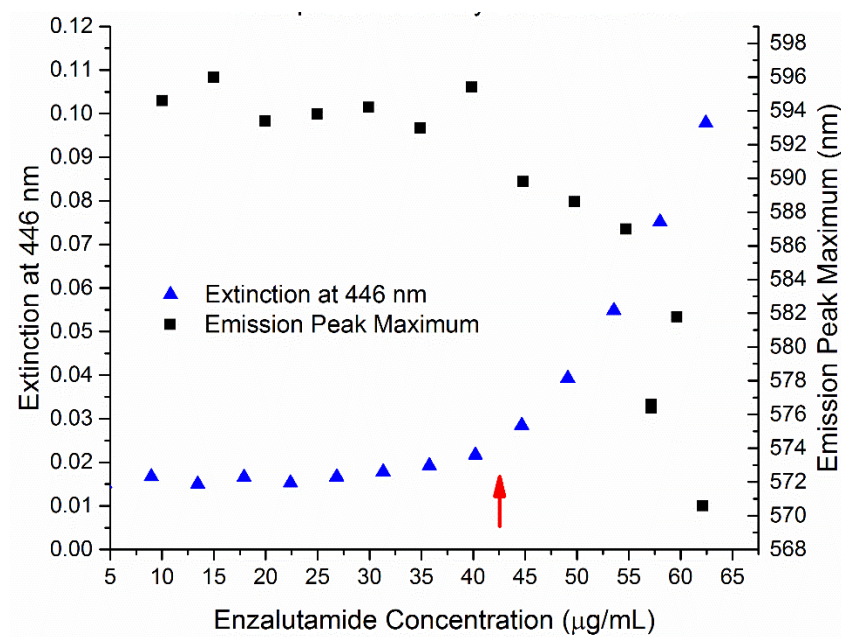
Figure 2-2. Example of UV extinction and fluorescence data used to determine the experimental amorphous solubility of enzalutamide. The arrow indicates the concentration where the scattering increases in the UV extinction experiment, indicating the formation of a second phase. Simultaneously, the fluorescence emission peak shifts to a lower wavelength.
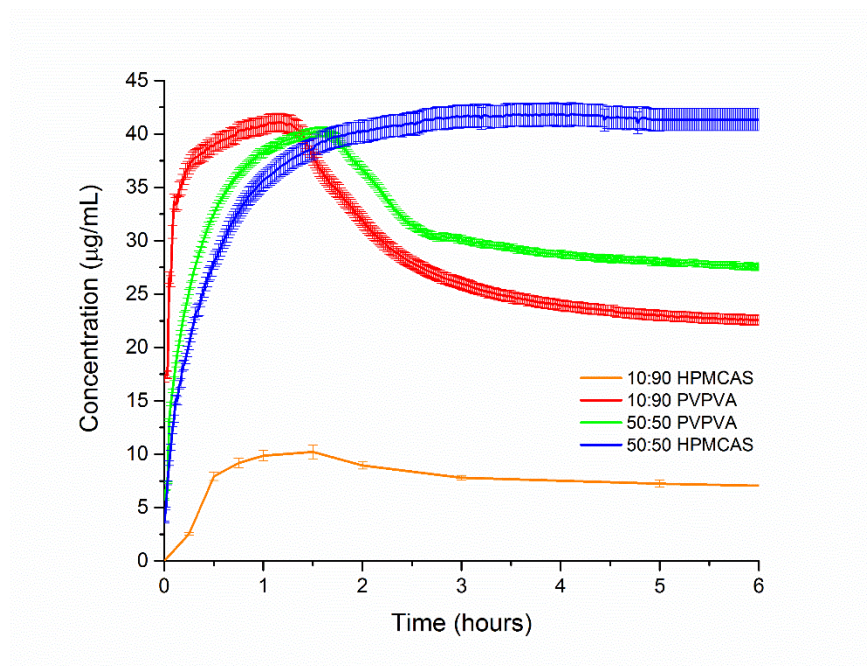
Figure 2-3. Dissolution profiles of ASDs formulated with either HPMCAS or PVPVA at low (10 wt. %) and high (50 wt. %) drug load in pH 6.5 50mM phosphate buffer under non-sink conditions. For the low drug loading HPMCAS dispersion, the concentration was measured following filtration and HPLC analysis due to interference of the small crystals with the UV absorbance measurements.
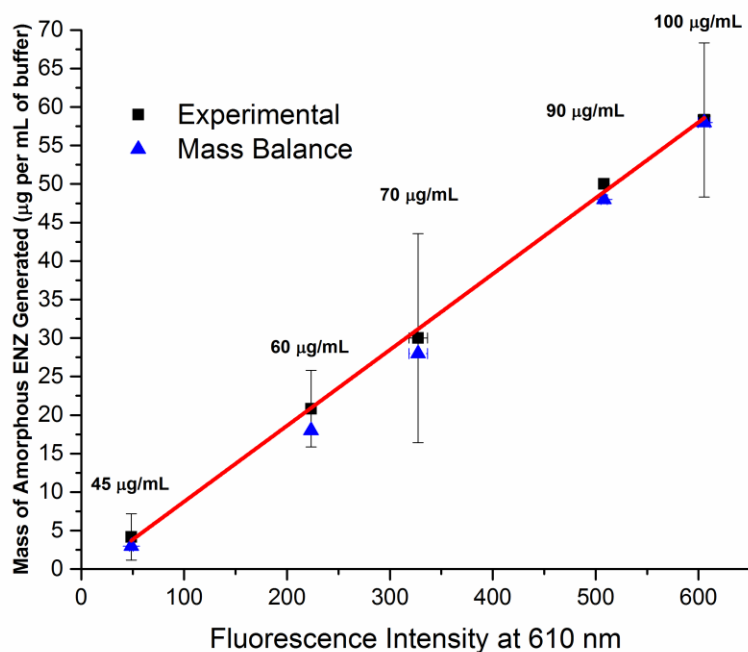
Figure 2-4. Mass of drug present as aggregates for various concentrations of enzalutamide (45-100 μg/mL) above the amorphous solubility and correlation to the Nile Red fluorescence intensity. The mass of drug present as drug aggregate was determined independently by centrifugation and weighing of the pellet. Experiments were performed in triplicate, x-axis error bars are smaller than data point size.
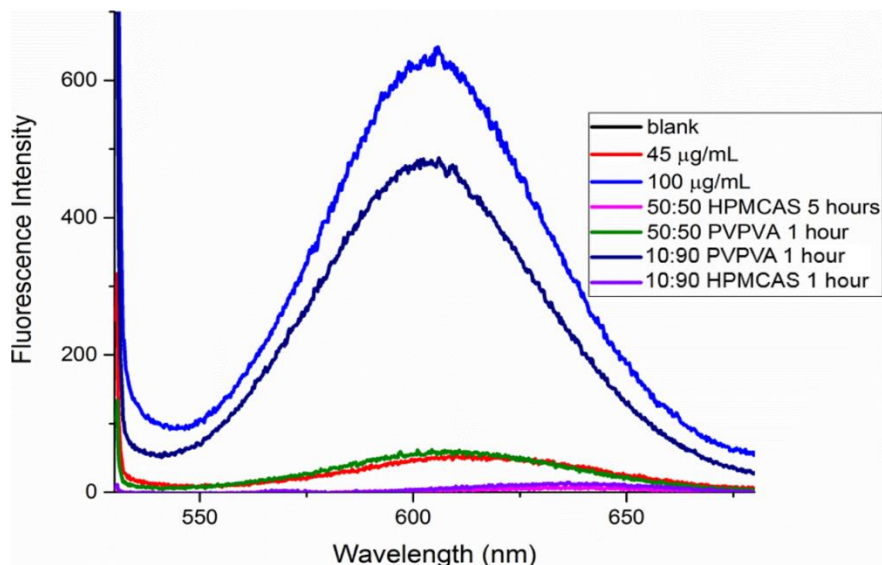
Figure 2-5. The fluorescence spectra of solutions derived from dissolution of 4 different ASDs of enzalutamide. The 10:90 Enz:PVPVA, 50:50 Enz:PVPVA, and 50:50 Enz:HPMCAS ASD samples were taken after 1 hour of dissolution. The 10:90 Enz:HPMCAS ASD sample was taken at 2 and 5 hours of dissolution and had similar fluorescence intensity.
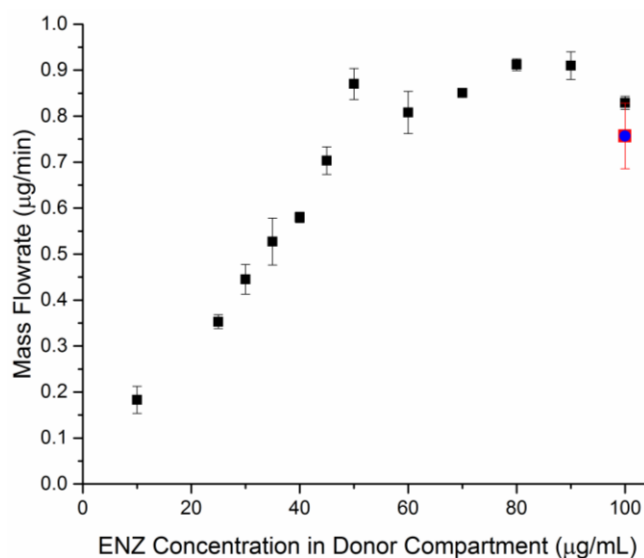
Figure 2-6. Mass flowrate into the receiver compartment versus initial enzalutamide concentration in the donor compartment. The red square represents the mass flow rate of enzalutamide derived from the 10:90 Enz:PVPVA ASD that underwent dissolution for 30 minutes prior to the diffusion cell experiment. The blue circle represents the enzalutamide mass flow in the presence of 900 µg/mL PVPVA in the donor compartment and this system has the same mass flow as the system derived from the10:90 Enz:PVPVA ASD.
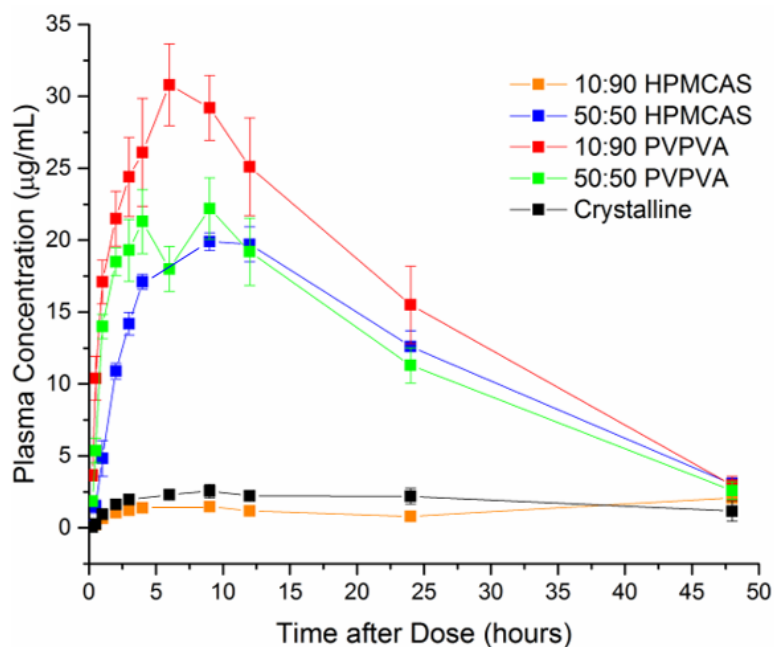
Figure 2-7. Mean plasma concentration vs time curve following oral dosing of various formulations to rats.
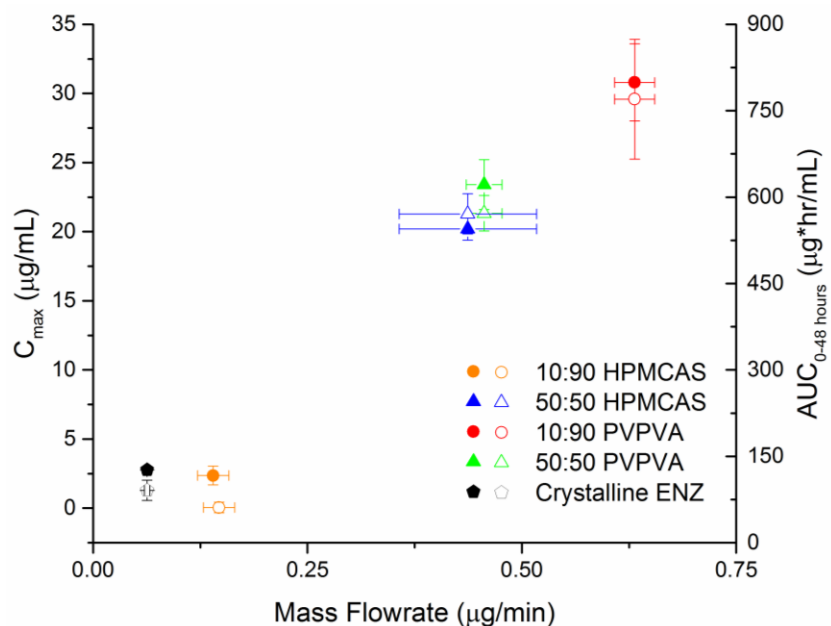
Figure 2-8. Mass flow (μg/min) measured in the side-by-side diffusion cell vs C_{max} (filled data points) and $AUC_{0-48\ hours}$ (open data points) of enzalutamide for four enzalutamide ASD formulations and the crystalline suspension.
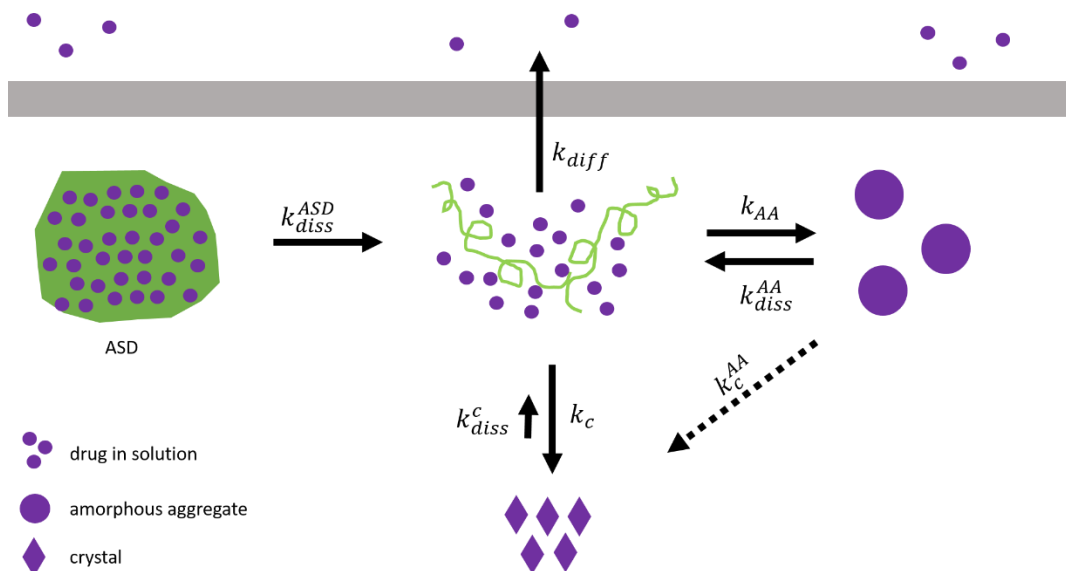
Figure 2-9. Different physical states of drug during ASD dissolution in diffusion cell. It is assumed that only drug in solution will diffuse across a membrane. k represents various rate constants: k_{diss}^{ASD} is the rate of ASD dissolution, k_c is the rate of crystallization of drug from solution, k_{AA} is the rate of formation of amorphous aggregates from drug in solution when the amorphous solubility is exceeded, k_{diss}^{AA} is the rate of dissolution of amorphous aggregates to replenish drug lost from solution by crystallization or permeation across the membrane, k_c^{AA} is the rate of crystallization of amorphous aggregates, k_{diss}^{c} is the rate of dissolution of crystals, and k_{diff} is the rate of diffusion of drug molecules across the membrane. Not shown is the crystallization of drug within the ASD matrix.

2.7 References

[1] L. Z. Benet, "The role of BCS (biopharmaceutics classification system) and BDDCS (biopharmaceutics drug disposition classification system) in drug development," *J. Pharm. Sci.*, vol. 102, no. 1, pp. 34–42, 2013.

[2] V. H. K. Li, "Influence of Drug Properties and Routes of Drug Administration on the Design of Sustained and Controlled Release Systems," in *Controlled Drug Delivery*, 1987, pp. 3–94.

[3] A. Fasano, "Novel approaches for oral delivery of macromolecules," in *Journal of Pharmaceutical Sciences*, 1998, vol. 87, no. 11, pp. 1351–1356.

[4] S. Sastry, J. Nyshadham, and J. Fix, "Recent technological advances in oral drug delivery - a review.," *Pharm. Sci. Technolo. Today*, vol. 3, no. 4, pp. 138–145, 2000.

[5] M. A. Rahman, A. Hussain, M. S. Hussain, M. A. Mirza, and Z. Iqbal, "Role of excipients in successful development of self-emulsifying/microemulsifying drug delivery system (SEDDS/SMEDDS)," *Drug Dev. Ind. Pharm.*, vol. 39, no. 1, pp. 1–19, 2013.

[6] S. T. Buckley, K. J. Frank, G. Fricker, and M. Brandl, "Biopharmaceutical classification of poorly soluble drugs with respect to 'enabling formulations,'" *Eur. J. Pharm. Sci.*, vol. 50, no. 1, pp. 8–16, 2013.

[7] A. C. F. Rumondor, P. J. Marsac, L. A. Stanford, and L. S. Taylor, "Phase behavior of poly(vinylpyrrolidone) containing amorphous solid dispersions in the presence of moisture," in *Molecular Pharmaceutics*, 2009, vol. 6, no. 5, pp. 1492–1505.

[8] T. Vasconcelos, B. Sarmento, P. Costa, and B. S. and P. C. Teo´ filo Vasconcelos, "Solid dispersions as strategy to improve oral bioavailability of poor water soluble drugs," *Drug Discov Today*, vol. 12, no. 23–24, pp. 1068–1075, 2007.

[9]   S. Onoue, H. Sato, K. Ogawa, Y. Kawabata, T. Mizumoto, K. Yuminoki, N. Hashimoto, and S. Yamada, "Improved dissolution and pharmacokinetic behavior of cyclosporine A using high-energy amorphous solid dispersion approach," *Int. J. Pharm.*, vol. 399, no. 1–2, pp. 94–101, 2010.

[10]   D. Engers, J. Teng, J. Jimenez-Novoa, P. Gent, S. Hossack, C. Campbell, J. Thomson, I. Ivanisevic, A. Templeton, S. Byrn, and A. Newman, "A solid-state approach to enable early development compounds: Selection and animal bioavailability studies of an itraconazole amorphous solid dispersion," *J. Pharm. Sci.*, vol. 99, no. 9, pp. 3901–3922, 2010.

[11]   C. Brough and R. O. Williams, "Amorphous solid dispersions and nano-crystal technologies for poorly water-soluble drug delivery," *International Journal of Pharmaceutics*, vol. 453, no. 1. pp. 157–166, 2013.

[12]   G. A. Ilevbare and L. S. Taylor, "Liquid–Liquid Phase Separation in Highly Supersaturated Aqueous Solutions of Poorly Water-Soluble Drugs: Implications for Solubility Enhancing Formulations," *Cryst. Growth Des.*, vol. 13, no. 4, pp. 1497–1509, Apr. 2013.

[13]   S. A. Raina, G. G. Z. Zhang, D. E. Alonzo, J. Wu, D. Zhu, N. D. Catron, Y. Gao, and L. S. Taylor, "Enhancements and limits in drug membrane transport using supersaturated solutions of poorly water soluble drugs," *J. Pharm. Sci.*, vol. 103, no. 9, pp. 2736–2748, 2014.

[14]   M. J. Jackson, S. J. Toth, U. S. Kestur, J. Huang, F. Qian, M. A. Hussain, G. J. Simpson, and L. S. Taylor, "Impact of polymers on the precipitation behavior of highly supersaturated aqueous danazol solutions," *Mol. Pharm.*, vol. 11, no. 9, pp. 3027–3038, 2014.

[15]   L. I. Mosquera-Giraldo and L. S. Taylor, "Glass−Liquid Phase Separation in Highly Supersaturated Aqueous Solutions of Telaprevir," *Mol. Pharm.*, vol. 12, no. 2, pp. 496–503, 2015.

[16] A. S. Indulkar, Y. Gao, S. A. Raina, G. G. Z. Zhang, and L. S. Taylor, "Exploiting the Phenomenon of Liquid-Liquid Phase Separation for Enhanced and Sustained Membrane Transport of a Poorly Water-Soluble Drug," *Mol. Pharm.*, vol. 13, no. 6, pp. 2059–2069, 2016.

[17] Committee for Medicinal Products for Human Use (CHMP) European Medicines Agency, "Enzalutamide European Public Assessment Report," vol. 44, no. April, 2013.

[18] D. E. Alonzo, G. G. Z. Zhang, D. Zhou, Y. Gao, and L. S. Taylor, "Understanding the behavior of amorphous pharmaceutical systems during dissolution," *Pharm. Res.*, vol. 27, no. 4, pp. 608–618, 2010.

[19] J. D. Hoffman, "Thermodynamic driving force in nucleation and growth processes," *J. Chem. Physics1*, vol. 29, no. 5, pp. 1192–1193, 1958.

[20] R. H. Bogner, S. B. Murdande, M. J. Pikal, and R. M. Shanker, "Solubility advantage of amorphous pharmaceuticals: II. application of quantitative thermodynamic relationships for prediction of solubility enhancement in structurally diverse insoluble pharmaceuticals," *Pharm. Res.*, vol. 27, no. 12, pp. 2704–2714, 2010.

[21] W. I. Higuchi and T. Higuchi, "Theoretical Analysis of Diffusional Movement Through Heterogeneous Barriers**University of Wisconsin, S-hool of Pharmacy, hladison 6," *J. Am. Pharm. Assoc. (Scientific ed.)*, vol. 49, no. 9, pp. 598–606, 1960.

[22] S. A. Raina, G. G. Z. Zhang, D. E. Alonzo, J. Wu, D. Zhu, N. D. Catron, Y. Gao, and L. S. Taylor, "Impact of Solubilizing Additives on Supersaturation and Membrane Transport of Drugs," *Pharm. Res.*, vol. 32, no. 10, pp. 3350–3364, 2015.

[23] T. G. Fox, "Influence of diluent and of copolymer composition on the glass temperature of a polymer system," *Bull. Am. Phys. Soc.*, vol. 1, no. 2, pp. 123–35, 1956.

[24] P. Greenspan and S. D. Fowler, "Spectrofluorometric studies of the lipid probe, nile red," *J. Lipid Res.*, vol. 26, no. 7, pp. 781–789, 1985.

[25] P. Greenspan, E. P. Mayer, and S. D. Fowler, "Nile red: A selective fluorescent stain for intracellular lipid droplets," *J. Cell Biol.*, vol. 100, no. 3, pp. 965–973, 1985.

[26] K. E. Cooksey, J. B. Guckert, S. A. Williams, and P. R. Callis, "Fluorometric determination of the neutral lipid content of microalgal cells using Nile Red," *J. Microbiol. Methods*, vol. 6, no. 6, pp. 333–345, 1987.

[27] N. S. Trasi and L. S. Taylor, "Thermodynamics of Highly Supersaturated Aqueous Solutions of Poorly Water-Soluble Drugs - Impact of a Second Drug on the Solution Phase Behavior and Implications for Combination Products," *J. Pharm. Sci.*, vol. 104, no. 8, pp. 2583–2593, 2015.

[28] K. Kiesow, F. Tumakaka, and G. Sadowski, "Experimental investigation and prediction of oiling out during crystallization process," *J. Cryst. Growth*, vol. 310, no. 18, pp. 4163–4168, 2008.

[29] I. De Albuquerque and M. Mazzotti, "Crystallization process design using thermodynamics to avoid oiling out in a mixture of vanillin and water," *Cryst. Growth Des.*, vol. 14, no. 11, pp. 5617–5625, 2014.

[30] L. Almeida e Sousa, S. M. Reutzel-Edens, G. A. Stephenson, L. S. Taylor, L. Almeida e. Sousa, S. M. Reutzel-Edens, G. A. Stephenson, and L. S. Taylor, "Assessment of the Amorphous 'Solubility' of a Group of Diverse Drugs Using New Experimental and Theoretical Approaches," *Mol Pharm*, vol. 12, no. 2, pp. 484–495, 2014.

[31] D. A. Lorenz, S. Konagurthu, R. J. Wald, J. A. Everett, S. Matz, Y. Takaishi, T. Sakai, R. Irie, S. Oba, H. Toyota, K. Nishimura, and A. Kanbayashi, "Formulations of enzalutamide," WO2014043208 A1, 2013.

[32] J. A. Gibbons, T. Ouatas, W. Krauwinkel, Y. Ohtsu, J. S. van der Walt, V. Beddo, M. de Vries, and J. Mordenti, "Clinical Pharmacokinetic Studies of Enzalutamide," *Clin. Pharmacokinet.*, vol. 54, no. 10, pp. 1043–1055, 2015.

[33]   G. E. Benoist, R. J. Hendriks, P. F. A. Mulders, W. R. Gerritsen, D. M. Somford, J. A. Schalken, I. M. van Oort, D. M. Burger, and N. P. van Erp, "Pharmacokinetic Aspects of the Two Novel Oral Drugs Used for Metastatic Castration-Resistant Prostate Cancer: Abiraterone Acetate and Enzalutamide," *Clinical Pharmacokinetics*, vol. 55, no. 11. pp. 1369–1380, 2016.

[34]   G. L. Flynn and T. J. Roseman, "Membrane diffusion II: Influence of physical adsorption on molecular flux through heterogeneous dimethylpolysiloxane barriers," *J. Pharm. Sci.*, vol. 60, no. 12, pp. 1788–1796, 1971.

[35]   A. S. Indulkar, J. E. Waters, H. Mo, Y. Gao, S. A. Raina, G. G. Z. Zhang, and L. S. Taylor, "Origin of Nanodroplet Formation Upon Dissolution of an Amorphous Solid Dispersion: A Mechanistic Isotope Scrambling Study," *J. Pharm. Sci.*, vol. 106, no. 8, pp. 1998–2008, 2017.

[36]   A. M. Stewart, M. E. Grass, T. J. Brodeur, A. K. Goodwin, M. M. Morgen, D. T. Friesen, and D. T. Vodak, "Impact of Drug-Rich Colloids of Itraconazole and HPMCAS on Membrane Flux in Vitro and Oral Bioavailability in Rats," *Mol. Pharm.*, vol. 14, no. 7, pp. 2437–2449, 2017.

[37]   D. E. Alonzo, Y. Gao, D. Zhou, H. Mo, G. G. Z. Z. Zhang, and L. S. Taylor, "Dissolution and precipitation behavior of amorphous solid dispersions," *J. Pharm. Sci.*, vol. 100, no. 8, pp. 3316–3331, 2011.

[38]   K. Six, G. Verreck, J. Peeters, M. Brewster, and G. Van Den Mooter, "Increased Physical Stability and Improved Dissolution Properties of Itraconazole, a Class II Drug, by Solid Dispersions that Combine Fast- and Slow-Dissolving Polymers," *J. Pharm. Sci.*, vol. 93, no. 1, pp. 124–131, 2004.

[39]   Y. Chen, C. Liu, Z. Chen, C. Su, M. Hageman, M. Hussain, R. Haskell, K. Stefanski, and F. Qian, "Drug-polymer-water interaction and its implication for the dissolution performance of amorphous solid dispersions," *Mol. Pharm.*, vol. 12, no. 2, pp. 576–589, 2015.

[40]   D. Law, E. A. Schmitt, K. C. Marsh, E. A. Everitt, W. Wang, J. J. Fort, S. L. Krill, and Y. Qiu, "Ritonavir-PEG 8000 Amorphous Solid Dispersions: In Vitro and in Vivo Evaluations," *J. Pharm. Sci.*, vol. 93, no. 3, pp. 563–570, 2004.

[41]   B. Li, S. Konecke, L. A. Wegiel, L. S. Taylor, and K. J. Edgar, "Both solubility and chemical stability of curcumin are enhanced by solid dispersion in cellulose derivative matrices," *Carbohydr. Polym.*, vol. 98, no. 1, pp. 1108–1116, 2013.

[42]   T. Kai, Y. Akiyama, S. Nomura, and M. Sato, "Oral absorption improvement of poorly soluble drug using solid dispersion technique.," *Chem. Pharm. Bull. (Tokyo).*, vol. 44, no. 3, pp. 568–71, 1996.

CHAPTER 3.   AMORPHOUS SOLID DISPERSIONS OF ENZALUTAMIDE AND NOVEL POLYMERS: INVESTIGATION OF RELATIONSHIPS BETWEEN POLYMER STRUCTURE AND PERFORMANCE METRICS

3.1   Abstract

Amorphous solid dispersions (ASDs) are a widely employed formulation technique for compounds with poor aqueous solubility. Polymers are an integral part of the ASD formulation, but mechanisms by which polymers lead to the generation and maintenance of supersaturated solutions, which in turn enhance oral absorption *in vivo*, are not well understood. Herein, commercially available polymers and a diverse group of synthesized cellulose derivatives were pre-screened for their ability to inhibit crystallization of enzalutamide, a poorly soluble compound used to treat prostrate cancer. ASDs were then prepared from the novel polymers, selecting a somewhat hydrophobic polymer that was extremely effective at inhibiting crystallization from supersaturated enzalutamide solutions, as well as a less effective, but more hydrophilic polymer. The permeation of drug evolved from the various formulations across a membrane was evaluated *in vitro* and compared to the amount of drug absorbed following oral dosing in rats. Good correlation was noted between the *in vitro* diffusion cell studies and the *in vivo* data. The ASD formulated with the less effective crystallization inhibitor outperformed the ASD prepared with the highly effective crystallization inhibitor in terms of the amount and rate of drug absorbed in vivo. This study provides valuable insight into key factors impacting oral absorption from enabling formulations, and how to best evaluate such formulations using *in vitro* approaches.

3.2   Introduction

The number of drugs designated as Biopharmaceutics Classification System (BCS) class II and IV compounds has increased in recent years; these poorly water soluble compounds now form the majority of drugs in development[1] (A. Fahr and X. Liu, *Expert Opin. Drug Delivery*, 2007, **4**, 403–416). Since the drug in an oral dosage form must first dissolve prior to absorption across the gastrointestinal tract, it is critical that formulation techniques are employed to enhance the dissolution rate and/or solubility; supersaturating formulations are of increasing interest for this purpose. Amongst supersaturating formulation strategies, amorphous solid dispersions comprising

a molecular level blend of drug and polymer, have demonstrated bioavailability advantages *in vivo*[2–4] (insert 1st manuscript reference). While the exact mechanisms by which ASD dissolution leads to supersaturated solutions are not fully understood, it generally recognized that the polymer role is to facilitate the release of drug from the amorphous matrix and to prevent subsequent crystallization[5,6]. The latter aspect is particularly important for rapidly crystallizing compounds because once crystallization commences, supersaturation is depleted and any solubility advantage is lost. Thus, it is important the polymer contains hydrophobic substituent groups to drive interaction with the drug in an aqueous environment to prevent crystallization and hydrophilic groups to interact with water and facilitate drug release from the ASD[7–9].

There are currently a limited number of polymers that have been used in commercial ASDs; the majority of Food and Drug Administration (FDA) approved ASDs are formulated with hypromellose, hypromellose acetate succinate or copovidone[10–12]. However, this small group of polymers is not sufficiently diverse in terms of chemistry to enable structure activity relationships to be systematically probed, and these polymers were not specifically designed for ASD formulation, rather they have been repurposed from other applications. In recent years, the synthesis of novel polymers specifically designed for use in ASDs, as well as to facilitate mechanistic understanding of key polymer functionality, has led to an increase in polymer diversity[9,13]. Ultimately, if polymers with enhanced properties can be identified, this may lead to more poorly soluble drugs being formulated as ASDs. Further, if improved mechanistic understanding of drug release and crystallization inhibition can be realized, in the future, polymers could be rationally selected based upon the physiochemical and structural properties of the drug. One challenge worth noting is the difficulty in achieving adequate and timely release of drug in a high drug loading ASD[14].

The role of the polymer in an ASD is multifaceted whereby the polymer needs to inhibit crystallization of drug during manufacture, keep the drug amorphous during storage in the solid state dosage form, to enhance the dissolution of the drug relative to the pure crystalline and amorphous forms, and to delay crystallization of drug from the supersaturated solution generated after dissolution. In order to inhibit crystallization, the polymer must interact with the drug through specific interactions such as van der Waals forces, ionic interactions, and hydrogen bonds,[7,15,16]

whereby the relative importance of different types of interaction may vary in the dry versus the hydrated system. In addition, the polymer must be sufficiently water soluble to dissolve and subsequently release the drug[15]. It has been found that high polymer solubility, with subsequent rapid drug release, may lead to fast drug crystallization[17] since highly water soluble polymers may show less tendency to interact with drugs[18]. Conversely, insoluble polymers may limit the amount of drug released leading to lower levels of supersaturation[19]. Therefore, polymers need an appropriate balance of functional groups to achieve the desired ASD performance in terms of both drug release and crystallization inhibition. However, it is currently unclear what the required balance between these two factors is. Moreover, it is unclear which *in vitro* tests are predictive of *in vivo* performance, with recent studies suggesting that flux measurements may provide greater insight than simple dissolution tests [20,21](reference 1st manuscript). The goal of this study was therefore to evaluate the crystallization inhibitory ability of a group of structurally diverse polymers, and to further evaluate the release properties and *in vivo* absorption performance of a subset of these polymers.

Enzalutamide, a biopharmaceutics classification system (BCS) class II compound was selected as the model compound. Enzalutamide, which is used to treat prostate cancer, does not ionize over physiologically relevant pH conditions. Structurally diverse polymers were screened for their ability to inhibit crystallization of enzalutamide from supersaturated solutions by measuring the nucleation induction time. From these results, two newly synthesized cellulose derivatives with a different balance of hydrophobic and hydrophilic moieties were selected for ASD formulation. The relative hydrophilicity of the polymers was evaluated by measuring the aqueous solubility and comparing solubility parameters. Permeation ability was measured using a side-by-side diffusion cell to measure flux. The amount of drug absorbed *in vivo* was determined by dosing the different formulations to rats and determining drug plasma levels. The choice of polymer was found to have a dramatic influence on both the rate and extent of drug absorption and the extent of permeation in the *in vivo* and *in vitro* studies respectively.

3.3   Materials & Methods

3.3.1   Materials

Abbreviations and details about the polymer used are summarized in Table 3-1. The following excipients were generously donated: HPMCAS (Shin-Etsu Co. Ltd, Tokyo, Japan), company), PVPVA (BASF, Ludwigshaven, Germany), HPC (Ashland Inc., Covington, Kentucky), PVP (BASF, Ludwigshaven, Germany), and Labrasol ALF (Gattefosse, Lyon, France). The novel cellulose derivatives were synthesized as described previously: HPC-Pen106-AA-H, HPC-Pen282-AA-H[22], HPC-C3OH-AA-H, Cellulose Propionate Trioxdecanoate[9], CA-Pen056-PEG-H2[9], CA-Pen056-HEA-H[9], CA Propionate 504-0.2 adipate 0.85[23], CA 320S Adipate 0.67[24], CA 320S Suberate 0.9[24], CA-Pen079-HEA-3MPA[25], CA-Un067-TMA-3MPA[25], Methylcellulose Adipate[26], MC1.6C5-AA-TSH-MC56, MC1.6C5-AA-H-MC56, ECN2.6C5-AA-H-TSH-N5020, ECN2.6C5-AA-H-N5020, EC2.2C5-AA-H-TSH, and EC2.1C5-AA-H-MCC33. Enzalutamide was obtained from ChemShuttle (Hayward, California), CA Ph was from Sigma-Aldrich (St. Louis, Missouri), and all organic solvents used were supplied by Fisher Scientific (Hampton, New Hampshire).

3.3.2   Hoy Solubility Parameter

The solubility parameter was calculated using Hoy's method[27]. In short, the chemical structure is used to calculate the solubility parameter which can be divided into separate intermolecular interactions: hydrogen bonding, dispersive, and polar. The values for each molecular moiety molar attraction functions are summed and the value for the solubility parameter is calculated using the following equation:

$$\delta_t = \sqrt{\delta_p^2 + \delta_h^2 + \delta_d^2} \qquad (3\text{-}1)$$

where the subscript t is for the total, p for polar, h for hydrogen bonding, and d for dispersive component.

3.3.3   Formulation Preparation

3.3.3.1   Self-Emulsifying Drug Delivery System Preparation

SEDDS were prepared by dissolving crystalline enzalutamide in Labrasol ® (Gattefosse, Saint-Priest, France) with a drug loading of 4.5% .

3.3.3.2   Amorphous Solid Dispersion Preparation

ASDs of enzalutamide were prepared by dissolving enzalutamide and polymer in an organic solvent and rapidly removing the solvent by rotary evaporation. Three different ASDs were prepared: 50% drug loading with CA Sub, and 10% and 50% drug loadings with HPC-Pen106. Methanol was used to prepare HPC-Pen106 ASDs and tetrahydrofuran was used to prepare CA Sub ASDs. A polymer blend ASD was prepared with 10% enzalutamide, 85% PVPVA, and 5% CA Suberate in a solvent mixture of 50% DCM and 50% methanol. A Buchi Rotovapor – R (New Castle, Delaware) with a Yamato BM 200 (Tokyo, Japan) water bath maintained at 25ºC was used to prepare the ASDs, followed by additional drying under vacuum at 35ºC for 1 hour to remove residual solvent. Samples were then ground to a powder using a mortar and pestle and stored in a desiccator prior to use.

3.3.4   In vitro Experiments

3.3.4.1   Nucleation Induction Time Determination

The average time to detect the onset of crystallization for supersaturated solutions of enzalutamide was determined in pH 6.5 50 mM phosphate buffer containing pre-dissolved polymer using an *in situ* UV dip probe as described by Mosquera-Giraldo *et al*[9]. The nucleation induction time i.e. the time when the first signs of crystallization could be detected, was determined as the point where there was an observed decrease in the absorbance maximum and a concurrent increase in the baseline signal. For enzalutamide the absorbance maximum is 237 nm and the baseline wavelength used was 446 nm. Some polymers did not readily dissolve in buffer, thus 1-10 ppm of polymer dissolved in an organic solvent was added to the solution to disperse/dissolve the polymer. Next, 245 µL of methanolic solution of 10 mg/mL enzalutamide was added to 35 mL of the polymeric solution magnetically stirred at 300 rpm and maintained at 37ºC, leading to an initial enzalutamide concentration of 70 µg/mL. The experiments were performed in triplicate.

3.3.4.2   Mass Flow Rate in Side-by-Side Diffusion Cell

The mass flow rates of enzalutamide formulations were measured using the method described in Section 2.3.2.8. In brief, ASDs were dissolved for 1 hr in 30 mL of pH 6.5 50 mM phosphate buffer, 37°C, prior to transfer to the donor compartment of side-by-side diffusion cell (PermeGear, Hellertown, PA). The donor compartment was separated from the receiver compartment by a

regenerated cellulose dialysis membrane with MW cutoff of 6-8 kDa (Spectra/Por 1, Spectrum Laboratories Inc., Rancho Dominguez, CA). The receiver compartment contained 30 mL of buffer and samples of 75 µL were taken every 5 minutes and analyzed via the high performance liquid chromatography (HPLC) method described previously in Section 2.3.2.8. The apparatus was maintained at 37°C and experiments were performed in triplicate.

3.3.5   In vivo Studies

In vivo studies were performed with male Sprague-Dawley rats purchased from Charles River Laboratories (Wilmington, MA) to determine the *in vivo* absorption and pharmacokinetics of enzalutamide ASDs and SEDDS. The rats had access to food and water throughout dosing. A suspension of each ASDs was prepared one hour prior to dosing, containing 5 mg/mL of enzalutamide, and dosed at 50 mg/kg. Blood samples were obtained in K_2EDTA coated tubes at the following time points after dosing: 15 minutes, 30 minutes, 1 hour, 2 hours, 3 hours, 6 hours, 9 hours, 12 hours, 1 day, 2 days, and 3 days. Similarly, the SEDDS formulations was dosed at 50 mg/kg and samples were taken at the same time points listed previously. The plasma samples were centrifuged at 3,000 g at -4°C for 10 minutes and stored at -15°C. Prior to analysis, the plasma samples were thawed and 10 µL of plasma was added to 275 µL acetonitrile with diclofenac as internal standard. Samples were mixed and centrifuged with the supernatant being retained. The supernatant of each samples was diluted 3-fold with 0.1% formic acid in water. The samples were then analyzed on a Sciex API5500™ mass spectrometer with a Turbo-Ion Spray source (m/z 465 > 209) (Framingham, Massachusetts) with a Fortis Pace C18 5µm, 30 x 2.1 mm column (Fortis Inc., St. John's, Canada) with a 0.1% formic acid in water and 0.1% formic acid in acetonitrile gradient. Analysis was performed with Sciex Analyst™ 1.6.2 software. The standard curves of enzalutamide had a least weighted appropriate regression fit up to $1/x^2$ quadratic and minimum R-squared value of 0.99. The plasma concentration data underwent non-compartmental curve fitting with WinNonlin (Certara, St. Louis, Missouri) to determine the area under curve from 0 to 48 hours (AUC_{0-48}) using the linear trapezoidal rule. The maximum plasma concentration, C_{max}, was found directly from the plasma samples. Additional pharmacokinetic analysis was performed using PKSolver[28], and add-in program for Microsoft Excel. Here, the data were fitted to a one compartment model assuming first order absorption and first order elimination.

3.4   Results

3.4.1   Induction Times

The induction time of enzalutamide at an initial concentration corresponding to approximately 1.5x the amorphous solubility was determined in the presence of 3 different polymer concentrations: 5 μg/mL, 25 μg/mL, and 50 μg/mL, and results are summarized in Figure 3-1. When 70 μg/mL of enzalutamide is added to solution, approximately 42 μg/mL enzalutamide exists as free drug molecularly dissolved in solution and the remaining enzalutamide is present as colloidal amorphous aggregates. Consequently, the polymer needs to inhibit crystallization of free drug in solution, as well as from the amorphous aggregates. Given that the crystalline solubility is 2.9 μg/mL, the supersaturation ratio (S) is the amorphous solubility/crystalline solubility, which is approximately 14.5. In the absence of polymers, the drug crystallized rapidly, with an induction time of ~15 min. HPMCAS inhibited crystallization for at least 16 hours, irrespective of polymer concentration. Three of the novel cellulose derivatives, P177, CA Sub, and ECN50, also inhibited crystallization for >16 h at the highest polymer concentration tested (50 μg/mL). Several polymer inhibited crystallization for >2 h, and can therefore theoretically have a large impact on supersaturation duration *in vivo* where small intestine transit times are typically less than 2 h[29]. The effectiveness was dependent on polymer concentration for some of the polymers, in particular CA Sub; this polymer delayed crystallization for approximately 5 hours at 5 μg/mL and inhibited crystallization for 16 hrs at higher concentrations. In contrast, the effectiveness of several other polymers as crystallization inhibitors (CA 320S Adip, CA Ph, PVPVA, PVP, HPMCAS and HPMC) did not show a dependence on polymer concentration.

The following structural features are common amongst the 4 polymers which most effectively inhibited crystallization at a concentration of 50 μg/mL: 1) cellulose backbone, 2) carbon chain in tether contains branched structures, 3) carboxylate group is located at the terminal end(s) of the tether, and 4) number of carbons in the tether is 6 or less. While these features were common to the most effective crystallization inhibitors, their inclusion does not guarantee that the polymer is effective as seen from evaluation of the structures of MC Adipate, MC-C5-AA-H2, MC-C5-AA-pTSH, EC-C5-AA-H2 0.7, and N50-C5-AA-pTSH. Those polymers had approximately the same effectiveness at delaying enzalutamide crystallization as the commercial polymers, PVP and PVPVA, which are not cellulose based. These observations point to the subtle differences in

structure that can impact crystallization inhibitory behavior, which are not readily apparent from simple comparisons of chemical functionality.

3.4.2 In vivo Rat Studies

ASDs were prepared with two cellulose derivatives namely HPC-Pen106 and CA Sub. These polymers were chosen based upon a consideration of their aqueous solubility as well as their crystallization inhibition properties. CA Sub inhibited crystallization for >16 hours and has an aqueous solubility of 3 mg/mL[8], whereas HPC-Pen106 delayed crystallization for 1 hour but had an aqueous solubility of 43.5 mg/mL[22]. The Hoy solubility parameter was calculated to qualitatively describe the relative hydrophilicity of the cellulose derivatives (Table 3-2). The polar and hydrogen bonding component of the solubility parameter were higher for HPC-Pen106 than CA Sub.

Two different drug loadings, 10% and 50%, were tested for HPC-Pen106 ASDs and one drug loading, 50%, for CA Sub ASDs. The *in vivo* performance of each of these ASDs was compared to two reference formulations, a crystalline suspension, and a formulation that mimics the commercial formulation. The commercial formulation is a self-emulsifying drug delivery system (SEDDS) prepared with Labrasol, a non-ionic surfactant, and has a very low drug loading of only 4.5%.

The 10:90 Enz:HPC-Pen106 ASD resulted in the highest area under the curve (AUC), and had the highest maximum concentration (C_{max}). In contrast, the CA Sub ASD was poorly absorbed yielding a profile that was quite similar to the crystalline slurry, although an extended absorption window as observed and the time until the maximum concentration (T_{max}) was achieved was delayed relative to the crystalline reference (Table 3-3). This also lead to a longer absorption half life (k_{abs}). However, no crystals were observed for the CA Sub ASD in the aqueous suspension for up to 5 hours, based on evaluation with a polarized light microscope, hence the low plasma concentrations cannot be accounted for due to crystallization of the formulation. The trend of C_{max} and AUC was: 10:90 Enz:HPC-Pen106 > 50:50 Enz:HPC-Pen106 > SEDDS> 50:50 Enz:CA Sub = Crystalline Slurry and pharmacokinetic parameters are summarized in Table 3-3.

3.4.3   Diffusion Cell Mass Flow Rate

The mass flow rate of enzalutamide across an artificial membrane was investigated for all ASD formulations to compare the amount of free enzalutamide present in the suspensions dosed in the *in vivo* study and to determine if this correlated with the amount of drug absorbed *in vivo* (Figure 3-3). The highest mass flow rates were observed for solutions derived from dissolution of the 10:90 Enz:HPC-Pen106 and the 50:50 Enz:HPC-Pen106 ASDs. The crystalline slurry control sample and 50:50 Enz:CA Sub ASD had the lowest mass flow rates, almost 5 times lower than the 10:90 HPC-Pen106 ASD.

3.5   Discussion

Enzalutamide crystallizes rapidly from supersaturated solutions, thus, to formulate an effective ASD, a polymer with several key properties is required. The polymer needs to ensure the amorphous form of the drug is produced during the manufacturing step, stabilize the amorphous drug in the solid-state for the duration of the product shelf-life, enhance the drug dissolution rate relative to the crystalline form, and delay crystallization from the supersaturated solution formed upon dissolution. To enhance the dissolution rate of a hydrophobic drug such as enzalutamide, the polymer must be sufficiently hydrophilic to dissolve in a reasonable timeframe, enabling release of the drug into the medium. This consideration suggests that more hydrophilic polymers may make the best ASD polymers. However, extremely hydrophilic polymers are typically not good crystallization inhibitors, whereby amphiphilic polymers have been found to be more effective[30,31]. This observation can be rationalized by considering that, in an aqueous environment, drug-polymer hydrogen bonding interactions are unlikely to be the predominant mechanism of interaction, due to competition from water, and thus hydrophilic polymers are likely to preferentially interact with water. Indeed, recent molecular dynamics simulations suggest that cellulose derivatives interact with high log P drugs in aqueous solution through the hydrophobic substituents on the cellulose backbone. However, polymers lacking sufficient hydrophilic groups tend to self-interact in water, rather than forming drug-polymer interactions[9], thus hydrophilic groups are also needed to interact with water and solvate the polymer. Therefore, the polymer must contain the "right balance" of hydrophobic and hydrophilic substituent groups be an effective polymer for ASD formulations. Efforts are underway to fully elucidate this balance, but it is becoming increasingly clear that

apparently small changes in chemical structure can lead to large differences in properties such as effectiveness of a crystallization inhibitor[9] .

The balance between properties that lead to an effective ASD polymer are exemplified in this study. First, the ability of structurally diverse polymers to delay enzalutamide crystallization from supersaturated solutions can be considered. Delaying crystallization from a supersaturated solution is a key requirement for an ASD polymer since many drugs will readily crystallize, however, one unresolved questions is: over what timeframe must this inhibition persist to lead to improved bioavailability? Clearly, given that gastrointestinal transit occurs over several hours, it might be inferred that an extended inhibition duration would lead to improved absorption. However, for many drugs, the window of absorption is actually quite short, in particular if absorption only occurs in a specific region of the gastrointestinal tract. Out of the 24 polymers tested (Table 3-1), 4 inhibited crystallization for longer than 5 hours, ample time to enable transit from the stomach to, and through the small intestine. These were HPMCAS, CA Sub, P177, and ECN-50. However, virtually all of the polymers showed some inhibitory effect. Since there were no obvious chemical or structural features that correlated with crystallization inhibition among the group of compounds tested, screening studies such as these are essential to identify leading polymer candidates. Intuitively, there is an expectation that polymers which inhibit crystallization for longer periods of time will be better ASD polymers, however, this ignores other important polymer characteristics discussed above. Hence, while screening for crystallization inhibition is important, it should clearly be combined with other *in vitro* tests to better identify new polymers suitable for ASD applications. Since the most appropriate *in vitro* tests are still under discussion, correlation to *in vivo* studies provides essential feedback on the development of the appropriate surrogate tests.

Importantly, we note from the *in vivo* studies, that a polymer which is a less effective crystallization inhibitor, namely HPC-Pen 106, leads to substantially improved absorption relative to the extremely effective crystallization inhibitor, CA Sub. This result highlights that there is indeed an interplay between effectiveness as a crystallization inhibitor and other key polymer properties, most notably polymer solubility in this instance. HPC-Pen106 has an aqueous solubility of 43.5 mg/mL[22] but delayed crystallization for only 1 hour. Conversely, CA Sub inhibited crystallization for 16 hours but has an aqueous solubility of approximately 3 mg/mL[8]. HPC-Pen contains a C5

side chain terminated by a COOH group while CA Sub has a similar tether in terms of the terminal functional group, but contains a C8 chain. The DS with respect to the COOH group is similar; 1.06 vs 0.9 for HPC-Pen versus CA Sub. The difference in the polymer solubility presumably accounts, in part, for the different levels of molecularly dissolved drug that evolves following dissolution. Molecularly dissolved drug can be evaluated using flux measurements to evaluate the rate of mass transfer across a membrane. It is generally accepted that only free drug is available for membrane transport, and that flux is directly proportional to the free drug concentration. Herein, the flux measurements (Figure 3-3) suggest that the amount of free drug evolved from the Ca Suberate dispersion is similar to that obtained from dissolution of the crystalline form, correlating well with the *in vivo* data where the AUC values for these two systems are comparable. Since no drug crystallization was observed for the Ca Sub ASD, the low free drug concentration can be attributed to the low polymer solubility combined with strong drug-polymer interactions in the matrix[19]. The low free drug concentration observed in the flux experiment was confirmed by conducting a release study, which showed that the maximum drug concentration attained was only ~3 µg/mL, which is very close to that obtained by dissolving crystalline drug (Figure 4). The polymer solubility alone cannot account for the low extent of drug release since the polymer has sufficient solubility to completely dissolve in solvent.   In contrast, much higher flux values are seen for the two HPC-Pen106 dispersions, and correspondingly, much higher AUC values are obtained (Table 3-3). Thus, the flux measurements on the various formulations appear to be a good in vitro surrogate for rank ordering *in vivo* performance.

The excellent *in vivo* performance of the dispersions formulated with HPC-Pen106 warrants further discussion, given the relatively poorer performance of this polymer as a crystallization inhibitor in our screening experiments. First, it should be noted that the local environment *in vivo* after dosing is very different from our lab experiment, in particular in terms of hydrodynamics, as well as fluid composition, where many endogenous substances such as bile salts are present. Both hydrodynamic conditions and bile salts are known to influence crystallization kinetics[32,33], and crystallization may well occur over a longer timeframe *in vivo* relative to in the lab experiment. Second, drug is absorbed following *in vivo* dosing, diminishing the amount of drug remaining in the intestinal compartment, relative to the closed compartment lab experiment. Thus, the rate of absorption relative to the crystallization time is likely to be important. Consequently, if absorption

is faster or occurs on a similar timescale to crystallization, dosing formulations that gives rise to a supersaturated solution, which have a higher rate of membrane transport, will increase the amount of drug reaching the systemic circulation for a drug with solubility limited absorption (assuming no complicating issues such as extensive first pass metabolism and/or efflux). It is of interest to note that the half-life for absorption (estimated from fitting a 1 compartment model to the *in vivo* data , Table 3-3) of the HPC-Pen106 dispersions is ~1hr. This confirms that a substantial portion of the drug is absorbed prior to crystallization. Further, the half-life is similar to the liquid SEDDS formulation (in which the drug is predissolved). This further suggests that dissolution is not the rate limiting step for the HPC-Pen106 dispersions. In contrast, the absorption half-lives for the crystalline suspension and the Ca Sub dispersion are at least twice as long, consistent with lower luminal concentrations and slower dissolution rates. It should also be noted that the dispersion containing a 50% drug loading with HPC-Pen106 has comparable performance to the SEDDS formulation which contains only 4.5% drug loading. This ASD formulation thus offers an advantage in terms of patient compliance in terms of final dosage form size and/or number of dosage units to be consumed, since considerably less excipient is required to achieve a formulation with comparable *in vivo* performance to the commercial formulation

3.6 Conclusion

Several effective solution crystallization inhibitors of enzalutamide were identified from a cohort of newly synthesized cellulose derivatives. Amorphous solid dispersions were subsequently fabricated from one of the most effective crystallization inhibitors, and a less effective, but more water soluble polymer. *In vitro* and *in vivo* tests carried out to characterize the new formulations showed a five-fold improvement in the extent of absorption for the ASD formulation with the polymer that was the less effective crystallization inhibitor, relative to a crystalline control. In contrast, a formulation with the polymer that was a more effective crystallization inhibitor, but which was less soluble, yielded minimal improvements in oral absorption relative to the crystalline control. *In vitro* flux experiments were a useful approach to rank order the various formulations in terms of the rate of membrane transport, which in turn showed a good correlation with the in vivo studies. This study highlights that overall performance of an ASD formulation is a complex interplay of drug and polymer properties.

Table 3-1. Name, structure, and organic solvent used to dissolve polymer in buffer for induction time experiments.

Name	Abbreviation	Structure	Organic Solvent
Hydroxypropyl methyl cellulose acetate succinate MF grade	HPMCAS	R = –H, –CH$_3$, –CH$_2$–CHOH–CH$_3$	None
Hydroxypropyl methyl cellulose E3 grade	HPMC	R = –H, –CH$_3$, –CH$_2$–CHOH–CH$_3$	None
Poly(vinylpyrrolidone) vinyl acetate VA 64	PVPVA		None
Poly(vinylpyrrolidone) K 29/32	PVP		None
Cellulose Acetate Phthalate	CA Ph		None
Hydroxypropyl cellulose	HPC		None
HPC-Pen106-AA-H	HPC-Pen106[22]	DS (-COOH): 1.06	None

Table 3-1 Continued
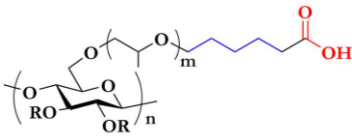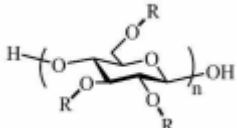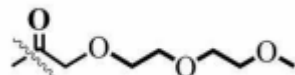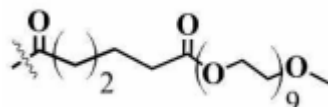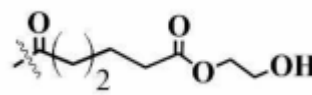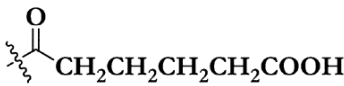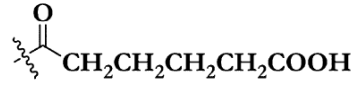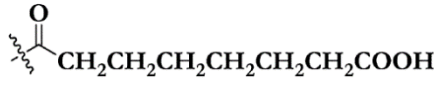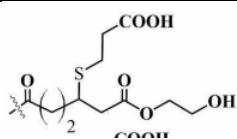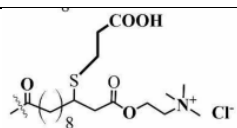
	HPC-Pen282	DS (-COOH): 2.88	
HPC-C3OH-AA-H	HPC-C3OH	(Laura will give me this structure)	
Cellulose Backbone Structure			
Cellulose Propianate Trioxdecanoate 202	CPT		DMF
CA-Pen056-PEG-H2	P126		THF
CA-Pen056-HEA-H	P125		THF
CA Propionate 504-0.2 adipate 0.85	CAP Adp[23]	$CH_2CH_2CH_2CH_2COOH$	THF
CA 320S Adipate 0.67	CA 320S Adip	$CH_2CH_2CH_2CH_2COOH$	THF
CA 320S Suberate 0.9	CA Sub	$CH_2CH_2CH_2CH_2CH_2CH_2COOH$	THF
CA-Pen079-HEA-3MPA	P177[25]		DMSO
CA-Un067-TMA-3MPA	P185-2		DMSO

Table 3-1 Continued
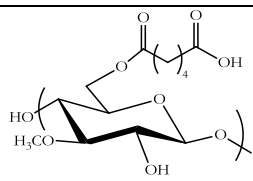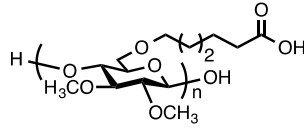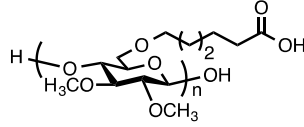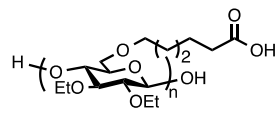
Methylcellulose Adipate	MC Adipate[26]		DMF
MC1.6C5-AA-TSH-MC56º	MC-C5-AA-pTSH		DMF
MC1.6C5-AA-H-MC56º	MC-C5-AA-H2		DMF
Ethyl Cellulose backbone			
ECN2.6C5-AA-H-TSH-N5020º	N50-C5-AA-pTSH	DS_{Et}:2.58	DMSO
ECN2.6C5-AA-H-N5020º	ECN50-C5-AA-H2	DS_{Et}: 2.58	THF
EC2.2C5-AA-H-TSH-MCE*	EC-C5-AA-pTSH	DS_{Et}:2.19	DMSO
EC2.1C5-AA-H-MCC33*	EC-C5-AA-H2 0.7	DS_{Et}: 2.19	THF

Table 3-2. The Hoy solubility parameter of enzalutamide and cellulose based polymers.

Compound	Total solubility parameter (δ_t)	Polar solubility parameter (δ_p)	Hydrogen bonding solubility parameter (δ_h)	Dispersive solubility parameter (δ_d)
Enzalutamide	31.4	4.3	15.2	27.1
HPMCAS-MF	25.8	16.0	14.6	14.1
CA Sub	21.0	12.1	8.2	15.1
HPC-Pen106	23.4	14.4	11.4	14.4

Table 3-3. Pharmacokinetic parameters following dosing of different enzalutamide formulations at 50 mg/kg oral dose.

Formulation	$AUC_{0\text{-inf}}$ ($\mu g \cdot h/mL$)	C_{max} ($\mu g/mL$)	T_{max} (h)	$t_{1/2}$ (h)	$t_{1/2ka}$ (h)
Crystalline Slurry	43.1 (4.6)	1.04 (0.03)	5.0 (1.0)	22.2	1.9
50:50 CA Sub	45 (14)	1.44 (0.34)	12.0 (6.2)	12.1	3.6
SEDDS	283 (11)	9.34 (0.42)	4.0 (1.0)	20.7	1.1
50:50 Pen106	305 (19)	11.7 (0.3)	3.0 (0.0)	14.7	0.9
10:90 Pen106	516 (137)	15.3 (2.1)	2.7 (0.3)	15.1	1.0
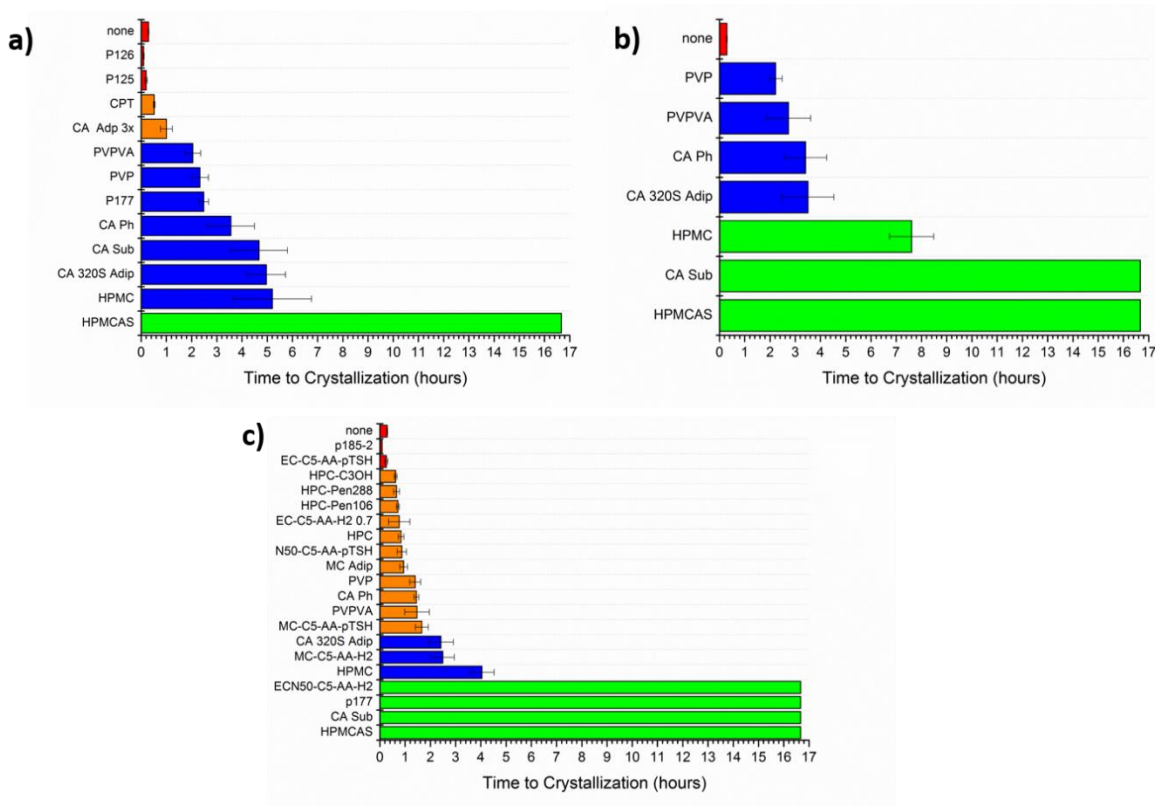
Figure 3-1. The average time to crystallization for supersaturated enzalutamide solutions with an initial concentration of 70 μg/mL in the presence of a) 5 μg/mL, b) 25 μg/mL, and c) 50 μg/mL of pre-dissolved polymer in buffer. Polymers shown had similar induction time as enzalutamide alone, those in orange 30 minutes – 2 hours, blue 2-6 hours, and green greater than 6 hours.
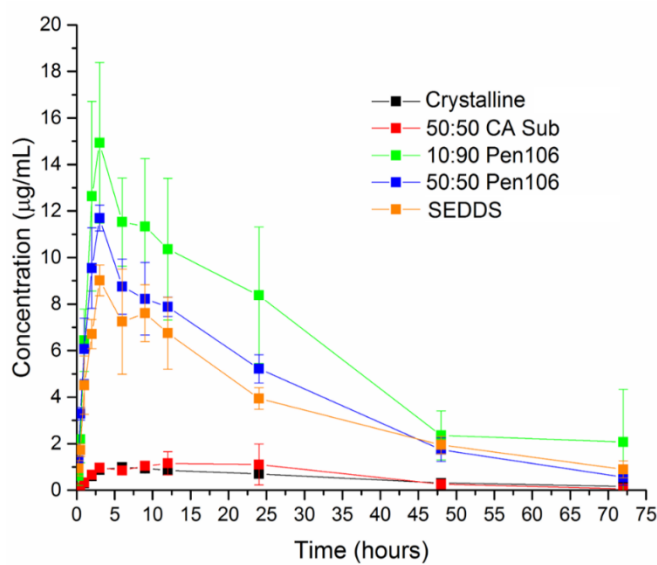
Figure 3-2. The plasma concentration versus time profiles for enzalutamide ASDs prepared with novel cellulose derivatives, SEDDS prepared with Labrasol, and a crystalline slurry.
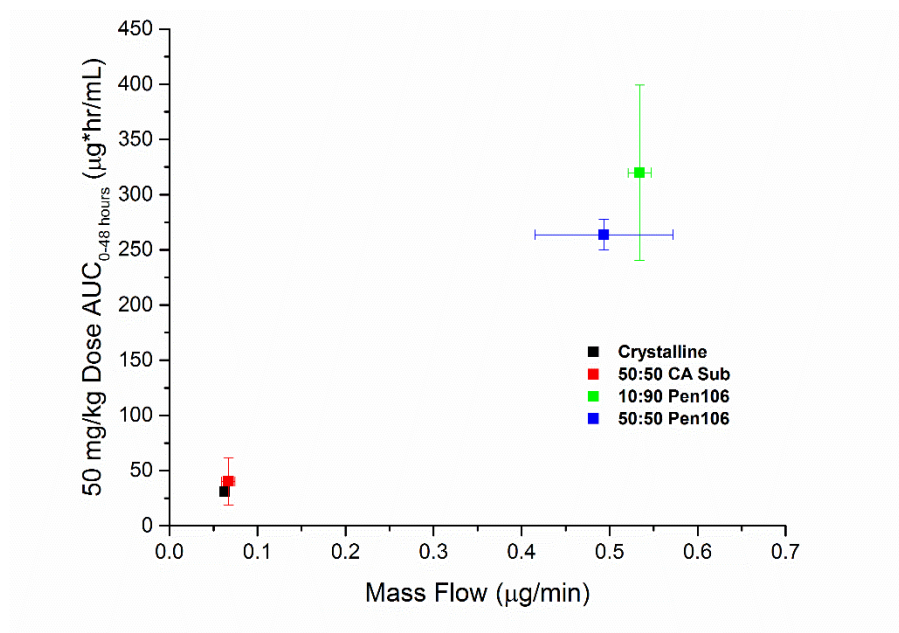
Figure 3-3. The mass flow rate vs AUC (0-48 hours) of enzalutamide formulations. The mass flow rate was measured in a side-by-side diffusion cell whereby a mass of formulation equivalent to 100 µg/mL enzalutamide as added to the donor compartment. A dose of 50 mg/kg was given to the rats with the AUC being reported for 0-48 hours.
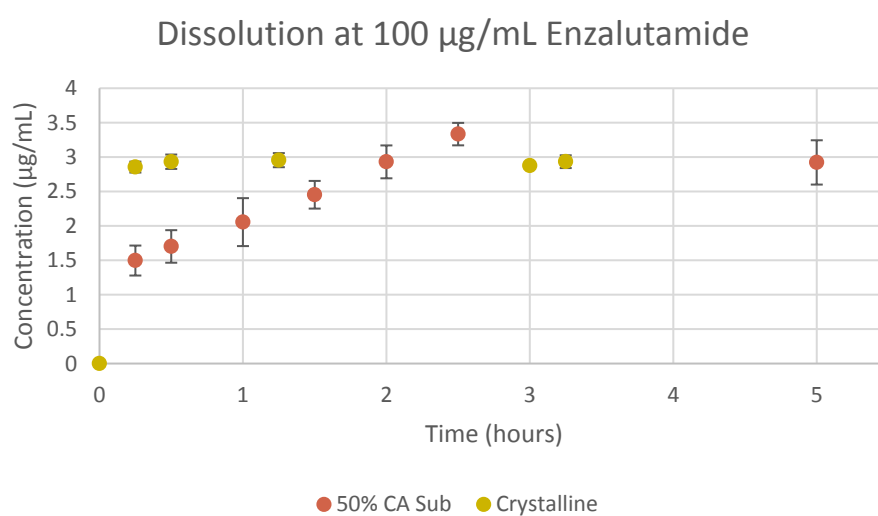
Figure 3-4. The dissolution profile of 50:50 CA Suberate ASD and crystalline slurry.

3.7 References

[1]   L. Z. Benet, "The role of BCS (biopharmaceutics classification system) and BDDCS (biopharmaceutics drug disposition classification system) in drug development," *J. Pharm. Sci.*, vol. 102, no. 1, pp. 34–42, 2013.

[2]   K. P. R. Chowdary and K. V. V Suresh Babu, "Dissolution, bioavailability and ulcerogenic studies on solid dispersions of indomethacin in water soluble cellulose polymers," *Drug Dev. Ind. Pharm.*, vol. 20, no. 5, pp. 799–813, 1994.

[3]   J. M. Miller, A. Beig, R. A. Carr, J. K. Spence, and A. Dahan, "A win-win solution in oral delivery of lipophilic drugs: Supersaturation via amorphous solid dispersions increases apparent solubility without sacrifice of intestinal membrane permeability," *Mol. Pharm.*, vol. 9, no. 7, pp. 2009–2016, 2012.

[4]   D. Law, E. A. Schmitt, K. C. Marsh, E. A. Everitt, W. Wang, J. J. Fort, S. L. Krill, and Y. Qiu, "Ritonavir-PEG 8000 Amorphous Solid Dispersions: In Vitro and in Vivo Evaluations," *J. Pharm. Sci.*, vol. 93, no. 3, pp. 563–570, 2004.

[5]   Y. Shibata, M. Fujii, A. Suzuki, N. Koizumi, K. Kanada, M. Yamada, and Y. Watanabe, "Effect of storage conditions on the recrystallization of drugs in solid dispersions with crospovidone," *Pharm. Dev. Technol.*, 2014.

[6]   J. X. Wu, M. Yang, F. Van Den Berg, J. Pajander, T. Rades, and J. Rantanen, "Influence of solvent evaporation rate and formulation factors on solid dispersion physical stability," *Eur. J. Pharm. Sci.*, 2011.

[7]   G. A. Ilevbare, H. Liu, J. Pereira, K. J. Edgar, and L. S. Taylor, "Influence of Additives on the Properties of Nanodroplets Formed in Highly Supersaturated Aqueous Solutions of Ritonavir," 2013.

[8]   L. I. Mosquera-Giraldo, N. Li, V. R. Wilson, B. L. B. Nichols, K. J. Edgar, and L. S. Taylor, "Influence of Polymer and Drug Loading on the Release Profile and Membrane Transport of Telaprevir," *Mol. Pharm.*, vol. 15, no. 4, pp. 1700–1713, Apr. 2018.

[9]   L. I. Mosquera-Giraldo, C. H. Borca, X. Meng, K. J. Edgar, L. V. Slipchenko, and L. S. Taylor, "Mechanistic Design of Chemically Diverse Polymers with Applications in Oral Drug Delivery," *Biomacromolecules*, vol. 17, no. 11, pp. 3659–3671, 2016.

[10] C. Brough and R. O. Williams, "Amorphous solid dispersions and nano-crystal technologies for poorly water-soluble drug delivery," *International Journal of Pharmaceutics*, vol. 453, no. 1. pp. 157–166, 2013.

[11] Y. Huang and W.-G. Dai, "Fundamental aspects of solid dispersion technology for poorly soluble drugs," *Acta Pharm. Sin. B*, vol. 4, no. 1, pp. 18–25, 2014.

[12] S. Baghel, H. Cathcart, and N. J. O'Reilly, "Polymeric Amorphous Solid Dispersions: A Review of Amorphization, Crystallization, Stabilization, Solid-State Characterization, and Aqueous Solubilization of Biopharmaceutical Classification System Class II Drugs," *Journal of Pharmaceutical Sciences*, vol. 105, no. 9. pp. 2527–2544, 2016.

[13] A. D. Gilley, H. C. Arca, B. L. B. Nichols, L. I. Mosquera-Giraldo, L. S. Taylor, K. J. Edgar, and A. P. Neilson, "Novel cellulose-based amorphous solid dispersions enhance quercetin solution concentrations in vitro," *Carbohydr. Polym.*, 2017.

[14] T. Xie and L. S. Taylor, "Dissolution Performance of High Drug Loading Celecoxib Amorphous Solid Dispersions Formulated with Polymer Combinations," *Pharm. Res.*, vol. 33, no. 3, pp. 739–750, 2016.

[15] Y. Chen, C. Liu, Z. Chen, C. Su, M. Hageman, M. Hussain, R. Haskell, K. Stefanski, and F. Qian, "Drug-polymer-water interaction and its implication for the dissolution performance of amorphous solid dispersions," *Mol. Pharm.*, vol. 12, no. 2, pp. 576–589, 2015.

[16] G. L. B. De Araujo, C. J. Benmore, and S. R. Byrn, "Local Structure of Ion Pair Interaction in Lapatinib Amorphous Dispersions characterized by Synchrotron X-Ray diffraction and Pair Distribution Function Analysis," *Sci. Rep.*, vol. 7, 2017.

[17]   T. Xie and L. S. Taylor, "Improved Release of Celecoxib from High Drug Loading Amorphous Solid Dispersions Formulated with Polyacrylic Acid and Cellulose Derivatives," *Mol. Pharm.*, vol. 13, no. 3, pp. 873–884, 2016.

[18]   C. J. Schram, S. P. Beaudoin, and L. S. Taylor, "Impact of polymer conformation on the crystal growth inhibition of a poorly water-soluble drug in aqueous solution," *Langmuir*, vol. 31, no. 1, pp. 171–179, 2015.

[19]   N. Li and L. S. Taylor, "Tailoring supersaturation from amorphous solid dispersions," *J. Control. Release*, vol. 279, pp. 114–125, 2018.

[20]   A. M. Stewart, M. E. Grass, T. J. Brodeur, A. K. Goodwin, M. M. Morgen, D. T. Friesen, and D. T. Vodak, "Impact of Drug-Rich Colloids of Itraconazole and HPMCAS on Membrane Flux in Vitro and Oral Bioavailability in Rats," *Mol. Pharm.*, vol. 14, no. 7, pp. 2437–2449, 2017.

[21]   P. Berben, J. Brouwers, and P. Augustijns, "The artificial membrane insert system as predictive tool for formulation performance evaluation," *Int. J. Pharm.*, vol. 537, no. 1–2, pp. 22–29, 2018.

[22]   Y. Dong, L. I. Mosquera-Giraldo, J. Troutman, B. Skogstad, L. S. Taylor, and K. J. Edgar, "Amphiphilic hydroxyalkyl cellulose derivatives for amorphous solid dispersion prepared by olefin cross-metathesis," *Polym. Chem.*, vol. 7, no. 30, pp. 4953–4963, 2016.

[23]   N. Kar, H. Liu, and K. J. Edgar, "Synthesis of cellulose adipate derivatives," *Biomacromolecules*, vol. 12, no. 4, pp. 1106–1115, 2011.

[24]   G. A. Ilevbare, H. Liu, K. J. Edgar, and L. S. Taylor, "Understanding polymer properties important for crystal growth inhibition-impact of chemically diverse polymers on solution crystal growth of ritonavir," *Cryst. Growth Des.*, vol. 12, no. 6, pp. 3133–3143, 2012.

[25]   X. Meng, S. Roy Choudhury, and K. J. Edgar, "Multifunctional cellulose esters by olefin cross-metathesis and thiol-Michael addition," *Polym. Chem.*, vol. 7, no. 23, pp. 3848–3856, 2016.

[26] H. C. Arca, L. I. Mosquera-Giraldo, L. S. Taylor, and K. J. Edgar, "Synthesis and characterization of alkyl cellulose ω-carboxyesters for amorphous solid dispersion," *Cellulose*, vol. 24, no. 2, pp. 609–625, 2017.

[27] K. L. Hoy, "New values of the solubility parameters from vapor pressure data," *J. Paint Technol.*, vol. 42, no. 541, pp. 76–118, 1970.

[28] Y. Zhang, M. Huo, J. Zhou, and S. Xie, "PKSolver: An add-in program for pharmacokinetic and pharmacodynamic data analysis in Microsoft Excel," *Comput. Methods Programs Biomed.*, 2010.

[29] S. K. Kim, "Small intestine transit time in the normal small bowel study.," *Am. J. Roentgenol. Radium Ther. Nucl. Med.*, 1968.

[30] G. A. Ilevbare, H. Liu, K. J. Edgar, and L. S. Taylor, "Maintaining supersaturation in aqueous drug solutions: Impact of different polymers on induction times," *Cryst. Growth Des.*, vol. 13, no. 2, pp. 740–751, 2013.

[31] M. J. Jackson, S. J. Toth, U. S. Kestur, J. Huang, F. Qian, M. A. Hussain, G. J. Simpson, and L. S. Taylor, "Impact of polymers on the precipitation behavior of highly supersaturated aqueous danazol solutions," *Mol. Pharm.*, vol. 11, no. 9, pp. 3027–3038, 2014.

[32] J. Chen, L. I. Mosquera-Giraldo, J. D. Ormes, J. D. Higgins, and L. S. Taylor, "Bile Salts as Crystallization Inhibitors of Supersaturated Solutions of Poorly Water-Soluble Compounds," *Cryst. Growth Des.*, vol. 15, no. 6, pp. 2593–2597, 2015.

[33] N. Li, L. I. Mosquera-Giraldo, C. H. Borca, J. D. Ormes, M. Lowinger, J. D. Higgins, L. V. Slipchenko, and L. S. Taylor, "A Comparison of the Crystallization Inhibition Properties of Bile Salts," *Cryst. Growth Des.*, vol. 16, no. 12, pp. 7286–7300, 2016.

CHAPTER 4.   POLYMER LOCATION DURING GLASS-LIQUID PHASE SEPARATION

4.1   Abstract

Amorphous solid dispersions (ASDs), which consist of a drug dispersed at a molecular level in a polymeric matrix, are increasingly being applied to improve the *in vivo* performance of poorly water-soluble drugs delivered orally. The polymer is a critical component, playing several roles including facilitating drug release from the ASD, as well as delaying crystallization from the supersaturated solution generated upon dissolution. Certain ASD formulations dissolve to produce colloidal amorphous aggregates. The interaction of polymer with these aggregates is poorly understood but is thought to be important for inhibiting crystallization in these systems. In this study, the impact of ionic polymers on the crystallization of enzalutamide from supersaturated solutions containing different amounts of amorphous aggregates was evaluated. The amount of polymer associated with the drug aggregates was also determined. When comparing hydroxypropylmethyl cellulose acetate succinate and Eudragit E PO ®, it was found that a similar amount of polymer associated with the amorphous aggregates. However, the crystallization tendency and physical properties of the amorphous aggregates, varied between the two polymers. In conclusion, in supersaturated solutions containing amorphous aggregates, association of a polymeric inhibitor with the aggregate is not the only required criterion to inhibit crystallization.

4.2   Introduction

Over the past decade there has been increasing interest in gaining an improved mechanistic understanding of the enhanced *in vivo* performance often observed for amorphous solid dispersions (ASDs) compared to crystalline drug, and in some instances, other solubility enhancing formulations. This interest has been driven by the large number of poorly aqueous soluble drugs in development[1]. For ASDs, the main excipient combined with the drug is a polymer, and in some instances, a surfactant is added[2]. The role of the polymer is to inhibit crystallization of the amorphous drug from the solid formulation during storage, to facilitate drug release, and for many drugs, to delay crystallization from the supersaturated solution generated upon dissolution. The

latter property is particularly important for drugs that crystallize from solution over biologically relevant time frames. Surfactants are typically added to improve processing and/or drug release. Ideally, ASD dissolution is rapid relative to the rate of absorption across the gastrointestinal membrane, and leads to the formation of a supersaturated solution; supersaturation is known to drive membrane transport. If the concentration of the drug in solution is below the amorphous solubility i.e. below the maximum achievable free drug concentration, the system is comprised of dissolved polymer and drug, and undissolved ASD. If, however, the ASD dissolves and results in a concentration that exceeds the amorphous solubility, amorphous aggregates can form as a result of liquid-liquid or glass-liquid phase separation (LLPS or GLPS)[3–6]. LLPS occurs if the resultant amorphous aggregates are above their glass transition temperature (Tg), whereas the process is termed GLPS if the amorphous aggregates are glassy, that is below their Tg. It is considered desirable that the drug undergo LLPS/GLPS following release from the ASD, since the amorphous aggregates that form in solution can act as a depot, rapidly replacing drug transferred across the membrane, maintaining the supersaturation at a maximum value, leading to high and sustained membrane flux[5,6]. The *in vivo* benefits of amorphous aggregates can only be realized if crystallization can be avoided. Thus, ASD dissolution is a complex process since the drug can undergo different phase transformations and exist in several different speciation states; molecularly dissolved drug, amorphous aggregates, undissolved ASD particles, or in crystalline form (Figure 2-9).

In a solution containing amorphous aggregates, the chemical potential of the drug in the aggregate and in the bulk solution phase is the same, and is higher than for the corresponding crystal[7]. Hence there is a driving for crystallization, and crystallization can occur in either the aggregates, or from the aqueous-rich phase. Given the important role of the polymer as a crystallization inhibitor, it is critical to understand the distribution of the polymer between the bulk aqueous solution and the drug aggregates. Raina *et al*. demonstrated that chemically diverse polymers showed variations in their distribution between the aqueous phase and the drug-rich aggregates, noting that the polymer distribution trended with the polymer hydrophobicity; hydrophilic polymers were found predominantly in the aqueous phase, amphiphilic polymers distributed between both phases while hydrophobic polymers were mainly present in the drug-rich phase[8]. They further noted that polymers that were effective crystallization inhibitors distributed between both aqueous and drug-

rich phases. Ueda and coworkers made a similar observation when studying a group of chemically related polymers and suggested that the extent of crystallization inhibition was related to the amount of polymer associated with the amorphous drug aggregates[9]. More recently, Wang et al have noted that the amount of polymer that coprecipitates with the drug correlates with the ability of the polymer to maintain solution supersaturation[10].

The purpose of this study was to further explore the impact of polymers on the crystallization tendency of highly supersaturated solutions containing amorphous drug aggregates, specifically exploring the relationship between crystallization and the amount of polymer interacting with the drug aggregates. To achieve this goal, the crystallization induction times for supersaturated solutions of enzalutamide were measured for solutions containing different amounts of colloidal drug species, with varying amounts of polymers, focusing on hydroxypropyl methylcellulose acetate succinate and Eudragit E PO ® as examples of negatively and positively charged polymers respectively at intestinal pH conditions. The amount of polymer associated with the drug-rich aggregates versus the amount remaining in aqueous solution was determined via chemical analysis. Transmission electron microscopy and fluorescence spectroscopy were used to further study the system.

4.3   Materials and Methods

4.3.1   Materials

4.3.1.1   Drug and Polymer Structures

Hydroxypropyl methylcellulose acetate succinate MF grade (HPMCAS) and Eudragit E PO ® were donated by Shin-Etsu Co. Ltd (Tokyo, Japan) and Evonik (Essen, Germany) respectively. The novel cellulose derivative, CA-Pen079-HEA-3MPA[11] (P177), was synthesized by the Edgar group as described previously. The molecular structures of these polymers, as well as that of the model drug, enzalutamide (ChemShuttle, Hayward, CA), are shown in Figure 4-1. Phenol, sulfuric acid, acid orange V, and chloroform were purchased from Fisher Scientific (Hampton, NH).

4.3.1.2 Dansylated HPMCAS Synthesis

Synthesis of dansylated 2-bromoethyl amine was achieved by slowly adding triethylamine (5.6 mL, 40 mmol) to a solution of dansyl chloride (5.0 g, 18.5 mmol) and 2-bromoethyl amine HBr (3.8 g, 18.5 mmol) in DMF (60 mL). The resulting solution was stirred overnight, and was then quenched with water. The product was extracted with EtOAc. The combined organic layers were washed with sat. aq. NaHCO3, followed by brine and were dried (MgSO4). The crude product was purified by column chromatography (1:1 EtOAc/hexanes) to give 1.16 g of pure N-dansyl-2-bromoethyl amine (17% yield). H1-NMR (300 MHz, CDCl3) d 8.2 – 8.8 (m, 3 H), 7.2 – 7.7 (m, 3 H), 5.9 (t, 1 H), 3.6 (t, 2 H), 3.3 (m, 2 H), 2.9 (s, 6 H)

Triethyl amine (8.6 mL, 62 mmol) was added to a solution of HPMCAS-MF (12 g) in DMF (70 mL). A solution of N-dansyl-2-bromoethyl amine (1.16 g, 3.1 mmol) in DMF (30 mL) was added, and the resulting solution was stirred for 3 days. The reaction mixture was poured into water (1.5 L) with vigorous stirring. The solution was acidified with 10% aq. HCl then the precipitate was collected by filtration, washed with water and dried to give 9.41 g of danylated HPMCAS. The quantification of the amount of dansyl attached to HPMCAS is described in Figures 4-.

4.3.1.3 Characterization of Dansylated HPMCAS

^{1}H and ^{13}C NMR were obtained using a Bruker Advance II spectrometer at 500 MHz and were analyzed using CD$_3$CN and C$_5$D$_5$N. ^{1}H NMR samples were analyzed in 10 mg mL^{-1} solutions in CD$_3$CN (δ 1.94 ppm) or C$_5$D$_5$N (δ 7.19, 7.55, and 8.71) with ^{13}C NMR in 50 mg mL^{-1} at 25 C in 5 mm o.d. tubes with a minimum of 32 and 5000 number of scans, respectively. A full description of the analysis is provided in the Supplemental Information.

Determination of DS (Dan-ethylene) for derivatized HPMCAS was a two step process by which the number of hydroxypropyl (HP) propylene oxide units (n = MS (propylene oxide)) were necessary to pre-determine due to its difficult to control oligomerizing nature during HPMCAS synthesis using the following equation:

$$\frac{I_{Backbone\ region}}{I_{CH3}^{HP}} = \frac{3H*DS_{CH3} + 3H*DS_{CH2,CH}^{HP}*n + 3H*DS_{Ac.} + 4H*DS_{S.}}{3H*DS_{CH3}^{HP}*n} \qquad (4\text{-}1)$$

This MS is equal to the integration number of methyl groups present on HP, and will be denoted as I_{CH3}^{HP}. This value was determined using AS-LG-grade HPMCAS by ^{1}H NMR in deuterated acetonitrile (CD$_3$CN), as well as the reported DS values for methoxy, acetyl, succinyl, and HP units (Figure 4-2). The MS value calculated from Figure 4-2 was incorporated into the overall number of protons present in the cellulosic backbone region of HPMCAS, 'b'. The integration of the protons in the cellulosic region (HPMCAS overlapping Dan-ethylene protons) and the ratio of the new and downfield aromatic proton peaks present on Dan-ethylene was used to calculate final DS (Dan-ethylene):

$$\frac{ax}{b+cx} = \frac{1}{d} \qquad (4\text{-}2)$$

where a is the number H of substituent away from backbone region, c is the number of H in cellulose backbone of new substituent, and d is the new integration of backbone region after setting ax integration to 1.

4.3.2 Methods

4.3.2.1 Nucleation Induction Time Measurements

The induction time i.e. the average time to detect the first signs of crystallization, was taken as the point where there was a decrease in absorbance at 237 nm, with a concurrent increase in the signal at the non-absorbing of 446 nm. Experiments were performed at varying initial concentrations of enzalutamide: 30, 35, 40, 45, 70, and 120 µg/mL, which represent concentrations below and above the concentration where aggregate formation occurs (GLPS, which is 42 µg/mL for the experimental conditions employed). Based on the GLPS concentration of 42 µg/mL, the solutions prepared at an added concentration of 45, 70 and 120 µg/mL contain 3, 28 and 78 µg/mL of amorphous aggregates and 42 µg/mL of molecularly dissolved enzalutamide. A stock solution of 10 mg/mL enzalutamide in methanol was aliquoted into 35 mL of 50 mM phosphate buffer, pH 6.5 containing pre-dissolved polymer. Eudragit E PO grade and HPMCAS MF grade were directly pre-dissolved in the buffer while P177 was initially dissolved in dimethyl sulfoxide prior to adding to buffer, such that the final concentration of organic solvent was 1ppm. The following concentrations of polymer were tested: 30, 35, 40, 45, 70, and 120 µg/mL. All induction time experiments were performed in triplicate.

4.3.2.2   Colloidal Amorphous Aggregate Size and Surface Charge

The size and zeta potential of amorphous aggregates at varying concentration of enzalutamide and polymer were determined using dynamic light scattering (DLS) and zeta potential measurements respectively. A 10 mg/mL stock solution of enzalutamide in methanol was added to a solution containing either P177, HMPCAS, or Eudragit E PO ® pre-dissolved in pH 6.5 50 mM phosphate buffer, to generate solutions containing different concentrations of drug and polymer. Samples were stirred at 300 rpm at 37°C for 5 minutes. Folded capillary zeta cell were used to measure zeta potential and particle size on a Nano-Zetasizer (Malvern Instruments, Westborough, MA) with dispersion technology software. The kinematic viscosity of solutions containing various concentrations of HPMCAS and Eudragit E PO ® solutions were determined at 37°C using a Vibro viscometer SV-10 (A&D Ltd., Japan) and this value was input into the DLS instrument software to determine the hydrodynamic diameter of the particles. For all measurements, a refractive index of 1.33 was used and all samples had a PDI < 0.5. Experiments were performed in triplicate.

4.3.2.3   Polymer Distribution in Different Phases

4.3.2.3.1   Colorimetric Experiments

The amount of HPMCAS in bulk aqueous solution versus that associated with amorphous aggregates of enzalutamide was determined by separation of the two phases and then determination of HPMCAS amount using a colorimetric assay. Solutions containing 120 μg/mL enzalutamide were generated in the presence of 25, 50, 100, 250, and 500 μg/mL HPMCAS. Enzalutamide was aliquoted in 15 mL of 25 μg/mL HPMCAS pre-dissolved in pH 6.5 50 mM phosphate buffer to generate an enzalutamide concentration of 120 μg/mL. This system was stirred at 300 rpm for 15 minutes at 37°C, and then additional HPMCAS was added to increase the polymer concentration to 50, 100, 250, or 500 μg/mL, and stirred for an additional 60 minutes. 2 mL samples were then removed and centrifuged at 21.1 g for 40 minutes at 37°C in a Legend Micro 21R Centrifuge (Fisher Scientific, Hampton, New Hampshire). The pellet was re-dissolved in 100 μL methanol and diluted to 2 mL with pH 6.5 phosphate buffer. The supernatant initially containing 250 μg/mL or 500 μg/mL HPMCAS was diluted 5-fold and 10-fold respectively with buffer. 50 μL of phenol and 5 mL of sulfuric acid were added to all samples, i.e. both the supernatant and re-dissolved pellet. Samples were kept at room temperature for 1 day to allow the color to develop. The absorbance at 490 nm was measured on a Varian Cary 300 Vio UV-visible Spectrophotometer

(Palo Alto, California). Standards were prepared with HPMCAS over a concentration range of 5-100 µg/mL. Experiments was performed in triplicate.

Similarly, the amount of polymer associated with enzalutamide aggregates was determined for Eudragit E PO ® by colorimetry. 2 mL samples were prepared at 50 and 100 µg/mL of Eudragit E PO ®. After addition of 10 mg/mL enzalutamide methanolic solution into polymer pre-dissolved in buffer to yield a concentration of 70 µg/mL, the samples were vortexed for 10 seconds. Samples were centrifuged at 21.1 g for 40 minutes at 37°C in a Legend Micro 21R Centrifuge (Fisher Scientific, Hampton, New Hampshire). The supernatant was diluted with 4 mL of chloroform. The pellet was re-dissolved in 4 mL chloroform and 2 mL of buffer. Both the supernatant and pellet solutions were vortexed prior to addition of 4 mL of 200 µg/mL acid orange V in 0.1M NaCl. Samples were then vortexed again and then kept stationary to allow separation of chloroform from the aqueous solution. The chloroform layer which contains acid orange complexed with Eudragit E PO ® was analyzed at an absorbance of 480 nm on a Varian Cary 300 Vio UV-visible Spectrophotometer (Palo Alto, California). Standards were prepared with Eudragit E PO ® at a concentration range of 0-100 µg/mL. All standards and samples were prepared in triplicate.

4.3.2.3.2 Fluorescence Spectroscopy

The fluorescence spectra of enzalutamide in the presence of dansylated HPMCAS (HPMCAS with a dansyl fluorophore attached) were used to evaluate the interaction of HPMCAS with the amorphous drug aggregates. Samples of enzalutamide with dansylated HPMCAS were analyzed on a Shimadzo (insert info). Enzalutamide ($20 - 120$ µg/mL) was added to dansylated HPMCAS (50 and 100 µg/mL) in buffer and subsequently vortexed for 5 seconds prior to measurements. The excitation wavelength was 380 nm with an excitation slit width of 5 and emission slit width of 5.

4.3.2.3.3 Transmission Electron Microscopy Imaging

An FEI Tecnai G 20 electron microscope (FEI, Hillsboro, Oregon, USA) equipped with a LaB6 source and operated at 200 keV was used to acquire bright field (BF) transmission electron micrographs. Samples were prepared by pipetting an aliquot of the liquid sample onto 300 mesh ultra-thin carbon coated copper TEM grids with a thickness of 3-4 nm (SPI supplies, West Chester, PA) placed on a cellulose filter paper. The solution was allowed to cascade down the surface of

the tilted grid as described before. [1] Elemental analysis was performed to identify the drug and the polymer using a X-MAX silicon drift detector (SDD) energy dispersive spectroscopy (EDX) detector (Oxford Instruments, Oxfordshire, UK). Fluorine was used as the distinguishing element since enzalutamide contains four fluorine atoms while the polymers do not. The beam spot size was chosen to be 4 to achieve the highest possible spatial resolution and a reasonable x-ray count rate. Image processing, including fast Fourier transform (FFT) was performed using Gatan Microscopy Suite Software®. FFT processing was utilized herein to confirm the presence of crystalline enzalutamide. Three grids of each sample were tested.

4.4   Results

The crystallization inhibition potential of a given polymer in the presence and absence of amorphous aggregates has not been extensively explored, but is of importance given the likely propensity of many ASD formulations to form these species during dissolution[12–15]. For drugs that crystallize over biologically relevant time frames, the polymer needs to inhibit crystallization of drug in bulk solution, as well as from any amorphous aggregates formed. As shown in Table 4-1, enzalutamide crystallizes within 15 minutes in the absence of polymer, both for supersaturated solutions that are free of aggregates, as well as from solutions containing aggregates. Enzalutamide is thus a fairly rapidly crystallizing compound and crystallization inhibitors are necessary to sustain supersaturation.

Figures 4-4, 4-5, and 4-6 compare the impact of different concentrations of various polymers on the induction times of supersaturated solutions free of amorphous aggregates (30-40µg/mL), and those containing different amounts of aggregates (solutions of concentration greater than 42 µg/mL initially contain amorphous aggregates prior to crystallization). It is apparent from Figures 4-4, 4-5, and 4-6 that the effectiveness of the various polymers at preventing crystallization depends on polymer type, amount, as well as the initial concentration of the enzalutamide solutions and hence the amount of amorphous aggregate formed. The polymers extend the supersaturation duration, by a few minutes or for several hours, depending on the system evaluated. It is particularly notable that Eudragit E PO ® is only effective at inhibiting crystallization at higher polymer concentrations and in solutions where there are few or no amorphous drug aggregates. P177 is an effective crystallization inhibitor for enzalutamide solutions that do not contain aggregates, and at higher

polymer concentrations for solutions containing a moderate amount of drug aggregates. At higher concentrations (≥50 µg/mL) HPMCAS is a highly effective crystallization inhibitor, maintaining supersaturation in enzalutamide systems containing a large amount of drug aggregates, as well as those without aggregates for several hours. These observations highlight quite dramatically that the perceived effectiveness of a given polymer as a crystallization inhibitor is highly dependent on the extent to which the polymer is "challenged" in terms of its concentration, and the initial drug concentration and hence the amount of aggregates. In the presence of drug aggregates, it is clearly more difficult to delay crystallization by a polymer, relative to in the absence of aggregates. Therefore, when evaluating polymers, concentrations of both drug and polymer should be meaningful relative to the likely final concentrations generated upon dissolution of the dosage form. Given the differences observed between the polymers in terms of their effectiveness as crystallization inhibitors in the systems with and without drug aggregates, the distribution of the polymer between the bulk aqueous phase and the drug-rich amount was assessed for Eudragit E PO ® and HPMCAS. Based on literature reports[9,10], the expectation was that the poor inhibitory impact of Eudragit E PO ® in the presence of the drug-rich aggregates might arise because of a low concentration of polymer associated with the drug-aggregates.

Table 4-2 and Table 4-3 show the amount of polymer associated with each of the two phases, bulk aqueous solution and drug-rich aggregates. It is apparent that the solution phase is depleted of polymer, and that a considerable amount of polymer is associated with the drug-rich phase. It should be noted that, in the absence of drug, polymer aggregates that could pelleted by centrifugation were formed at concentrations at or above 250 µg/mL of HPMCAS (Table 4-4). Hence, meaningful interpretations could only be made for HPMCAS concentrations lower than then concentration. For systems containing an initial Eudragit E PO ® or HPMCAS concentration of 50 -100 µg/mL, the resultant drug-rich pellet contained approximately 20% w/w of polymer, with no difference in polymer amount being observed depending on polymer type.

Given the amount of polymer associated with drug-rich phase, it was important to determine if the amorphous solubility was reduced. A second component that mixes substantially with the drug-rich phase would be expected to reduce the value of the amorphous solubility[16–20]. However, it was found that the amorphous solubility of enzalutamide in the presence of 500 µg/mL HPMCAS

or 100 µg/mL Eudragit E PO ® was the same as for enzalutamide in buffer, namely 42 µg/mL. This suggests that the polymer that is associated with the drug-rich phase is probably not intimately mixed with the drug, and therefore does not impact the thermodynamic activity of the drug-rich phase. To further investigate the polymer location, TEM imaging was performed.

TE micrographs for HPMCAS and enzalutamide are shown in Figure 4-7. Approximately spherical enzalutamide droplets of diameter ranging from ~100-200nm are present and surrounded by regions of polymer. This was confirmed by the elemental composition of each of those regions using EDX. Fluorine (present in enzalutamide but not polymer) was used here to locate each component. The analyzed spherical nanospecies displayed 24 ± 6 % fluorine demonstrating that they are drug-rich, while the surrounding regions displayed 4 ± 2 % fluorine indicating that they are polymer-rich. Based on the image, HPMCAS appears to be associated with the drug-rich droplet perimeter, but not mixed with the droplet. FFT of the droplets shown in Figure 4-7a did not exhibit any order indicating that those droplets were amorphous. On the other hand, Figure 4-7b indicates the presence of crystal planes which was confirmed using the FFT analysis as displayed in Figure 4-7c. The FFT, in Figure 4-7c, indicates the presence of crystals in multiple orientations. It should be highlighted that polymer was not visible around the crystallized drug droplets. When a higher concentration of HPMCAS was used, no crystallization was observed in the sample (Figure 4-7d) and the presence of polymer aggregates of approximate size 20-50 nm are apparent. In the case of the Eudragit E PO ®-enzalutamide system, the size range of the droplets is much larger, with agglomerates of the droplets being visible. Again, the polymer appears to be associated with the periphery of the drug. Figure 4-8b shows an agglomerate which appears to have undergone crystallization in the presence of this polymer.

The TEM images suggest that the polymer associates with the drug-rich aggregates at the drug-water interface. Therefore, it would be anticipated that the zeta potential would change in the presence of the polymer. This was found to be the case whereby the surface charge of amorphous aggregates generated during GLPS varied with polymer (Figure 4-9). In the absence of polymers, the zeta potential was negative. When HPMCAS was present, the zeta potential became more negative, while with Eudragit E PO ®, the zeta potential was large and positive (Figure 4-9). In order for colloidal species, such as amorphous aggregates, to be physically stable through

electrostatic repulsion the zeta potential of the colloidal species should be less than -30 mV or greater than +30 mV [21–23]. If the surface charge is between -30 mV and +30 mV the solution has the propensity to ripen over time. Thus none of the polymers stabilized enzalutamide amorphous aggregates solely through electrostatic stabilization (Figure 4-9).

The size of the colloidal species in the absence and presence of polymer was also of interest, especially in terms of correlation to the TEM images, recognizing that DLS measures the hydrodynamic diameter. Polymer interaction with the droplet surface would be expected to impact the size measured, especially if agglomeration is prevented. In samples prepared with drug alone, the size of the drug-rich droplets increased rapidly with increasing drug concentration, most likely due to the agglomeration of the glassy droplets. The presence of polymer impacted the hydrodynamic diameter of the colloidal species, Figure 4-10. With HPMCAS, the size of the colloidal species was 200-400nm. For Eudragit E PO ®, the droplets ranged in size between approximately 200 and 1100 nm. Eudragit E PO ® was not tested above a drug concentration greater than 70 µg/mL due to rapid crystallization. The smallest amorphous aggregates (80 nm) were observed for 70 µg/mL enzalutamide and 50 µg/mL HPMCAS. An approximately inverse relationship was observed for the size of amorphous aggregates and the concentration of Eudragit E PO ® in 70 µg/mL enzalutamide. A reduction of amorphous aggregates size was only observed for higher polymer concentrations (50 and 100 µg/mL Eudragit E PO ®) in 70 µg/mL enzalutamide. However, in some systems, a bimodal size distribution was observed, suggesting that some agglomerates had formed, consistent with the TEM data.

In order to better understand the interaction of polymers with the amorphous enzalutamide drug-rich aggregates, HPMCAS, labeled with an environment sensitive fluorescence tag, was utilized. The fluorescence emission spectrum of dansyl, which was used as the label, is highly dependent on the polarity of the local environment. In a less polar environment, the fluorescence intensity increases, and the emission peak shifts to a lower wavelength, relative to a polar environment. To confirm that covalent linkage of dansyl to HPMCAS led to environment sensitivity, the fluorescence emission spectrum of the labeled polymer in water and dichloromethane was compared, with data show in Figure 4-11. A blue shift is observed for the dansylated HPMCAS (d-HPMCAS) spectrum in dichloromethane in comparison to buffer, and the peak intensity

increase. It was also determined that d-HPMCAS showed a similar effectiveness as a crystallization inhibitor as the non-labeled polymer, confirming that the polymer retained functionality as an inhibitor after labeling. Next, d-HPMCAS was added to solutions with different initial enzalutamide concentrations, containing different amounts of drug-rich aggregates. For enzalutamide solutions at a concentration below the amorphous solubility, both drug and polymer are molecularly dissolved and minimal interactions are anticipated between the solvated species. At concentrations above the amorphous solubility, enzalutamide will undergo GLPS with the formation of amorphous aggregates whereby this drug-rich phase is less polar than water. Hence, if d-HPMCAS associates with the amorphous aggregates, its emission characteristics are expected to change. In contrast, if there is no interaction, d-HPMCAS should have the same spectrum as in buffer or the low concentration enzalutamide solutions. The fluorescence spectra of d-HPMCAS in buffer and enzalutamide solutions of different concentrations above and below the GLPS concentrations are shown in Figure 4-12. All spectra show a peak at approximately 437 nm, irrespective of the presence or absence of enzalutamide. In water, there is a broad, low intensity peak at around 535 nm which is present at around 528 nm at low enzalutamide concentrations. As the concentration increases beyond the amorphous solubility (42 µg/mL), new peaks emerge at 469 nm and 487 nm, and the emission peak has increased in intensity, whereby the overall maximum has shifted to a much lower wavenumber, and the peak found at lower concentrations now presents as a shoulder at around 535nm. This suggests that the dansylated portion of d-HPMCAS experiences two environments in the presence of the drug-rich aggregates, a less polar environment where the polymer is interacting with the aggregates, and the more polar aqueous environment. This is consistent with the results present above that demonstrate that HPMCAS distributes between both phases. To check that dansylation did not impact the distribution of the polymer in terms of the amount associated with the aggregates versus the amount in bulk aqueous solution, the polymer concentration was assayed in each phase, and was not found to be substantially different from that of the unlabeled polymer.

4.5   Discussion

Colloidal amorphous drug aggregates are frequently observed in aqueous solutions[24]. Of particular note, they form when the concentration of drug in solution exceeds the amorphous solubility[7] of the compound in a given medium. This suggests that solubility enhancing formulations, designed

to generate supersaturated solutions *in vivo*, are potentially prone to form amorphous aggregates following release of the drug from the formulation. To date, amorphous aggregate formation has been shown to occur *in vitro* following dissolution of certain amorphous solid dispersions, as a result of pH change[25], following dissolution of a drug salt[26], and following dilution of a concentrated organic solution of a drug[3,13]. Because most drugs have melting points above room temperature, the amorphous form is metastable with respect to the crystal and there is thermodynamic driving force for crystallization. Hence, when amorphous aggregates form in solution, the solution remains supersaturated and crystallization is favored. Given that a metastable equilibrium exists between drug present in the amorphous aggregate and drug in the bulk aqueous solution, i.e. the chemical potential of the drug in each phase is equal, there is an equal driving force for crystallization from each phase, although other factors important for crystallization such as molecular mobility vary between each phase. When the amorphous solubility is exceeded, either aggregate formation or crystallization are inevitable, whereby formation and maintenance of aggregates is preferred over crystallization from a solubility enhancement and drug delivery perspective, since aggregates co-exist with supersaturated bulk aqueous solution, while crystal formation results in a depletion of the supersaturation. It is widely recognized that supersaturated solutions show improved membrane transport and lead to a greater extent of permeation[27,28]. Therefore, inhibiting crystallization in systems containing drug aggregates is desirable. Indeed, recent studies, both *in vitro* and *in vivo*, point to the advantageous properties of aggregate containing systems[15]. These studies suggest that the aggregates act as a reservoir, dissolving to replace drug absorbed across a membrane, thereby maintaining supersaturation at a maximized value, driving membrane transport, and potentially enhancing absorption in vivo[3,5,6,29,30].

To maintain solution supersaturation, effective crystallization inhibitors that can prevent drug crystallization from both the drug-rich phase and the bulk solution phase are necessary. This requires that polymer associates with drug present in each phase. This concept was discussed by Raina *et al* in a study with felodipine where it was noted that the amount of polymer associated with the amorphous aggregates appeared to correlate with the polymer hydrophobicity, for a given initial polymer concentration[8]. Further, it was found that polymers that had a high affinity for either the aqueous phase, or the drug-rich phase, were poor crystallization inhibitors. Therefore, it was suggested that a required criterion for effective polymeric inhibitor in systems containing drug-

rich colloids, is that the polymer distribute between both phases. Clearly, following distribution, the polymer must then inhibit crystallization in each phase. Ueda *et al*. studied a several HPMC derivatives of differing hydrophobicities and also found that the amount of polymer associated with the drug-rich aggregates increased with polymer hydrophobicity[9]. They further concluded that a greater extent of crystallization inhibition was observed for systems where there was more polymer associated with the drug-rich aggregates. Similar conclusions were drawn by Wang *et al*. when studying supersaturated solutions of posaconazole and HPMCAS, namely that increased association of polymer with the drug-aggregates leads to supersaturation for a longer period of time[10].

For the two polymer studied herein, we find that although the amount of polymer associated with the drug-rich aggregates is the same, the effectiveness of each polymer as a crystallization inhibitor varies considerably. Hence our results do not agree with the conclusions of Ueda *et al*[9]. and Wang *et al.,*[10] namely that crystallization inhibition correlates with the amount of polymer associated with the aggregate phase. By considering crystallization mechanisms, we can attempt to rationalize, at least to some extent, our observations. The first important consideration is that crystallization can occur from either phase. Therefore, an effective polymer must be able to prevent crystallization from the bulk solution phase. This can be evaluated by studying crystallization from aggregate-free solutions, i.e. those at a concentration below the amorphous solubility. We note that, in the absence of aggregates up to 40 µg/mL enzalutamide, and at polymer concentration of 50 µg/mL, Eudragit E PO ® is an effective inhibitor of solution crystallization. Therefore, the relatively poor performance of Eudragit E PO ® relative to HPMCAS in the presence of aggregates appears be related to the ability of each polymer to inhibit crystallization from the aggregate phase. One possible explanation that can be ruled out is that mixing of the polymer with the drug aggregate phase reduces the drug chemical potential, and hence the driving force for crystallization, and that this occurs to a different extent for each polymer. If this were the case, the amorphous solubility, which depends on the chemical potential of the drug in the aggregate phase, would be reduced in the presence of the polymer, with the extent of the reduction depending on the amount of polymer mixed with the drug and any mixing non-idealities. Since no change in the amorphous solubility of enzalutamide in the presence of either polymer was observed, this suggests that the polymer is mainly associated with aggregate surface.

The interaction of each polymer with the aggregate surface is supported by the zeta potential data (Figure 4-9), as well as the TEM images (Figure 4-7 and 4-8). It is widely accepted that heterogeneous nucleation reduces the barrier for nucleation, and hence nucleation at an interface typically proceeds more readily. The interface of the drug-rich aggregate with the solvent is likely a highly favorable site for heterogeneous nucleation. Altering the surface chemistry of an interface via additives can be expected to enhance or retard nucleation, depending on how the additive interacts with the interface. Our results demonstrate that, in the presence of polymers, it is much harder to inhibit crystallization in systems containing aggregates, relative to in aggregate-free supersaturated solutions, with inductions times trending downwards as the number of aggregates increases. This observation supports the conjecture that the presence of aggregates is favorable for crystallization. It should be noted that the supersaturation is equivalent for solutions with an initial concentration of 42 µg/mL and above, because once the amorphous solubility is reached, excess drug above this concentration forms a new phase (the aggregates), and the chemical potential of the drug in each phase remains constant. However, several systems showed a marked decrease in induction time when the concentration increases from just below the amorphous solubility (40µg/mL) to just above the amorphous solubility (45µg/mL), as shown in Figures 4-4,4-5, and 4-6. Further decreases in induction time are apparent as the amount of aggregates is increased and higher amounts of polymer are required. Therefore, the aggregates tend to enhance the crystallization tendency of the system, and therefore crystallization inhibition is essential.

The cellulose derivatives, P177 and HPMCAS, which are anionic at the pH tested, were effective crystallization inhibitors at concentrations above and below the amorphous solubility. HPMCAS has been shown to be effective at maintaining supersaturation for multiple structurally diverse, poorly water-soluble compounds[5,31–37]. The effectiveness of HPMCAS has been attributed to the presence of hydrophobic regions that can interact with the drug in aqueous solution, as well as the presence of a charge arising from carboxylic acid groups that ionize at pHs above 5-6, which interacts with water[32,33,38]. Overall, these chemical features lead to amphiphilic properties and it has been demonstrated that HPMCAS adsorbs at the drug crystal:water interface. These molecular features should also drive interaction with the drug aggregates, and results with fluorescently labeled HPMCAS (Figure 4-12) confirm close interaction of the polymer with enzalutamide aggregates. Considering these chemical features, it might be anticipated that Eudragit E PO ®

would exhibit similar behavior to HPMCAS since it is an amino methacrylate copolymer and thus contains both hydrophobic moieties as well as the cationic amino group which is ionized at pH 6.5. This polymer does indeed interact with enzalutamide aggregates, where the same amount of polymer associates with the aggregates as observed for HPMCAS. However, despite the equivalent polymer concentration associated with the aggregates, Eudragit E PO ® was far less effective at inhibiting enzalutamide crystallization than HPMCAS. This observation suggests that a more detailed understanding of drug-polymer interactions and structure at the drug:polymer:water interface will be necessary in order to fully understand our experimental observations.

4.6   Conclusion

Enzalutamide crystallizes rapidly from supersaturated solutions. Both anionic and cationic polymers, specifically HPMCAS and Eudragit E PO ®, are effective crystallization inhibitors in homogenous, single phase supersaturated solutions, i.e. solutions at a concentration below the amorphous solubility. When colloidal drug-rich aggregates are formed, the polymers become less effective at maintaining supersaturation, and a greater polymer concentration is required to extend induction times. Analysis of the amount of each polymer associated with the drug-rich aggregates demonstrated that approximately the same amount is present for each polymer. However, HPMCAS more effectively stabilizes the drug-rich aggregates against both crystallization and size enlargement. The stabilization against crystallization in supersaturated aqueous solutions containing enzalutamide aggregates appears to be mediated by interactions between the drug and the polymer at the aggregate:water interface. These systems warrant more detailed investigations to probe the mechanism of crystallization inhibition at a molecular level.

Table 4-1. The induction time of enzalutamide in the absence of polymer.

Concentration (µg/mL)	Time (minutes)
30	15 (0)
35	9 (1)
40	8 (1)
45	5 (1)
70	9 (2)
120	12 (3)

Table 4-2. HPMCAS location in enzalutamide solutions containing 42 µg/mL of molecularly dissolved drug and 78 µg/mL of amorphous aggregates after 1.25 hours of mixing.

HPMCAS Concentration (µg/mL)	HPMCAS Concentration in Solution (µg/mL)	w/w% HPMCAS:ENZ Amorphous Aggregates
25*	19.2 (5.2)	12.9 (4.2)
25	21.0 (12.5)	9.6 (1.0)
50	29.9 (2.4)	19.7 (1.0)
100	88.2 (5.2)	20.4 (1.0)

* Reading taken after 15 minutes

Table 4-3. Eudragit E PO ® location in enzalutamide solutions containing 42 µg/mL of molecularly dissolved drug and 28 µg/mL of amorphous aggregates.

Eudragit E PO ® Concentration (µg/mL)	Eudragit E PO ® Concentration in Solution (µg/mL)	w/w% Eudragit E PO ®:ENZ Amorphous Aggregates
50	45.1 (10.8)	22.5 (0.7)
100	92.5 (9.3)	18.9 (1.4)

Table 4-4. Amount of polymer that forms pellets in buffer alone.

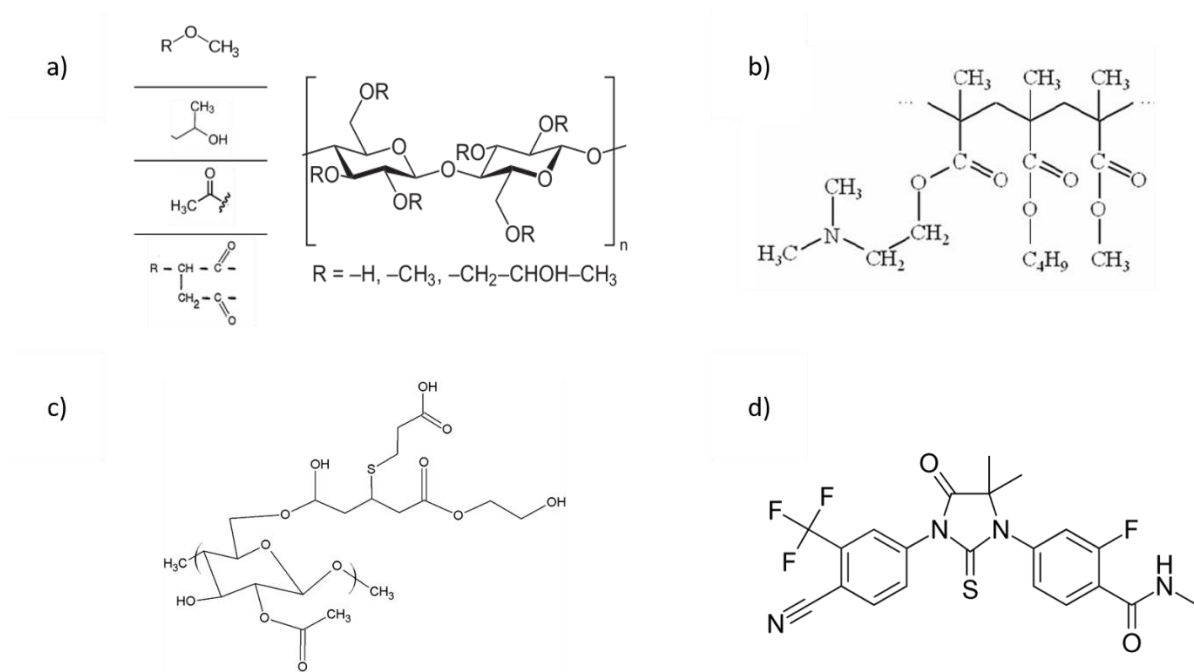| Polymer	Polymer Concentration (μg/mL)	Polymer Concentration in Pellet (μg/mL)
Eudragit E PO ®	100	0
HPMCAS	100	0
	250	12.3 (4.0)
	500	35.1 (10.8)

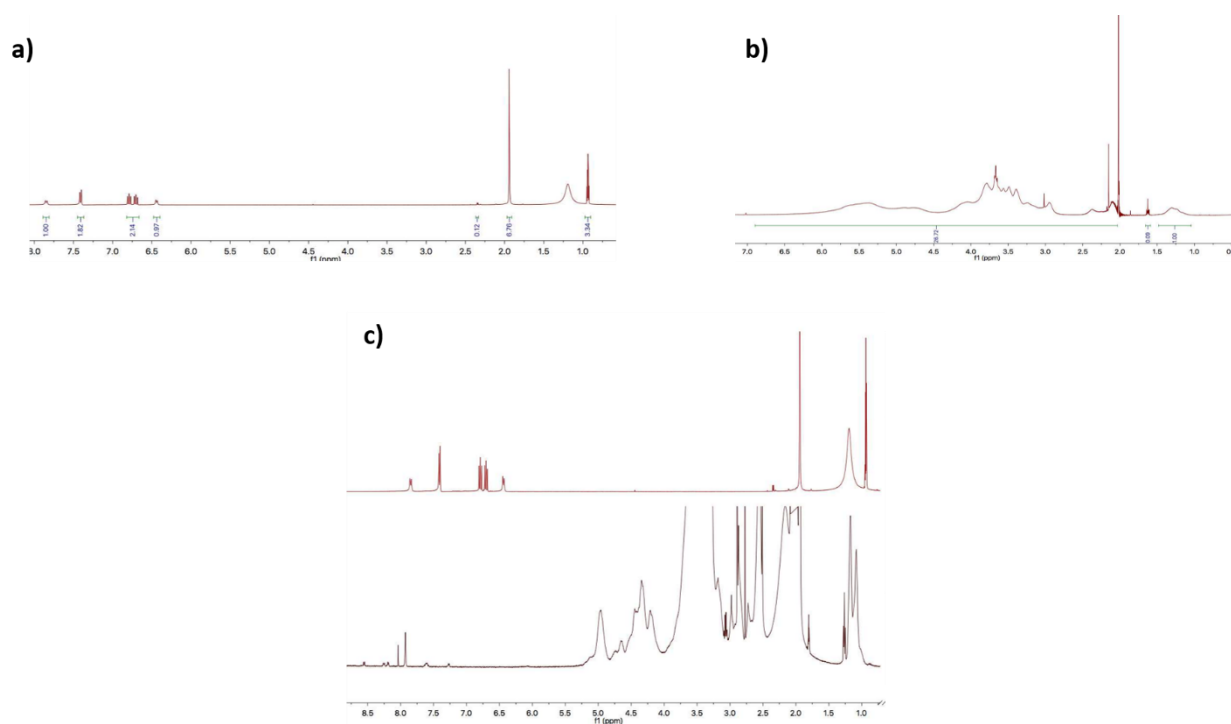Figure 4-1. Structures of a) HPMCAS, b) Eudragit E PO ®, c) P177, and d) enzalutamide.

Figure 4-2. The ^{1}H NMR spectra of a) dansyl chloride in deuterated acetonitrile, b) HPMCAS in deuterated pyridine, and c) dansyl-Chloride (top) vs. dansylated-HPMCAS (bottom) in deuterated acetonitrile.
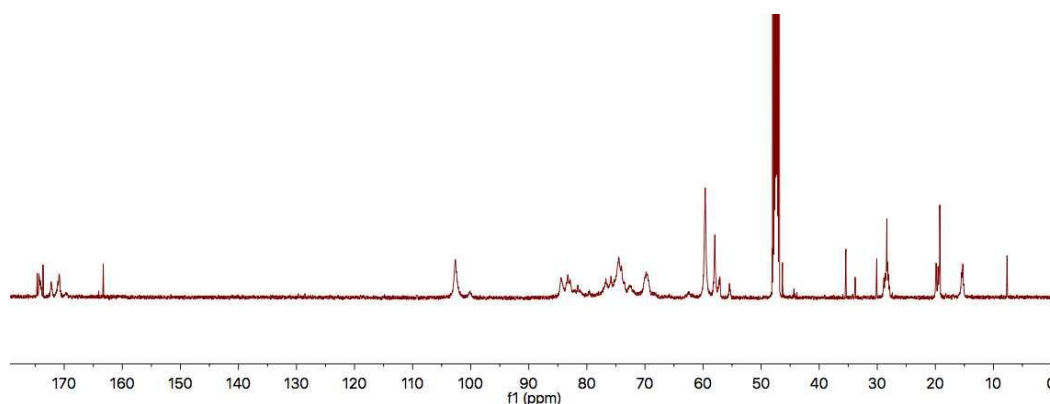
Figure 4-3. The ^{13}C NMR spectra of dansylated-HPMCAS in deuterated acetonitrile.
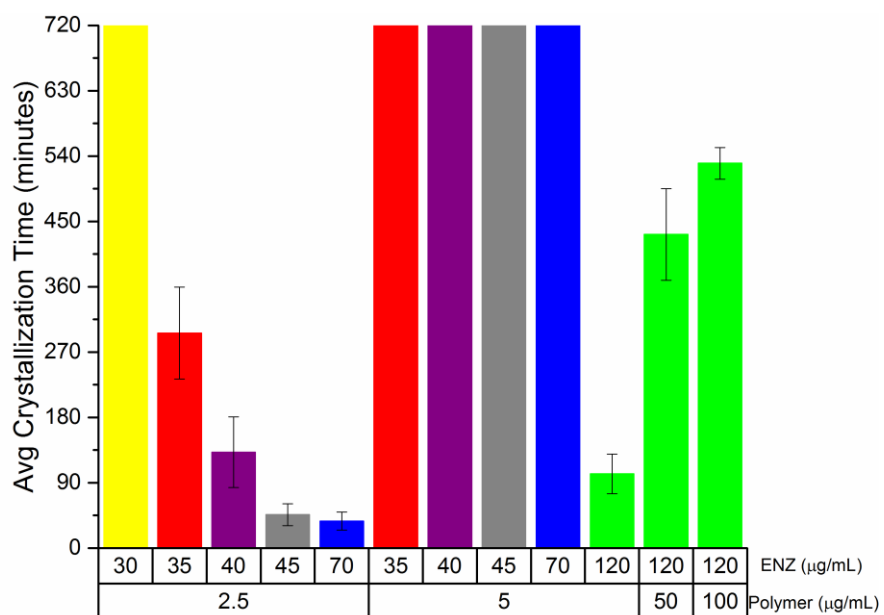

Figure 4-4. The induction time of enzalutamide solutions of varying initial concentrations in the presence of different amounts of HPMCAS.
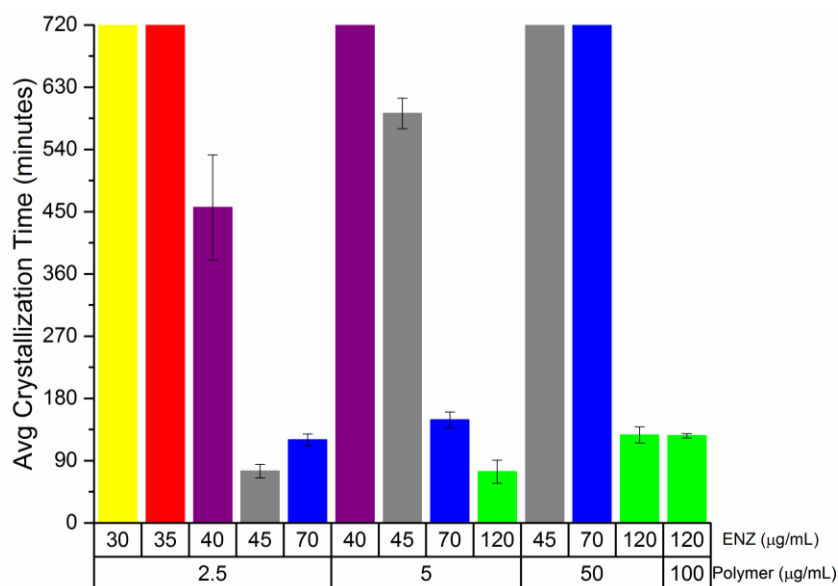
Figure 4-5. The induction time of enzalutamide solutions of varying initial concentrations in the presence of different amounts of P177.
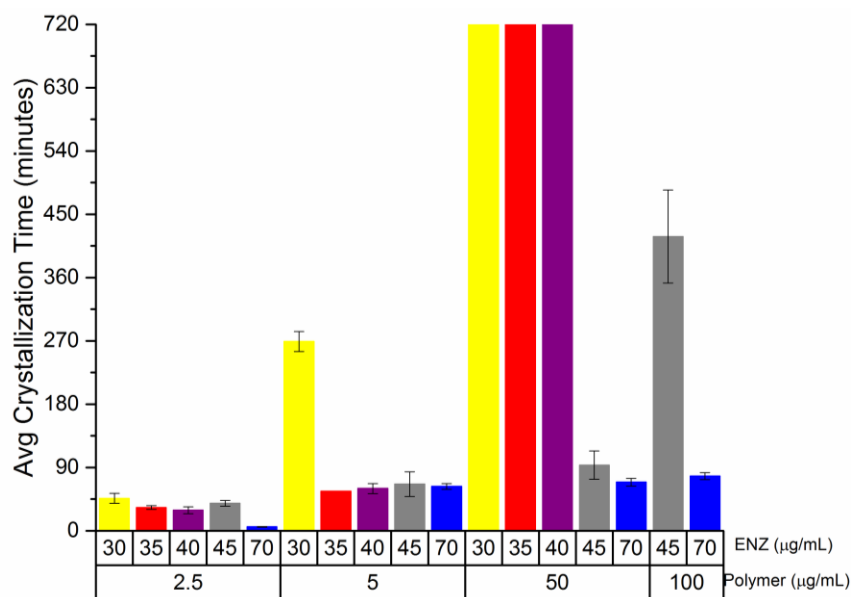

Figure 4-6. The induction time of enzalutamide solutions of varying initial concentrations in the presence of different amounts of Eudragit E PO ®.
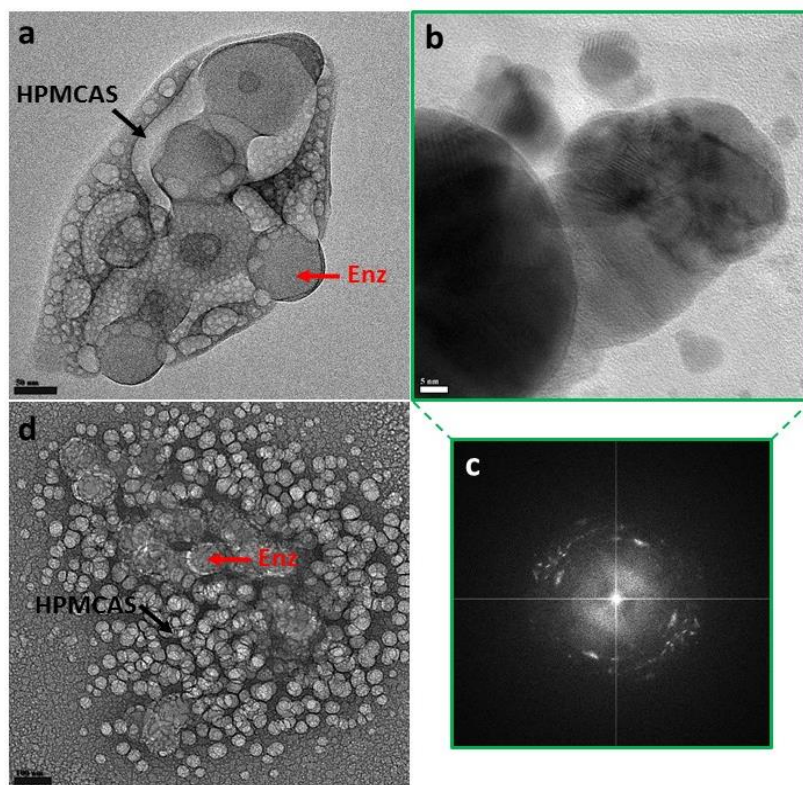
Figure 4-7. BF TE micrographs of (a) Enz (120 µg/mL):HPMCAS (100 µg/mL) aggregates (b) Enz (120 µg/mL):HPMCAS (100 µg/mL) aggregates after crystallization (c) FFT of (b) confirming the presence of order due to crystallized Enz and (d) Enz (120 µg/mL)-HPMCAS (500 µg/ml) showing both drug and polymer aggregates.
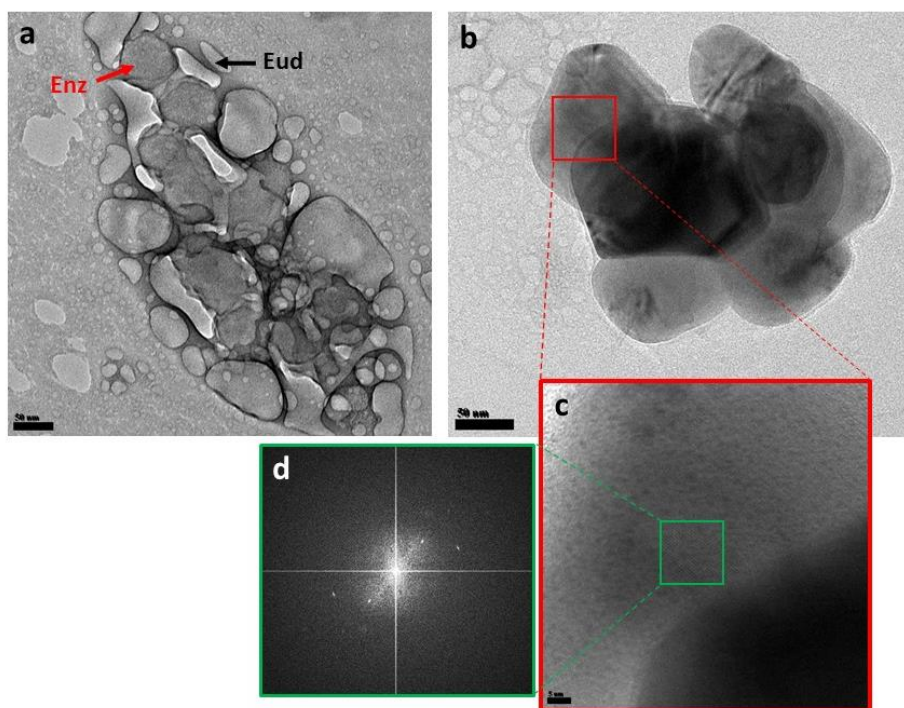
Figure 4-8. BF TE micrographs of (a) Enz (70 µg/mL):Eud (100 µg/mL) aggregates (b) Enz:Eud aggregates underwent crystallization, zoomed in region displaying order (d) FFT of (c) confirming the presence of order due to crystallized Enz.
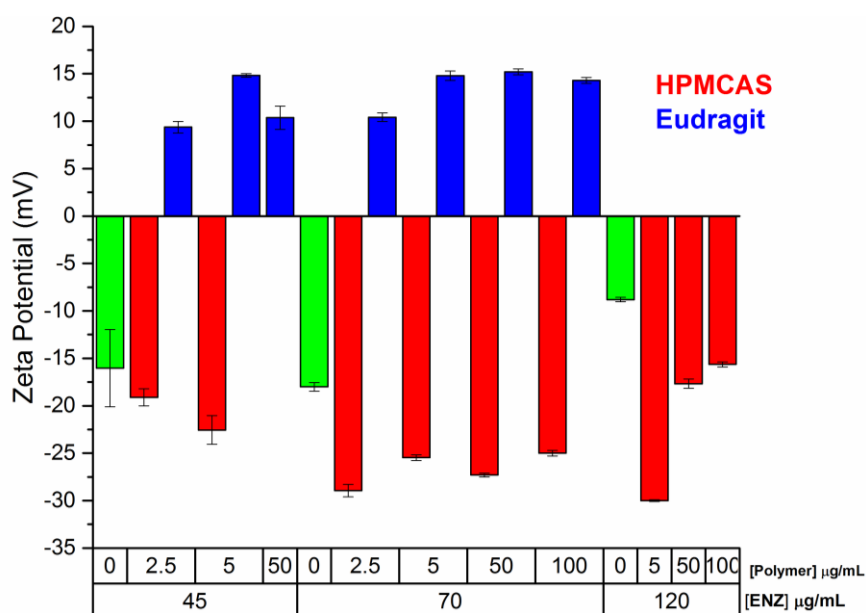

Figure 4-9. The zeta potential of amorphous aggregates of enzalutamide in the presence of varying concentrations of polymer.

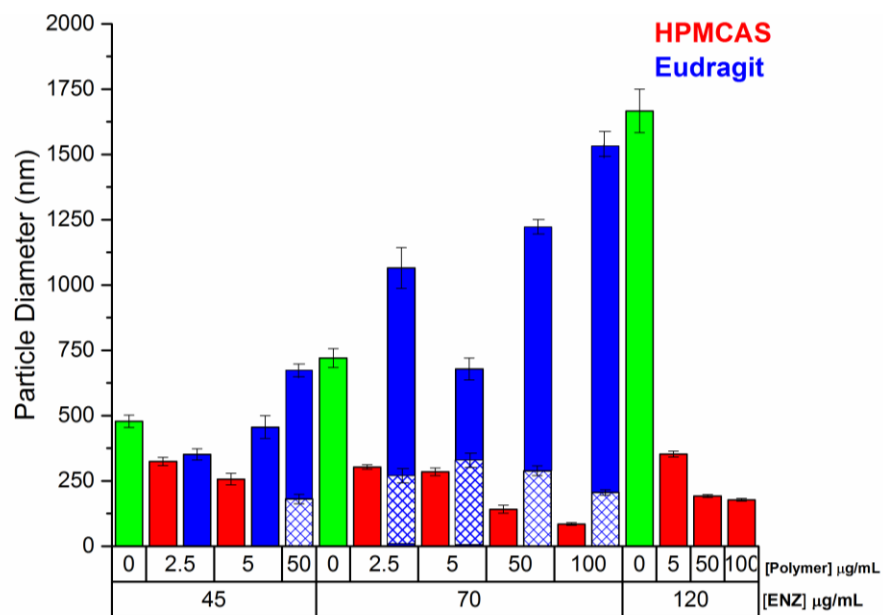Figure 4-10. The diameter of amorphous aggregates formed in the presence and absence of polymers HPMCAS and Eudragit E PO ®. A bimodal distribution was observed for Eudragit E PO ® samples.
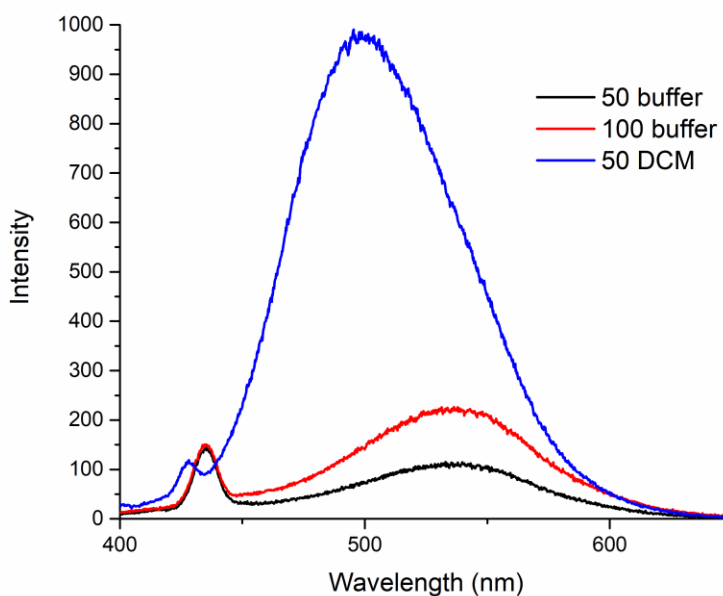

Figure 4-11. The fluorescence spectra of 50 and 100 µg/mL dansylated HPMCAS in buffer and dichloromethane (DCM).
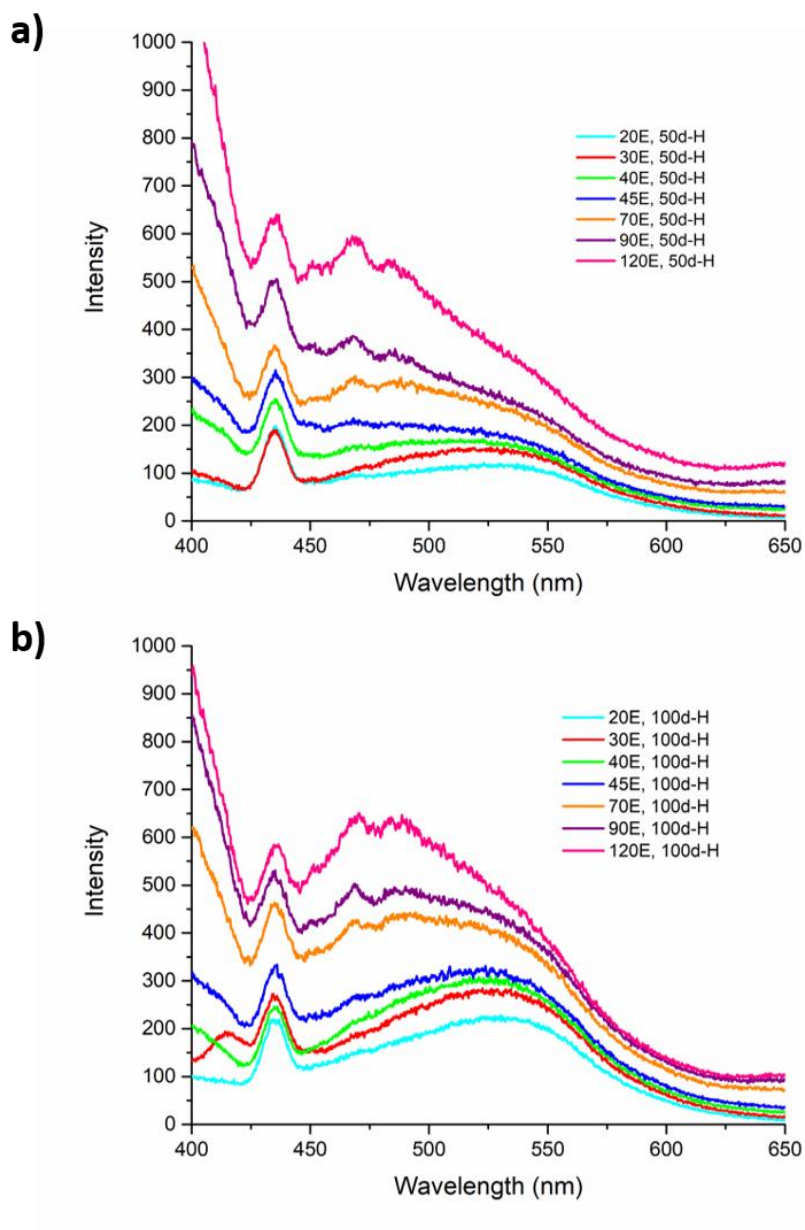
Figure 4-12. The fluorescence spectra of a) 50 and b) 100 µg/mL dansylated HPMCAS in varying concentrations of enzalutamide.

4.7 References

[1]   L. Z. Benet, "The role of BCS (biopharmaceutics classification system) and BDDCS (biopharmaceutics drug disposition classification system) in drug development," *J. Pharm. Sci.*, vol. 102, no. 1, pp. 34–42, 2013.

[2]   S. Baghel, H. Cathcart, and N. J. O'Reilly, "Polymeric Amorphous Solid Dispersions: A Review of Amorphization, Crystallization, Stabilization, Solid-State Characterization, and Aqueous Solubilization of Biopharmaceutical Classification System Class II Drugs," *Journal of Pharmaceutical Sciences*, vol. 105, no. 9. pp. 2527–2544, 2016.

[3]   L. I. Mosquera-Giraldo and L. S. Taylor, "Glass−Liquid Phase Separation in Highly Supersaturated Aqueous Solutions of Telaprevir," *Mol. Pharm.*, vol. 12, no. 2, pp. 496–503, 2015.

[4]   A. S. Indulkar, J. E. Waters, H. Mo, Y. Gao, S. A. Raina, G. G. Z. Zhang, and L. S. Taylor, "Origin of Nanodroplet Formation Upon Dissolution of an Amorphous Solid Dispersion: A Mechanistic Isotope Scrambling Study," *J. Pharm. Sci.*, vol. 106, no. 8, pp. 1998–2008, 2017.

[5]   S. A. Raina, G. G. Z. Zhang, D. E. Alonzo, J. Wu, D. Zhu, N. D. Catron, Y. Gao, and L. S. Taylor, "Enhancements and limits in drug membrane transport using supersaturated solutions of poorly water soluble drugs," *J. Pharm. Sci.*, vol. 103, no. 9, pp. 2736–2748, 2014.

[6]   A. S. Indulkar, Y. Gao, S. A. Raina, G. G. Z. Zhang, and L. S. Taylor, "Exploiting the Phenomenon of Liquid-Liquid Phase Separation for Enhanced and Sustained Membrane Transport of a Poorly Water-Soluble Drug," *Mol. Pharm.*, vol. 13, no. 6, pp. 2059–2069, 2016.

[7]   L. S. Taylor and G. G. Z. Zhang, "Physical chemistry of supersaturated solutions and implications for oral absorption," *Advanced Drug Delivery Reviews*. 2016.

[8]   S. A. Raina, B. Van Eerdenbrugh, D. E. Alonzo, H. Mo, G. G. Z. Zhang, Y. Gao, and L. S. Taylor, "Trends in the Precipitation and Crystallization Behavior of Supersaturated Aqueous Solutions of Poorly Water-Soluble Drugs Assessed Using Synchrotron Radiation," *J. Pharm. Sci.*, vol. 104, no. 6, pp. 1981–1992, 2015.

[9]   K. Ueda, K. Higashi, K. Yamamoto, and K. Moribe, "Inhibitory effect of hydroxypropyl methylcellulose acetate succinate on drug recrystallization from a supersaturated solution assessed using nuclear magnetic resonance measurements," *Mol. Pharm.*, 2013.

[10]   S. Wang, C. Liu, Y. Chen, A. (Donghua) Zhu, and F. Qian, "Aggregation of Hydroxypropyl Methylcellulose Acetate Succinate under Its Dissolving pH and the Impact on Drug Supersaturation," *Mol. Pharm.*, p. acs.molpharmaceut.8b00633, Aug. 2018.

[11]   X. Meng, S. Roy Choudhury, and K. J. Edgar, "Multifunctional cellulose esters by olefin cross-metathesis and thiol-Michael addition," *Polym. Chem.*, vol. 7, no. 23, pp. 3848–3856, 2016.

[12]   M. J. Jackson, U. S. Kestur, M. A. Hussain, and L. S. Taylor, "Dissolution of Danazol Amorphous Solid Dispersions: Supersaturation and Phase Behavior as a Function of Drug Loading and Polymer Type," *Mol. Pharm.*, 2016.

[13]   G. A. Ilevbare and L. S. Taylor, "Liquid–Liquid Phase Separation in Highly Supersaturated Aqueous Solutions of Poorly Water-Soluble Drugs: Implications for Solubility Enhancing Formulations," *Cryst. Growth Des.*, vol. 13, no. 4, pp. 1497–1509, Apr. 2013.

[14]   K. J. Frank, U. Westedt, K. M. Rosenblatt, P. Hölig, J. Rosenberg, M. Mägerlein, G. Fricker, and M. Brandl, "The amorphous solid dispersion of the poorly soluble ABT-102 forms nano/microparticulate structures in aqueous medium: Impact on solubility," *Int. J. Nanomedicine*, vol. 7, pp. 5757–5768, 2012.

[15]   A. M. Stewart, M. E. Grass, T. J. Brodeur, A. K. Goodwin, M. M. Morgen, D. T. Friesen, and D. T. Vodak, "Impact of Drug-Rich Colloids of Itraconazole and HPMCAS on Membrane Flux in Vitro and Oral Bioavailability in Rats," *Mol. Pharm.*, vol. 14, no. 7, pp. 2437–2449, 2017.

[16] N. S. Trasi and L. S. Taylor, "Dissolution performance of binary amorphous drug combinations - Impact of a second drug on the maximum achievable supersaturation," *Int. J. Pharm.*, 2015.

[17] N. S. Trasi and L. S. Taylor, "Thermodynamics of Highly Supersaturated Aqueous Solutions of Poorly Water-Soluble Drugs - Impact of a Second Drug on the Solution Phase Behavior and Implications for Combination Products," *J. Pharm. Sci.*, vol. 104, no. 8, pp. 2583–2593, 2015.

[18] N. Li and L. S. Taylor, "Tailoring supersaturation from amorphous solid dispersions," *J. Control. Release*, vol. 279, pp. 114–125, 2018.

[19] L. Lindfors, P. Skantze, U. Skantze, M. Rasmusson, A. Zackrisson, and U. Olsson, "Amorphous drug nanosuspensions. 1. Inhibition of ostwald ripening," *Langmuir*, 2006.

[20] L. Lindfors, S. Forssén, P. Skantze, U. Skantze, A. Zackrisson, and U. Olsson, "Amorphous drug nanosuspensions. 2. Experimental determination of bulk monomer concentrations," *Langmuir*, 2006.

[21] R. H. Müller, G. E. Hildebrand, R. Nitzsche, and B.-R. Paulke, "Zetapotential und Partikelladung in der Laborpraxis," *Paperb. APV*, vol. 37, 1996.

[22] T. M. Riddick, "Zeta-meter manual," *New York Zeta-m. Inc*, 1968.

[23] C. Jacobs and R. H. Müller, "Production and characterization of a budesonide nanosuspension for pulmonary administration," *Pharm. Res.*, vol. 19, no. 2, pp. 189–194, 2002.

[24] A. N. Ganesh, E. N. Donders, B. K. Shoichet, and M. S. Shoichet, "Colloidal aggregation: From screening nuisance to formulation nuance," *Nano Today*. 2018.

[25] A. S. Indulkar, K. J. Box, R. Taylor, R. Ruiz, and L. S. Taylor, "pH-Dependent Liquid-Liquid Phase Separation of Highly Supersaturated Solutions of Weakly Basic Drugs," *Mol. Pharm.*, 2015.

[26]   Y. Song, X. Yang, X. Chen, H. Nie, S. Byrn, and J. W. Lubach, "Investigation of Drug-Excipient Interactions in Lapatinib Amorphous Solid Dispersions Using Solid-State NMR Spectroscopy," *Mol. Pharm.*, 2015.

[27]   J. Brouwers, M. E. Brewster, and P. Augustijns, "Supersaturating drug delivery systems: The answer to solubility-limited oral bioavailability?," *Journal of Pharmaceutical Sciences*, vol. 98, no. 8. pp. 2549–2572, 2009.

[28]   P. Berben, J. Brouwers, and P. Augustijns, "The artificial membrane insert system as predictive tool for formulation performance evaluation," *Int. J. Pharm.*, vol. 537, no. 1–2, pp. 22–29, 2018.

[29]   L. I. Mosquera-Giraldo, N. Li, V. R. Wilson, B. L. B. Nichols, K. J. Edgar, and L. S. Taylor, "Influence of Polymer and Drug Loading on the Release Profile and Membrane Transport of Telaprevir," *Mol. Pharm.*, vol. 15, no. 4, pp. 1700–1713, Apr. 2018.

[30]   D. E. Alonzo, Y. Gao, D. Zhou, H. Mo, G. G. Z. Z. Zhang, and L. S. Taylor, "Dissolution and precipitation behavior of amorphous solid dispersions," *J. Pharm. Sci.*, vol. 100, no. 8, pp. 3316–3331, 2011.

[31]   L. E. Appel, W. C. Babcock, D. T. Friesen, R. J. Ray, D. T. Smithey, S. L. Shamblin, and R. M. Shanker, "Pharmaceutical dosage forms comprising a low-solubility drug and a polymer." Google Patents, 04-Jun-2009.

[32]   D. T. Friesen, R. Shanker, M. Crew, D. T. Smithey, W. J. Curatolo, and J. A. S. Nightingale, "Hydroxypropyl methylcellulose acetate succinate-based spray-dried dispersions: An overview," *Mol. Pharm.*, vol. 5, no. 6, pp. 1003–1019, 2008.

[33]   W. Curatolo, J. A. Nightingale, and S. M. Herbig, "Utility of hydroxypropylmethylcellulose acetate succinate (HPMCAS) for initiation and maintenance of drug supersaturation in the GI milieu," *Pharm. Res.*, vol. 26, no. 6, pp. 1419–1431, 2009.

[34]   F. Tanno, Y. Nishiyama, H. Kokubo, and S. Obara, "Evaluation of Hypromellose Acetate Succinate (HPMCAS) as a Carrier in Solid Dispersions," *Drug Dev. Ind. Pharm.*, vol. 30, no. 1, pp. 9–17, 2004.

[35] M. Van Speybroeck, R. Mols, R. Mellaerts, T. Do Thi, J. A. Martens, J. Van Humbeeck, P. Annaert, G. Van den Mooter, and P. Augustijns, "Combined use of ordered mesoporous silica and precipitation inhibitors for improved oral absorption of the poorly soluble weak base itraconazole," *Eur. J. Pharm. Biopharm.*, vol. 75, no. 3, pp. 354–365, 2010.

[36] H. Konno and L. S. Taylor, "Influence of different polymers on the crystallization tendency of molecularly dispersed amorphous felodipine," *J. Pharm. Sci.*, vol. 95, no. 12, pp. 2692–2705, 2006.

[37] S. A. Raina, G. G. Z. Zhang, D. E. Alonzo, J. Wu, D. Zhu, N. D. Catron, Y. Gao, and L. S. Taylor, "Impact of Solubilizing Additives on Supersaturation and Membrane Transport of Drugs," *Pharm. Res.*, vol. 32, no. 10, pp. 3350–3364, 2015.

[38] D. B. Warren, H. Benameur, C. J. H. Porter, and C. W. Pouton, "Using polymeric precipitation inhibitors to improve the absorption of poorly water-soluble drugs: A mechanistic basis for utility," *Journal of Drug Targeting*, vol. 18, no. 10. pp. 704–731, 2010.

VITA

Venecia R. Wilson received her Bachelors in Science in Agricultural & Biological Engineering and a Bachelors of Science in Pharmaceutical Sciences with a concentration in Medicinal Chemistry and Molecular Pharmacology from Purdue University, West Lafayette campus in 2013. In fall 2013,Venecia joined the Industrial and Physical Pharmacy department. Venecia will be joining Merck KGaA GoGlobal Inhouse Consulting program upon completion of her PhD.